

English translation of the monthly «Avtomacheskaya Svarka» (Automatic Welding) journal published in Russian since 1948

Founders: E.O. Paton Electric Welding Institute of the NAS of Ukraine
International Association «Welding»

Publisher: International Association «Welding»

Editor-in-Chief B.E.Paton

Editorial board:

Yu.S.Borisov	V.F.Khorunov
A.Ya.Ishchenko	I.V.Krivtsun
B.V.Khitrovskaya	L.M.Lobanov
V.I.Kirian	A.A.Mazur
S.I.Kuchuk-Yatsenko	
Yu.N.Lankin	I.K.Pokhodnya
V.N.Lipodaev	V.D.Poznyakov
V.I.Makhnenco	K.A.Yushchenko
O.K.Nazarenko	A.T.Zelnichenko
I.A.Ryabtsev	

International editorial council:

N.P.Alyoshin	(Russia)
U.Diltey	(Germany)
Guan Qiao	(China)
D. von Hofe	(Germany)
V.I.Lysak	(Russia)
N.I.Nikiforov	(Russia)
B.E.Paton	(Ukraine)
Ya.Pilarczyk	(Poland)
G.A.Turichin	(Russia)
Zhang Yanmin	(China)
A.S.Zubchenko	(Russia)

Promotion group:

V.N.Lipodaev, V.I.Lokteva
A.T.Zelnichenko (exec. director)

Translators:

A.A.Fomin, O.S.Kurochko,
I.N.Kutianova, T.K.Vasilenko

Editor:

N.A.Dmitrieva

Electron galley:

D.I.Sereda, T.Yu.Snegiryova

Address:

E.O. Paton Electric Welding Institute,
International Association «Welding»,
11, Bozhenko str., 03680, Kyiv, Ukraine
Tel.: (38044) 200 67 57, 200 82 77
Fax: (38044) 200 04 86, 200 82 77
E-mail: journal@paton.kiev.ua
http://www.nas.gov.ua/pwj

State Registration Certificate
KV 4790 of 09.01.2001

Subscriptions:

\$324, 12 issues per year,
postage and packaging included.
Back issues available.

All rights reserved.

This publication and each of the articles
contained herein are protected by copyright.
Permission to reproduce material contained in
this journal must be obtained in writing from
the Publisher.

Copies of individual articles may be obtained
from the Publisher.

CONTENTS

SCIENTIFIC AND TECHNICAL

Kuchuk-Yatsenko S.I., Kyrian V.I., Kazymov B.I. and Khomenko V.I. Assessment of deformability of pipe steel joints made by automatic continuous flash-butt welding 2

Andreev V.V., Efremenko E.M. and Moskovich G.N. Simulation of electric circuit as a stage in development of power source with controllable shape of alternating current 7

Dyadin V.P. and Yurko L.Ya. Experimental evaluation of δ_{1c} -curve temperature shift and brittle-tough transition of structural steels and welded joints by the results of standard tests 11

Moravetsky S.I. Detachability of slag crust in arc welding (Review). Part 2. Character of the effect of main factors on detachability of slag crust 20

Mohyla P., Hlavaty I. and Tomcik P. Cause of secondary hardening in Cr-Mo-V weld metal during long-term heat exposure 24

Tyurin Yu.N., Kuskov Yu.M., Markashova L.I., Chernyak Ya.P., Berdnikova E.N., Popko V.I., Kashnaryova O.S. and Alekseenko T.A. Effect of low-frequency resonance oscillations on structure and crack resistance of deposited high-chromium cast iron 27

INDUSTRIAL

Keitel S. and Neubert J. Laser based girth welding technologies for pipeline construction 31

Shlepakov V.N. and Kotelchuk A.S. Experience of manufacture and application of seamless flux-cored wire for electric arc welding 37

Kulik V.M., Savitsky M.M., Elagin V.P. and Demchenko E.L. Capabilities of application of high-strength low-alloy pipe steels for manufacture of high-pressure vessels 43

Gulakov S.V. and Burlaka V.V. Automatic control drive of electrode movement trajectory for the arc surfacing machines 48

BRIEF INFORMATION

Levchenko O.G., Savitsky V.V. and Lukianenko A.O. Information-calculation system for hygienic characteristics of welding electrodes 52

Theses for a scientific degree 54

INFORMATION

Flash-butt welding of rod reinforcement in reconstruction of Olympic NSC (Kiev) 56

Abstracts of works on innovation projects of the NAS of Ukraine 10, 19, 42, 51



ASSESSMENT OF DEFORMABILITY OF PIPE STEEL JOINTS MADE BY AUTOMATIC CONTINUOUS FLASH-BUTT WELDING

S.I. KUCHUK-YATSENKO¹, V.I. KYRIAN¹, B.I. KAZYMOV¹ and V.I. KHOMENKO²

¹E.O. Paton Electric Welding Institute, NASU, Kiev, Ukraine

²CJSC «Pskovelektrosvar», Russia

Peculiarities of formation of high quality flash-butt welded joints on pipes are analyzed. Factors affecting the results of impact tests of standard specimens are considered. Toughness properties of metal in the welding zone have been studied by using different impact test methods. It is shown that metal of as-welded joint made at optimum parameters has sufficiently high resistance to impact loads. Conditions for performing flash-butt welding and inspection of the joints providing high operating reliability of pipelines have been determined.

Key words: *flash-butt welding, pipelines, joint quality, impact testing methods, joint zone, impact toughness, operating reliability*

One of the important tasks in construction of pipeline systems is ensuring their operating reliability. It is solved by specifying a number of technical and technological requirements pertaining both to welding performance, and to the properties of site (circumferential) butt joints. Mechanical properties of the latter are represented by values of strength and ductility, and they should meet the requirements of standards [1, 2]. In addition, in order to prevent fractures in butt joint operation because of the most characteristic defects, inherent to the applied welding process, also specified are the requirements to the value of joint metal impact toughness representing the energy consumed in fracture of a standard sample.

Over the recent decades the method of impact testing of samples with a sharp mechanical notch (*KCV*) of depth $h = 2$ mm with radius $r = 0.25$ mm at the bottom, has become the dominant method that was due to a high probability of formation of sharp stress raisers in welds, including crack-like ones. Nowadays such a testing procedure and established values of impact toughness are extended to all the welded joints, irrespective of the process of their welding. In keeping with the requirements of [1], average value of impact toughness of metal of welded joints on pipes of strength class X52–X70 at -20°C testing temperature should be not less than 34.4, and minimum value should be 29.4 J/cm^2 . These *KCV* values were determined allowing for the inevitable and admissible defects for joints made by electric arc welding processes. These defects include external crack-like defects (one- and two-sided lacks-of-penetration — lacks-of-fusion) of up to 1 mm depth and up to 30 mm length, weld root concavity (shrinkage of down to 2 mm depth and length of up to 1/6 of welded butt joint perimeter), as well as internal lacks-of-penetration both be-

tween the layers and around the contour of the edges. In addition, in electric arc welding there is a high probability of appearance of various kinds of cracks, which are not allowed in welded joints. Their detection, however, by industrial NDT methods presents certain difficulties in a number of cases.

Transfer of the testing procedure and the above standard *KCV* requirements to welded joints made by other welding methods, is not always justified by far. In the case of absence of the above defects in the weld, ensuring *KCV* values on the level of 34.4 J/cm^2 for all the zones of the joints should be recognized as unpractical as such requirements make pipeline construction more complicated and lead to excessive consumption of material means. API-1104 standard is advanced in this respect [2]. It does not specify the impact toughness values; they are indicated by the customer in the form of special requirements that are defined allowing for specific conditions of pipeline construction and operation. Such an approach is directed to simultaneous solution of the two main tasks: lowering of failure probability of the pipelines in operation with the most probable defects in circumferential butt joints, characteristic for the applied welding process, and minimization of construction costs.

Many years of experience of operation of various diameter welded pipelines, including high-capacity gas- and oil pipelines of 1420 mm diameter, shows the high reliability of circumferential welds, made by automatic flash-butt welding. Mechanical properties of these joints meet all the requirements of the standards, in keeping with which large-scale construction of the main and industrial pipelines is performed, except for individual cases when special requirements are made to the value of impact toughness (mainly in welding large diameter pipelines operating at below zero temperatures).

Compared to electric arc fusion welding, flash-butt welding has principal differences in joint formation,



which need comprehensive analysis, and should be taken into account at substantiation of the procedure of fitness-for-purpose assessment of welded joints of pipes made by flash-butt welding.

Flash-butt welding is one of pressure welding processes in which there is no molten metal in the joint zone (weld), thus eliminating all the prerequisites for formation of such hazardous defects as cracks. In performance of welding in the optimum mode other defects are also absent in the joint zone (JZ), which could detract from joint performance. Such a welding mode is determined by statistical treatment of mechanical testing data obtained during investigation of weldability of each typesize of pipes under the condition that inadmissible welding defects are completely absent in the joints. Mechanical properties should correspond to the requirements of standards, made of pipe welded joints. Assessment of welding quality is performed by breaking welded butt joints through JZ [3]. From admissible defects in flash-butt welding, only local clusters of nonmetallic inclusions can be present in individual JZ regions with maximum area of 20–30 mm² [4, 5], but as they do not influence the static strength of the joints [6] they should not be regarded as defects. Considering the structural condition, such nonmetallic inclusions should be regarded as one of the kinds of structural inhomogeneity, presence of which is admissible in the pipe metal. In some works such JZ regions are called «mat spots» [7, 8]. Maintenance of the specified parameters of optimum welding mode in flash-butt welding is ensured by a computerized system of control and monitoring without intervention of welding operator. This is the determinant factor in ensuring the high operating reliability of more than 70,000 km of various pipelines, including more than 10,000 km of pipelines of 1420 mm diameter welded by flash-butt process [9, 10], that have been operating unfailingly for more than 30 years under different natural conditions, including artic regions of West Siberia (Figure 1). Average value of impact toughness of these joints, determined at testing of standard samples with a sharp mechanical notch, the tip of which is located in JZ center, is equal to 30–40 J/cm² in the scatter band of KCV values in the range of 14.3–56.3 J/cm² (20 °C testing temperature). Such values of impact toughness of JZ metal are largely due to mechanical inhomogeneity that forms as a result of varying degrees of metal strengthening in the welding zone. The magnitude of plastic deformation at the final stage of welding, i.e. upsetting, varies, depending on the temperature gradient in pipe welding zone (on both sides of JZ). As a result, the joint metal in its cross-section differs essentially by hardness, and, therefore, also mechanical properties ($\sigma_{0.2}$, σ_t). JZ has the smallest hardness value. Hardness of adjacent regions of the welding zone is higher than that of the pipe metal. In welding of pipes produced now from low-carbon low-

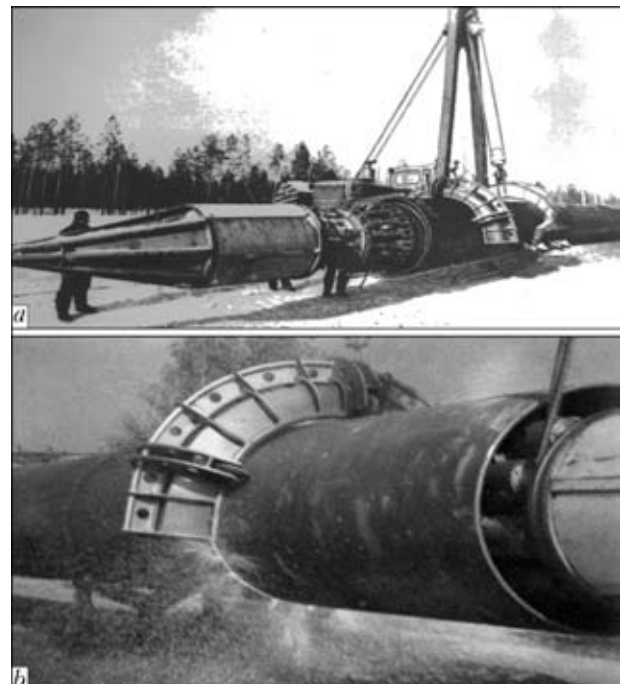


Figure 1. «Sever-1» welding complex in the construction route of 1420 mm diameter pipeline in West Siberia: *a* – position of welding machine in the pipeline before feeding the next pipe to be welded on; *b* – welding operation

alloyed steels, the width of JZ region can be within 0.5–5 mm, depending on the welding mode. Difference in hardness, and, therefore, strength of this region, compared to the adjacent regions of the zone of thermomechanical strengthening can be up to 30 %, and in welding of pipes from carbon steels it can be higher. The length of individual regions of the welding zone depends on the initial metal properties determined by its production technology, and welding mode.

As shown by testing of standard samples for static tension and bending, as well as of large-scale samples and pipe segments, mechanical inhomogeneity, on the whole, does not have a negative impact on the strength and ductility of welded joints [6, 11]. In this case, a narrow section of the JZ with lowered mechanical properties is plastically deformed due to contact strengthening together with the adjacent sections of the thermomechanical strengthening zone. Unlike that, at determination of impact toughness by the standard procedure (KCV) development of the fracture process is localized within a narrow section of JZ metal, located between the regions of the thermomechanical strengthening zone with higher strength properties, due to high values of concentration ($\alpha_\sigma = 3.45$) and stress gradient. As a result, in connection with a small metal volume involved in the process of plastic deformation at impact, the energy consumption for sample fracture essentially decreases compared to homogeneous material [4, 5]. This is indicated by the shown in Figure 2, *a* fracture surface of such a sample without any noticeable side shrinkages and low value of impact toughness.

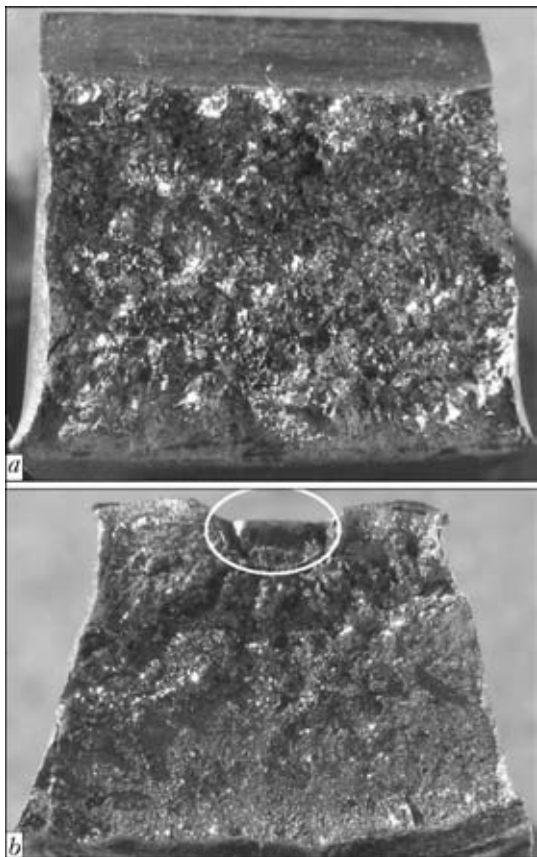


Figure 2. Fracture surface of impact samples of welded joints after their testing in as-welded condition with a standard mechanical notch, $KCV = 32 \text{ J/cm}^2$ (a) and without an artificial notch with structural inhomogeneity (marked by an oval), $KD = 161 \text{ J}$ (b)

At the same time, the nature of fracture of impact samples of flash-butt welded joints without artificial mechanical stress raiser in the JZ, but with the characteristic for flash-butt welding admissible defects differs in principle from the one described above.

Fractures of samples with such defects located at their surface had the form of a trapezoid, because of considerable shrinkage of their side faces (Figure 2, b) that essentially increased the energy consumption for fracture which is denoted as KD according to [5]. Results of testing impact samples of a standard size ($10 \times 10 \times 55 \text{ mm}$) without notches with structural inhomogeneity of various dimensions in the JZ by KD parameters turned out to be as follows: at $4.4 \times 2.5 \text{ mm} - 247.2 \text{ J}$; $4.0 \times 3.5 \text{ mm} - 261.6 \text{ J}$; $4.7 \times 2.0 \text{ mm} - 161.2 \text{ J}$, where the first value corresponds to the linear size of the defect on the impact sample surface, and the second value is the same, but in-depth of the sample.

Sections of structural inhomogeneity in the JZ located at some distance from the sample surface, practically do not affect the results of testing at impact loading. Such samples did not fail.

Thus, impact testing of standard samples with a sharp notch in JZ does not reproduce the pattern of deformation and fracture of a welded joint with admissible defects that may occur at flash-butt welding.

Values of fracture energy for samples with admissible defects (without an artificial notch) are much higher than those of samples from sound joints with a standard notch as a result of involvement of thermomechanical strengthening zone regions adjacent to JZ, into plastic deformation, which has a determinant role in the fracture process. This is indicative of the fact that impact toughness values of flash-butt welded joints with a sharp notch through the JZ are largely determined not by the properties of the joint metal, but by the stressed state induced in it. Thus, impact toughness values obtained on samples with a standard notch through the JZ, inadequately represent fracture resistance of a welded joint with admissible flash-butt welding defects, and, therefore, they cannot be a reliable characteristic of its fitness-for-purpose.

Proceeding from the above, an unambiguously positive reply can be given to one of the main questions: are the obtained values of KCV impact toughness of the metal of flash-butt welded joints in as-welded condition indeed sufficient to ensure reliable performance of pipelines under the conditions of service. It should be also taken into account that KCV values correlate with fracture mechanics characteristics (K_{1c}, δ_c). Their required level for prevention of welded joint fracture is directly related to the type and dimensions of the most probable defects, characteristic of the accepted welding process, including crack-like defects, the maximum dimensions of which are determined by the resolution of the used inspection techniques. Therefore, absence of hazardous defects in the metal of flash-butt welded joints guarantees their integrity at lower impact toughness values compared to the welding processes, in which cast metal forms in the welding zone. This is confirmed by many years of commercial operation of flash-butt welded pipelines.

Considering the known fact that «brittleness is not a property of a structural material and is determined not only by its structural state, but also by an essential influence of structural-technological factors ...» [12], in assessment of impact toughness of flash-butt welded joints it is important to create such a stress-strain state in the tested sample that the nature of its deformation and fracture corresponded to samples with admissible defects. Here, the main testing condition is ensuring simultaneous plastic deformation of the metal of JZ and thermomechanical strengthening zone. Such a task can be solved by reducing the depth of the mechanical notch down to zero (samples without an artificial stress raiser), changing their number and location in the welded joint.

In publications there is an example of localization of plastic deformation and fracture in the specified narrow volume of the tested impact sample by making two additional notches in the plane of location of the main notch on the side faces adjacent to it. Additional notches are similar to the main one in shape and size [13].



In [14], noting the practical absence of defects in flash-butt welded joints, it is proposed to lower stress concentration in standard *KCV* samples at the expense of reducing the notch depth. Testing conducted at PWI at the temperature of 20 and -20 °C of flash-butt welded joints on large-diameter pipes from steels of different strength grades, at different absolute values of notch depth h with radius $r = 0.25$ mm in standard samples, confirmed the potential of such an approach. With reduction of the depth of mechanical notch to $h = 1$ mm impact toughness values increase more than 2 times compared to a notch with $h = 2$ mm. Increase of the values occurs as a result of increase of the volume of metal involved in plastic deformation.

To determine the level of toughness properties of metal of flash-butt welded joints, it is necessary to eliminate JZ constraint by the adjacent large volumes of stronger metal of thermomechanically strengthened zone in the standard sample. With this purpose additional «straightening grooves» with geometrical parameters of the standard notch, located parallel to the notch through the JZ, were made in the high-hardness regions of thermomechanically strengthened zone.

Figure 3, *a* shows a schematic of making samples of flash-butt welded joints of 10 × 10 × 55 mm size with a standard notch through the JZ and two additional grooves. Such grooves are made in parallel to the notch through the JZ at distance $k = h$ (where k is the distance between the axes of the central and additional notches) on both sides from its center. In such a sample, in keeping with Neuber theory [15] stress concentration is mutually lowered, compared with one central notch, and practically equal conditions of plastic deformation of the metal of JZ and thermomechanically strengthened zone are created.

By analogy with accepted designations of impact energy and impact toughness, representing the concentrator type *KV*, *KCV*, we will introduce *K3V* and *KC3V* symbols for the proposed sample with three notches. Figure 4, *a* shows a typical nature of fracture in impact testing of samples with three notches from sound flash-butt welded joints, the characteristics of which meet the requirements of standards, and Figure 4, *b* shows defective joints, not meeting these requirements. Fracture energy of impact samples (with three notches 2 mm deep with 0.25 mm radius) of welded joints of pipe steel of X70 strength grade in as-welded condition, is as follows:

- in sound joints made in the optimal mode, at

$$T_{\text{test}} = 20 \text{ }^{\circ}\text{C} \quad K3V = \frac{114.6-254.3}{177} \text{ J}, \text{ at } T_{\text{test}} = -20 \text{ }^{\circ}\text{C}$$

$$K3V = \frac{112.8-214.4}{130} \text{ J};$$

- in defective joints made with mode violation (inadmissible defects found in fractures), at $T_{\text{test}} = 20 \text{ }^{\circ}\text{C}$ $K3V = \frac{4.8-21.0}{11.5} \text{ J}$. At testing of sound flash-butt welded joints it is established that the welding

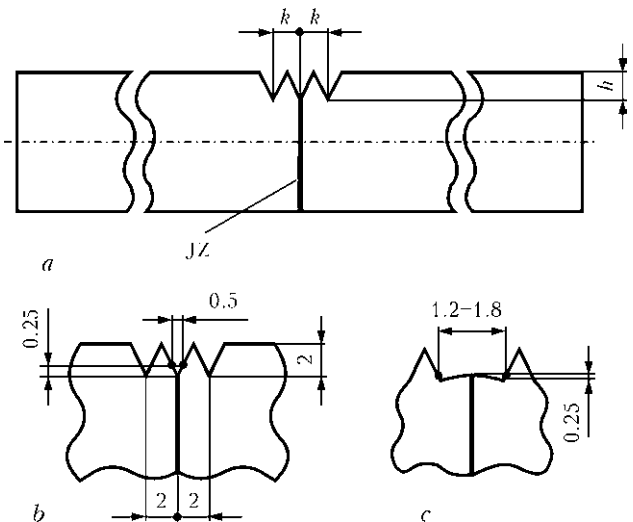


Figure 3. Schematic of *KC3V* impact sample: *a* — notch location; *b* — region of a sample with notches before testing; *c* — central notch after testing

zone, including JZ and thermomechanical strengthening zone, on the whole, has a high deformation ability, and, hence, high values of impact toughness. Here JZ was subjected to considerable plastic deformation at tension. While before testing the distance between the notch edges at its tip in accordance with its notch radius was equal to 0.5 mm ($2r = 2 \times 0.25$), after testing it increased 2.4–3.6 times (see Figure 3, *b* and *c*). These data are indicative of considerable ductility of JZ metal and its sufficiently high resistance not only to initiation, but also to propagation of cracks. In some samples micro- and macrocracks appeared at the bottom of the central notch through JZ (Figure 5), but they did not propagate any further. Final fracture of the sample in the shear mode was brought about by cracks initiating in the tips of the two side notches (see Figure 4, *a*).

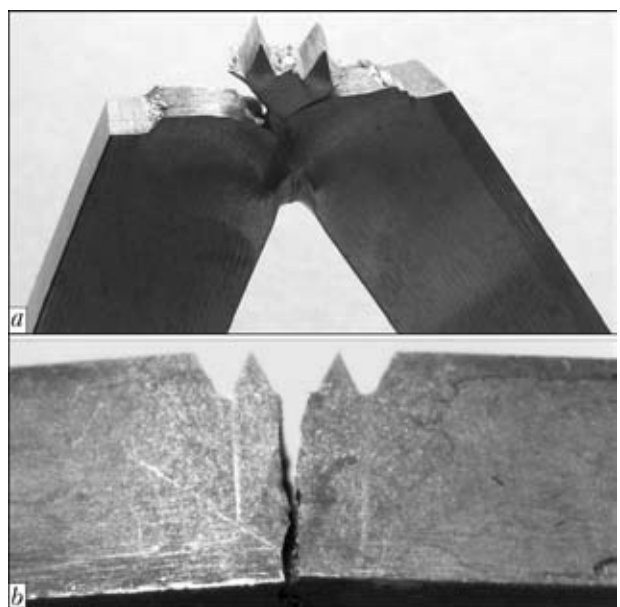


Figure 4. Typical nature of fracture of *KC3V* samples cut out of joints made in the optimum mode (sound joint) (*a*) and in modes with violation of the main parameters (defective joints) (*b*)

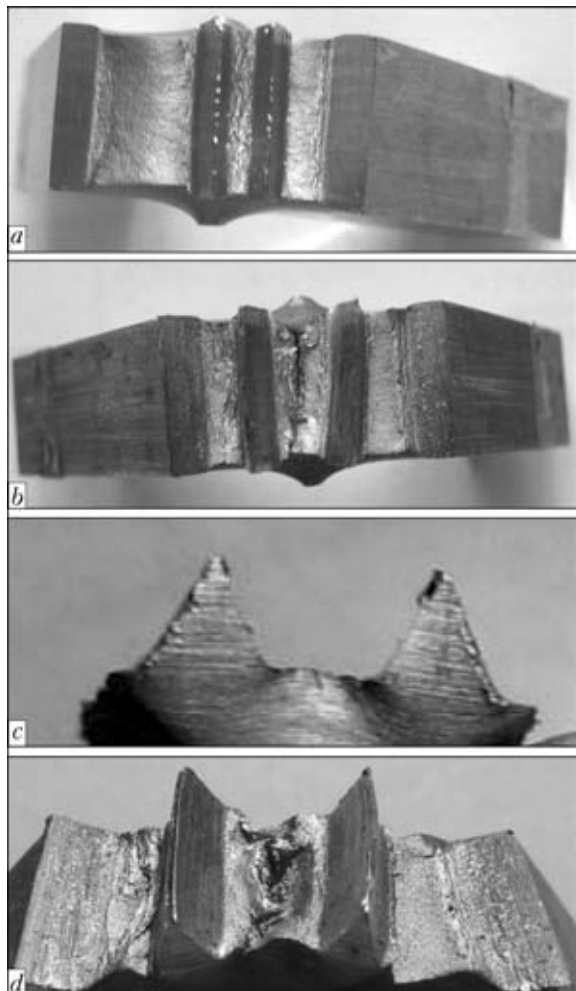


Figure 5. Nature of deformation of the zone of central notch of KC3V samples with micro- (a, c) and macrocracks (b, d); a, b – top view; c, d – side view

It is important that the proposed testing type allows revealing, alongside the NDT methods [16, 17], butt joints with inadmissible defects in the JZ. Such samples fail only through the central notch with low values of K3V fracture energy (see Figure 4, b).

At testing samples of a standard size with three notches from a sound joint of steel of strength grade X70 (samples from welded sectors of pipes supplied by Khartsyzsk plant, with impact toughness of pipe metal of more than 300 J/cm^2 at 20°C) in as-welded condition had the energy consumed in fracture (K3V) on average equal to 177 J at 20°C temperature, and to 130 J at -20°C . Standard impact samples (with one notch) of the same joints at 20°C temperature had KV of about 30 J, on average.

CONCLUSIONS

1. Values of impact toughness obtained on standard samples with a sharp notch KCV through JZ in as-

welded condition, do not represent the true fracture resistance of welded joints of pipes made by flash-butt welding, with the characteristic admissible defects. In this case, one of the factors determining KCV level, are not the properties of the welding zone metal proper, but its mechanical heterogeneity.

2. Conducted investigations with application of the procedure of impact testing of samples with three parallel notches changing the stress-strain state in the welding zone, showed that the metal of flash-butt welded joint, on the whole, and all its zones (JZ and thermomechanical strengthening zone) in as-welded condition have a sufficiently high resistance to impact loading.

3. Investigation results account for the confirmed by practical experience high operational reliability of welded pipelines. There is every ground to eliminate the requirements of application of postweld heat treatment of flash-butt welded joints, which is recommended to increase the impact toughness values.

1. SP 105-34-96: Guidelines. Performance of welding operations and quality control of welded joints. Introd. 01.10.96.
2. API STANDARD 1104: Welding of pipelines and related facilities. 19 ed., Sept. 1999.
3. Kuchuk-Yatsenko, S.I. (1992) *Flash-butt welding*. Kiev: Naukova Dumka.
4. Kuchuk-Yatsenko, S.I., Kirian, V.I., Kazymov, B.I. et al. (2006) On methodology for control of fitness-for-purpose of flash-butt welded joints in pipelines. *The Paton Welding J.*, **10**, 2–6.
5. Kuchuk-Yatsenko, S.I., Kirian, V.I., Kazymov, B.I. et al. (2008) Peculiarities of impact toughness tests of automatic flash-butt welded joints on pipes. *Ibid.*, **10**, 5–10.
6. Kuchuk-Yatsenko, S.I., Zhemchuzhnikov, G.V., Kazymov, B.I. et al. (1980) Influence of flash-butt welding defects on strength of joints at low temperatures. *Avtomatich. Svarka*, **12**, 1–3.
7. Kuchuk-Yatsenko, S.I., Lebedev, V.K. (1965) *Continuous flash-butt welding*. Kiev: Naukova Dumka.
8. Kuchuk-Yatsenko, S.I., Kazymov, B.I., Zagadarchuk, V.F. et al. (1984) Formation of mat spots in flash-butt welded joints. *Avtomatich. Svarka*, **11**, 23–26.
9. Paton, B.E., Lebedev, V.K., Kuchuk-Yatsenko, S.I. (1979) Complex «Sever-1» for flash-butt welding of position welds of large diameter pipes. *Ibid.*, **11**, 41–45.
10. Mazur, I.I., Serafin, O.M., Karpenko, M.P. (1989) Resistance welding of pipelines: ways of improvement. *Stroitelstvo Truboprovodov*, **4**, 8–11.
11. Kuchuk-Yatsenko, S.I., Lebedev, V.K. (1978) *Continuous flash-butt welding*. Kiev: Naukova Dumka.
12. Pisarenko, G.S., Novikov, N.V. (1970) About actual problems of investigation of carrying capacity of cryogenic pressure vessels. *Problemy Prochnosti*, **8**, 3–12.
13. Bakshi, O.A., Kukin, A.G., Monoshkov, A.N. (1970) Method of evaluation of reliability of materials and welded joints operating at low temperature conditions. *Ibid.*, **8**, 70–73.
14. Rakhmanov, A.S., Zandberg, A.S. (1985) Impact toughness as the criterion for evaluation of brittleness of joints made by resistance welding. *Stroitelstvo Truboprovodov*, **10**, 41–43.
15. Neuber, G. (1947) *Stress concentration*. Moscow: Gostekhizdat.
16. Troitsky, V.A., Radko, V.P., Yushchak, P.T. (1981) Ultrasonic control of quality of joints made by flash-butt welding. *Avtomatich. Svarka*, **4**, 38–40.
17. Kuchuk-Yatsenko, S.I., Radko, V.P., Kazymov, B.I. et al. (1996) Complex control of joints made by flash-butt welding. *Tekhnich. Diagnostika i Nerazrush. Kontrol*, **4**, 46–50.



SIMULATION OF ELECTRIC CIRCUIT AS A STAGE IN DEVELOPMENT OF POWER SOURCE WITH CONTROLLABLE SHAPE OF ALTERNATING CURRENT

V.V. ANDREEV, E.M. EFREMENKO and G.N. MOSKOVICH
E.O. Paton Electric Welding Institute, NASU, Kiev, Ukraine

The paper shows the effectiveness of simulation of electric circuit for power sources of alternating current of a controllable shape at evaluation of output power characteristics and methods of their regulation.

Key words: arc welding, power sources, alternating current, simulation, current of a controllable shape

Welding electrical equipment at present time is designed based on up-to-date element base allowing obtaining the characteristics of power supplies which provide increase of the quality of welded joints with simultaneous improvement of the economic factors. However, achievement of these goals is related with complication of hardware and functional constituents of developed equipment. It requires a development of special electric regulation systems, performance of complex mathematical calculations for selection of that or another elements of the electric circuit and construction of expensive physical models.

Such tasks can be solved with the help of modern packages for mathematic and simulation modelling [1] with a less labor content and higher efficiency. These packages were used during development of the

electric circuits for power supplies of alternating current of a controllable shape. Study [2] showed that control of the shape of direct and reversed polarity current is very perspective, since it allows performing alternating current MIG/MAG welding of high strength steels and aluminum preserving high indices of the mechanical properties of deposited metal. It was also noted that elimination of chemical elements is smaller in comparison with direct current welding.

Some circuits of investigated alternating current supplies are given below. In the first circuit, a diode bridge, consisting of $VD1$ - $VD4$ diodes with inductance $L1$ in its diagonal [4], is connected in series with secondary winding of transformer $T1$ instead of thyristor bridge [3] in contrast to existing developments. A regulator consisting of two thyristors of opposite-parallel connection $VS1$, $VS2$ and resistor $R1$ is connected to primary winding circuit of the transformer.

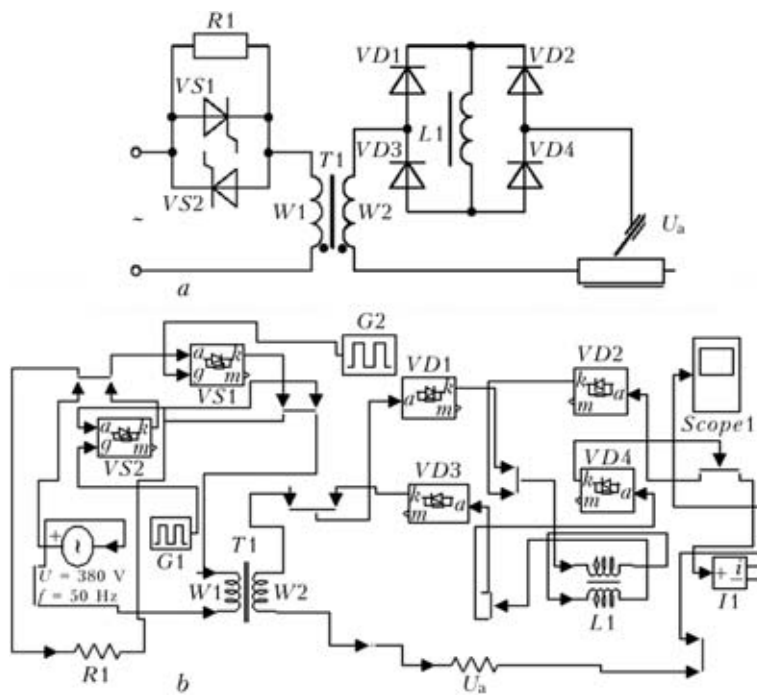


Figure 1. Electric circuit of the power source of alternating current of the controllable shape (a) and its simulation model with recording devices $I1$, $Scope1$ and pulse generator (b)

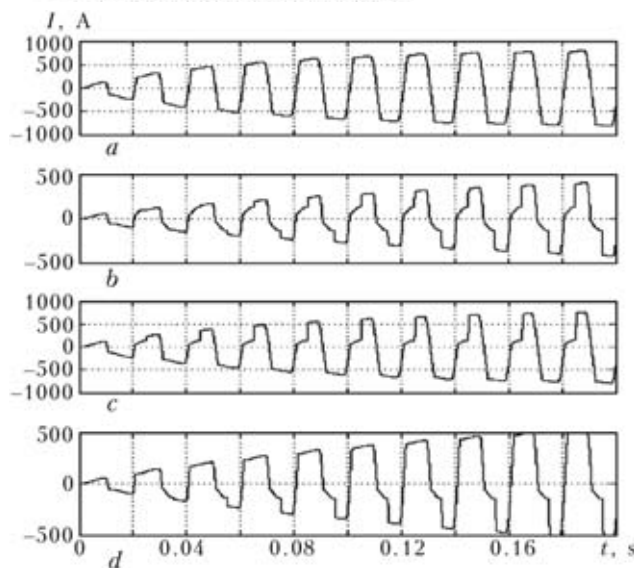


Figure 2. Oscillograms of load current of the power source (see Figure 1, *b*) obtained at different values of control pulse phases by thyristors VS1 and VS2: *a* – 0 and 0.010; *b* – 0.005 and 0.015; *c* – 0.005 and 0.010; *d* – 0 and 0.015 s

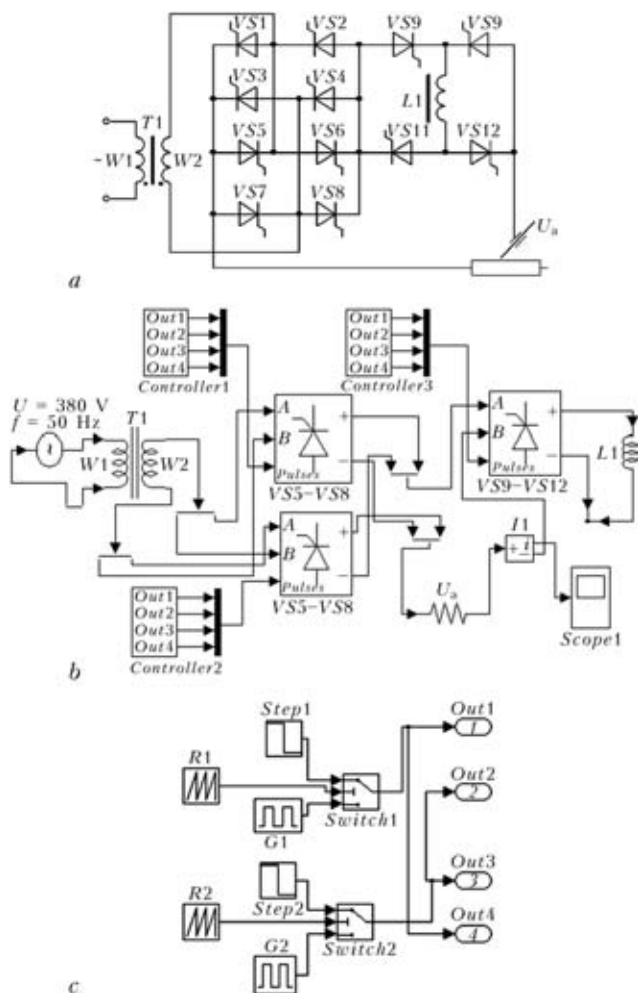


Figure 3. Electric circuit of the power source of balanced and unbalanced alternating current of low frequency (*a*) and simulation models of given power supply (*b*) and block of phase regulation Controller (*c*)

Here and in further circuits a load (arc) is represented by linear element, i.e. pure resistance.

Regulation of load current output is carried out on the primary circuit of a reducing transformer in which current is in several times lower than in the secondary circuit. Such an approach significantly widen power capabilities of power supply and allows applying it for arc welding as well as for electroslag technologies at current value of 10 kA and higher. At that the power supply has higher reliability and relatively small price. Pulse generators G1 and G2 for phase regulation by VS1 and VS2 thyristors, current meter I1 and oscilloscope Scope1 are used in the simulation model (see Figure 1, *b*), developed in MATLAB package. Such parameters as inductance of choke-accumulator L1, impedance of resistor R1, connection time of thyristors VS1, VS2 were varied in significantly wide ranges during simulation process for obtaining welding current of necessary shape and rate of its rise at polarity change. The oscillograms, given in Figure 2, showed the possibility of providing load current integrity and relatively high alternating rate as well as obtaining of different shapes of current of direct and reversed polarity in operation from the power supply (see Figure 1, *a*).

The second circuit (Figure 3, *a*) is a basis of power part of the source of balanced and unbalanced alternating current of low frequency [5]. Preliminary investigations of submerged-arc welding showed that reduction of frequency of welding current up to 12–16 Hz has positive effect on structure of deposited weld metal. Such welding is carried out from the power supply with a discrete regulation of current frequency and independent regulation of duration of its half cycles based on the thyristor regulator. It is built only on two bridge circuits which are switched to the secondary winding of power transformer [6]. This indicate a relationship between the welding current frequency, weld pool free oscillation frequency and technological indices of welding quality. However, presence of welding current ripple with 100 Hz frequency at two or more half cycles, forming that current, is characteristic for the electric circuit of such power supply. The third thyristor bridge VS9–VS12, having choke-accumulator L1 in its diagonal, is connected to output of double-bridge regulator VS1–VS4 and VS5–VS8 for reduction of current ripples. The regulation of frequency of welding current is performed similar to the scheme of work [6], namely, through development of positive and negative polarity pulses of determined duration and their modulation.

It should be noted that the duration of pulses of direct and reversed polarity current can be regulated independently in a wide range that significantly increases efficiency of modulation mode.

Simulation model of given power source, shown in Figure 3, *b*, contains three controllers Controller 1–3, designed for phase regulation of duration of direct

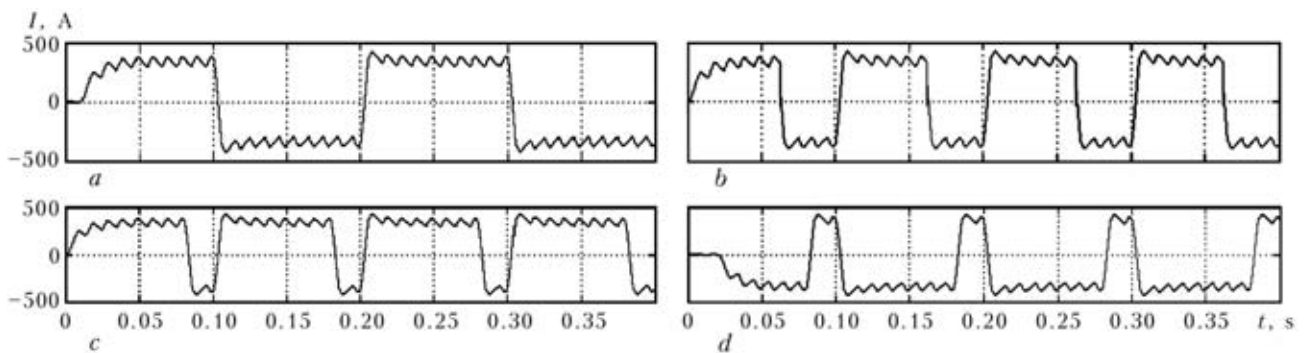


Figure 4. Oscillograms of balanced (*a*) and unbalanced (*b*) alternating current of low frequency obtained at different values of pulse duration of load current of reversed and direct polarity: *a* – 0.1 and 0.1; *b* – 0.08 and 0.02; *c* – 0.06 and 0.04; *d* – 0.02 and 0.08 s

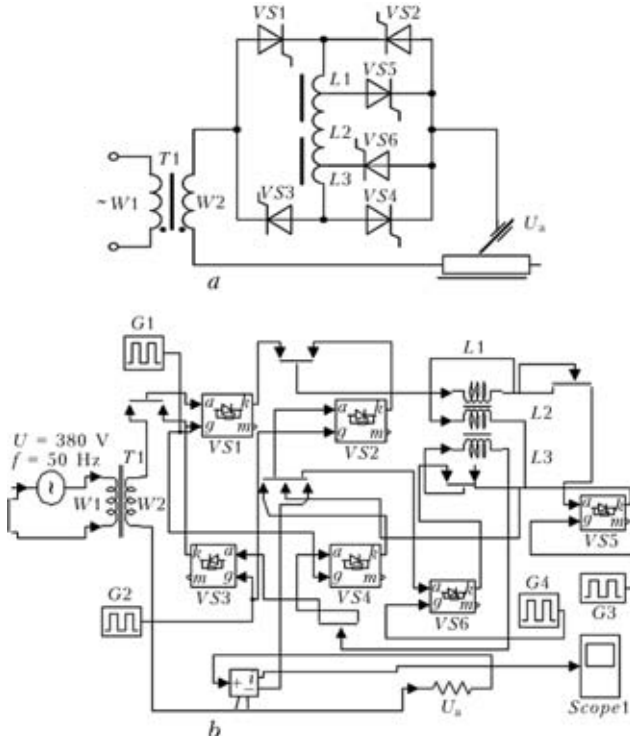


Figure 5. Electric circuit of the power source of alternating current of the controlled shape (*a*) and its simulation model with recording devices developed in MATLAB package medium (*b*)

and reversed polarity current, as well as device for current measurement I_1 and oscillograph $Scope1$ besides three thyristor rectifying bridges $VS1-VS4$, $VS5-VS8$, $VS9-VS12$ as in the basic electric circuit. The outputs $Out1-Out4$ of each controller (see Figure 3, *c*) are connected to controlling electrodes gates of thyristors *Pulses* of corresponding rectifying bridges. The regulation of duration of pulses of direct and reversed polarity current is carried out using given model, consisting of a generator of different shape signals *Step*, *R*, *G* and controlled switch of signals *Switch*. The oscillograms of load current, representing work of power supply in balanced and unbalanced modes, are shown in Figure 4.

The next example considers one of the variants of the power supply of alternating current of the controllable shape. The electric circuit of the power supply [7] and its model are shown in Figure 5. In this scheme two thyristors $VS5$ and $VS6$, linked to each

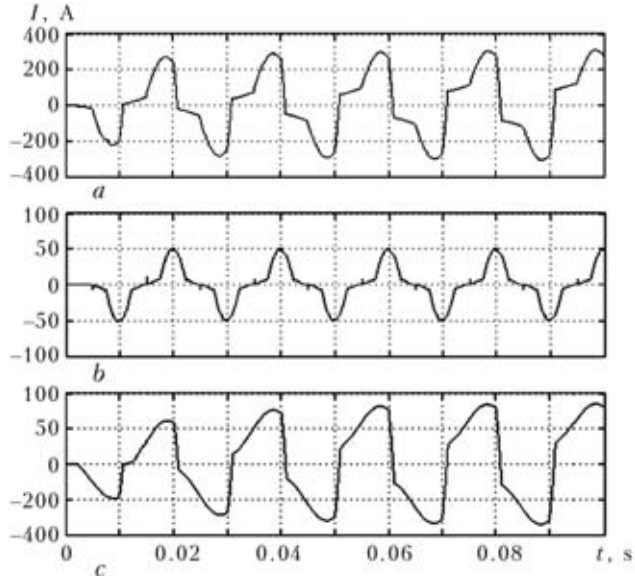


Figure 6. Oscillograms of load current of the controlled shape (see Figure 5, *b*) at different values of turn-on time of thyristors $VS1-VS4$, $VS5$ and $VS6$: *a* – 0–0.01, 0.05 and 0.0015, *b* – 0.005–0.015, 0.0075 and 0.0175; *c* – 0.0025–0.0125, 0.005 and 0.015 s

other, are additionally connected to the output of the bridge by alternating current and part of choke winding together with transformer $T1$, thyristor bridge $VS1-VS4$ and choke $L1$ on its diagonal. This solution allowed controlling the values and shape of principal current, including rectangular one, as well as shape of the pulse which is superimposed on the principle current (Figure 6) using pulse generator $G1-G4$. Such a combined power supply increases performance of the whole system at transition processes that has significant importance in submerged-arc welding where a lag of power supply is the reason for oscillation of mode parameters of welding process.

Therefore, the simulation during development of welding power supplies allows evaluating the capabilities of different circuits, various ways of regulation of power parameters and perspective of practical application, except for physical modelling.

1. Diakonov, V.P. (2005) *MATLAB 6/5 SP1/7/0 Simulink 5/6. Principles of application*. Library of Professional Series. Moscow: SOLOMON-Press.
2. Maxl, G., Posch, G. (2008) MAG-Wechselstromschweißen von hochfesten Feinkornbaustählen. *Schweiss- und Prüftechnik*, 3, 35–38.



3. Zaks, M.I., Kagansky, B.A., Pechenin, A.A. (1988) *Transformers for electric arc welding*. Leningrad: Energoatomizdat.
4. Andreev, V.V., Efremenko, O.M., Zaruba, I.I. *AC power source of controllable shape for arc and slag technologies*. Pat. 47333 Ukraine. Int. Cl. B 23 K 9/10, 9/00. Publ. 25.01.2010.
5. Andreev, V.V., Moskovich, G.N., Zhernosekov, A.M. et al. (2008) Specifics of low-frequency AC arc welding. *Svarshchik*, 6, 19–21.
6. Lebedev, V.K., Andreev, V.V., Moskovich, G.N. *Arc welding power source*. USSR author's cert. 1542721. Int. Cl. B 23 K 9/00, 9/10. Publ. 15.02.90.
7. Paton, B.E., Lebedev, V.K., Zaruba, I.I. et al. *Arc welding power source*. USSR author's cert. 1294523. Int. Cl. B 23 K 9/00. Publ. 07.03.87.

DEVELOPMENT OF METHODS OF ADAPTIVE CONTROL AND IMPORT REPLACING EQUIPMENT OF THE ORBITAL COMPLEXES FOR AUTOMATIC TIG WELDING OF POSITION JOINTS OF 89–219 MM DIAMETER PIPELINES DURING CONSTRUCTION AND REPAIR OF REACTORS OF NUCLEAR POWER PLANTS OF UKRAINE

(Innovation project of the NAS of Ukraine,
realized in the E.O. Paton Electric Welding Institute)

Obtaining of the reliable data on arc current and voltage signals is very important during automatization of the processes of orbital arc welding (OAW). It is a well-known fact that OAW automatic machines operate under conditions of high level of electromagnetic fields which result in significant «noise» of signals in measurement and control channels. Different methods of increase of their stability are to be used for improving the quality of monitoring system. In the scope of this work it was proposed to use a method of wavelet transform for processing of initial sensor signals. In this case, reconstruction of measuring signals allows significantly improving a signal-to-noise ratio and thereby increasing quality of the OAW process control. The wavelet transform of time sequence of current and voltage signals lies in their decomposition according to base of determined functions with the help of scaling and transfer.

The wavelet transform provides a two-dimensional representation of signal in contrast to the Fourier transform. At that its frequency and time are the independent variables, i.e. there is a possibility to analyze the properties of the process in time as well as frequency areas. The task of optimum selection of the wavelet is not solved at present time. Therefore, the researchers are to solve it by means of selection of different variants of the mother wavelets. Haar, Morlet and Daubechies wavelets were used in solving the task of selection. The Daubechies wavelets of the 5th order provide the best metrological indecies as it was shown by solving the model problems using MATLAB package.

Welded tubular elements are widely used in manufacture of the reactors of nuclear power plants. One of the main factors, determining their reliability and serviceability, are the residual stresses (RS), originating in pipes during welding. It is considered that stresses on the base of their determination are to be constant and area of controllable surface of the object is flat during determination of the RS in welded elements using experimental methods. It was experimentally determined that a surface curvature in which the RS are investigated influences on an error during their determination. Therefore, a numerical experiment using finite-element method was made for evaluation of influence of the surface curvature on the error of determination of the RS. The results of numerical experiment and their analysis showed that the errors of RS calculation technique do not exceed 8 % in a pipe of 89 mm diameter.



EXPERIMENTAL EVALUATION OF δ_{1c} -CURVE TEMPERATURE SHIFT AND BRITTLE-TOUGH TRANSITION OF STRUCTURAL STEELS AND WELDED JOINTS BY THE RESULTS OF STANDARD TESTS

V.P. DYADIN and L.Ya. YURKO

E.O. Paton Electric Welding Institute, NASU, Kiev, Ukraine

Investigation results are given on fracture toughness based on the deformation criterion for the most common domestic low-alloy structural steels of different thicknesses. An approach to evaluation of the brittle-tough transition temperature depending on the thickness of the investigated rolled metal is suggested. Shift of the basic deformation δ_{1c} -curve depending on the thickness of the rolled metal and its standard strength characteristics was experimentally verified.

Keywords: structural steels, welded joints, impact toughness, Charpy specimen, crack resistance characteristics, plane deformation, metal thickness, temperature shift, brittle-tough transition

Conventional criteria of transition from the plane stressed state to plane strain are insufficiently studied and require an experimental confirmation. The approach suggested in study [1] to possible evaluation of temperature shift for deformation criterion δ_{1c} depending on the specimen thickness is not an exception either, and requires an experimental verification as well.

Study [1] suggested that the lower temperature bound, where it is possible to make some changes when using the deformation criterion of fracture mechanics, should be limited by temperature $T_{28 J}$, at which the Charpy impact specimen fracture energy is 28 J at the lower bound of scatter. This limitation is of a certain interest, as it allows comparing temperature shifts both by the load and deformation criteria of fracture mechanics relative to a single point corresponding to $T_{28 J}$ for standard Charpy impact specimens.

Below we give results of experimental studies of metal of the welded joints on the most common low-alloy structural steels. The temperature shift of the deformation δ_{1c} -curve was determined according to study [1].

Fracture toughness of weld metal. Consider investigation results on the characteristic of crack resistance δ_c (δ_{1c}) of the weld metal made with electrodes of the ANO-TM grade (base metal 09G2S, thickness $t = 40$ mm).

The weld was made in several passes into the X-groove, after which the resulting welded joint was cut normal to the weld axis into pieces to make the following test specimens:

- three-point test specimens according to GOST 25.506-85 (type 4) to determine deformation characteristic δ_c (δ_{1c});

- impact bend test specimens (Charpy specimens) according to GOST 9454-78 (type 9);
- tensile test specimens according to GOST 6996-66 (type 2).

Specimens for evaluation of characteristic δ_c and for impact bend tests, having thickness of 35 mm, were made with a notch oriented along the weld axis, normal to the plate plane. Crack opening displacement δ_c was determined in compliance with MP-170-85.

According to [1, 2], crack resistance characteristic δ_{1c} under the plane strain conditions was determined from the results of standard mechanical tests:

$$\delta_{1c} = 0.5A\alpha_v/\sigma_{0.2}, \quad (1)$$

where α_v is the impact toughness of the Charpy specimens (KCV) at the corresponding test temperatures, J/cm^2 ; A is the correlation coefficient (in the given case, $A = 0.1$ for low-alloy and low-carbon steels); and $\sigma_{0.2}$ is the yield stress of the material, MPa.

The specimens were cooled with liquid nitrogen in a petrol bath. Temperature of the specimens during the tests was monitored by using a thermocouple.

Mechanical properties of the weld metal made with electrodes ANO-TM at $T_{test} = +20$ (-60) °C were as follows: $\sigma_t = 569$ (598) MPa, $\sigma_{0.2} = 428$ (455) MPa, $\delta = 30.7$ (30) %, and $\psi = 67.7$ (67) %.

The test results for the weld metal are presented in Table 1 and in Figures 1-3.

Fracture of the specimens was of a brittle and quasi-brittle character over the entire temperature range used to investigate toughness characteristic δ_c . Brittle fracture of the specimens until reaching the general yield was observed at a temperature down to -20 °C. At a temperature of -15 °C, fracture of a specimen took place at the point of reaching the general yield of the material beneath the notch. At the same time, no marked stable crack growth was fixed, as can be well seen in Figure 2.

Evaluation of characteristic δ_c at room temperature and analysis of the specimen fracture surfaces showed

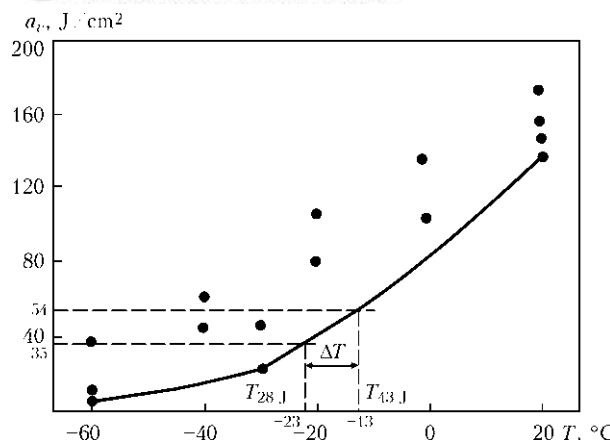


Figure 1. Temperature dependence of impact toughness (minimal values) of weld metal made by using electrodes ANO-TM (ΔT – value of temperature shift from formula (6))

an insignificant stable crack growth to a depth of about 0.4–0.6 mm, which was followed by an unstable crack growth by the quasi-brittle mechanism (see Figure 2). No drop of a load during the stable crack growth was fixed in the loading diagrams.

To plot the theoretical curve shown in Figure 3, we use the minimal values of specific impact toughness of the Charpy specimens from the studied welded joint for determination of the temperature shift of basic curve δ_{lc} . Then we find a temperature corresponding to a value of 35 J/cm² in the curve (in this case, it was -23 °C) (see Figure 1). And, by using linear extrapolation, we determine yield stress $\sigma_{0.2}$ and tensile strength σ_t of the welded joint corresponding to this temperature (441 and 583 MPa, respectively).

By involving the relationship from study [3] between the calculated value of strain hardening n^c and strength characteristics $\sigma_{0.2}$ and σ_t of the material

$$n^c = -0.18 + 0.22\sigma_t/\sigma_{0.2}, \quad (2)$$

we find the calculated value of n^c at a temperature of -23 °C ($n^c = 0.11$).

If strain ε_t at the point of a loss of plastic stability of the material is known [4], the value of strain hardening n can be calculated more precisely from the following formula:

$$n = \varepsilon_t/(1 + \varepsilon_t). \quad (3)$$



Figure 2. Fracture surface of specimens tested to three-point bending at different temperatures

Table 1. Crack resistance characteristics δ_c of the weld made with electrodes ANO-TM at three-point bending of 35 mm thick specimen

T_{test} , °C	δ_c , mm	Probable stable growth of crack, mm
-60	0.024	–
-36	0.044	–
-23	0.078	–
-15	0.139	–
+20	0.266	Up to 0.4
+20	0.323	Up to 0.6

According to studies [1, 5], the value of characteristic δ_c is expressed in terms of a function of n , β , α and δ_{lc} :

$$\delta_c = f(\beta(t))\delta_{lc}, \quad (4)$$

where $f(\beta(t))$ at $t > 10$ mm can be determined from the following expression:

$$f(\beta(t)) = \left(\frac{2}{\sqrt{3}} \right)^{\frac{n+1}{n}} \times \\ \times \left[1 - \alpha + \alpha^2 + \frac{(1 - 10.24/(t + 5.24))(1 + \alpha)}{2} \times \right. \\ \times \left. \left\{ \frac{(1 - 10.24/(t + 5.24))(1 + \alpha)}{2} - \alpha - 1 \right\} \frac{1-n}{2n} \times \right. \\ \times \left. \left\{ 1 - \frac{(1 - 10.24/(t + 5.24))(1 + \alpha) + 2\alpha}{4} \right\} / (1 - \alpha)^{1/n}. \right] \quad (5)$$

To simplify, take a mean value of $\alpha = 0.3$ [1, 6] for the given welded joint with $f(\beta(t))$ at a temperature of -23 °C.

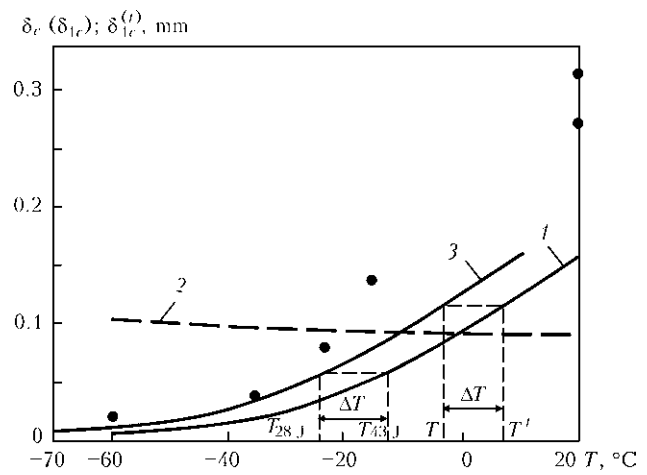


Figure 3. Temperature dependence of crack resistance characteristics of metal: 1 – theoretical curve δ_{lc} calculated from formula (1); 2 – condition from formula (9); 3 – theoretical curve $\delta_{lc}^{(t)}$ at $\Delta T = 10$ °C calculated from formula (7); points – experimental values of δ_c

Given that with the specific fracture energy of the Charpy specimens equal to 35 J/cm^2 the temperature is only -23°C , a change in yield stress of the studied welded joint is insignificant and, therefore, can be ignored. In this case, based on study [1], the link between temperature shift ΔT and basic deformation curve δ_{lc} can be expressed by the following dependence:

$$a_v^{T_{28J} + \Delta T} \approx a_v^{T_{28J}} f(\beta(t)) = 54 \text{ J/cm}^2. \quad (6)$$

The corresponding value of impact toughness is shown in Figure 1. It can be seen from the Figure that the value of impact toughness of the Charpy specimen equal to 54 J/cm^2 corresponds to a temperature of -13°C . Therefore, temperature shift ΔT is 10°C .

By using the approach suggested in study [1], it is possible to find theoretical deformation curve $\delta_{lc}^{(t)}$ shown in Figure 3 by shifting basic dependence (1) to a value of ΔT :

$$\delta_{lc}^{(t)} = 0.5 A a_v^{(t)} / \sigma_{0.2}^{(t)}, \quad (7)$$

where $\delta_{lc}^{(t)}$ is the corrected characteristic of fracture toughness δ_{lc} on a condition of a through crack propagating in a structural element with thickness t and temperature T ; $a_v^{(t)}$ is the impact toughness of the Charpy specimen corresponding to corrected temperature T^t allowing for thickness $T^t = T + \Delta T$; and $\sigma_{0.2}^{(t)}$ is the yield stress at corrected temperature T^t .

As seen from Figure 3, calculated curve $\delta_{lc}^{(t)}$ describes well enough the experimental values of δ_c .

It should be noted that the test temperature of impact specimens equal to $+20^\circ\text{C}$ does not yet provides the upper values of specific fracture energy a_v^{\max} in the tough state along the lower bound of scatter. This makes evaluation of characteristic δ_i (critical crack opening displacement at the moment of initiation of fracture in the tough state) from the results of the impact tests somewhat difficult. At the same time, an insignificant stable tough growth of a crack to a depth of about 0.4–0.6 mm, as well as achieving the general yield state of the material beneath a notch were fixed in determination of characteristic δ_c at room temperature and analysis of specimen fracture surfaces. Therefore, the value of δ_i in the general yield state beneath the notch can be evaluated allowing for this fact and for the following dependence from study [2]:

$$\delta_c = \delta_i + \Delta l \frac{\sigma_t}{\sigma_{0.2}} \frac{n}{(1-n)^2}, \quad (8)$$

where Δl is the value of the stable crack growth.

It follows from expressions (1) and (8), as well as from the data of Table 1 that $\delta_i \approx 0.2 \text{ mm}$.

Then, allowing for dependence (1), the value of the specific fracture energy in the tough state can be easily found from the lower bound of the scatter ($a_v^{\max} = 170 \text{ J/cm}^2$).

At the same time, when using the non-linear fracture mechanics approaches for qualification of welded joints on a number of critical structures (deepwater off-shore stationary platforms, main pipelines, etc.), first of all it is necessary to eliminate the probability of brittle fracture of structural elements having a defect in a region of nominal elastic strains.

Thus, according to the requirements [7] worked out in collaboration with CRISM «Prometey» for metal of the welded joints on the most critical and heavily-loaded structural elements, the value of critical crack opening displacement should meet the following condition:

$$\delta_c \geq 1.35 t \frac{\sigma_{0.2}}{E}, \quad (9)$$

where E is the elasticity modulus of the material, MPa; and $\sigma_{0.2}$ is the proof stress of this material, MPa.

This level at $\sigma_{0.2} = 360\text{--}450 \text{ MPa}$ is close to the requirements of the Canadian standard [6], as well as standards DNV and API for steels used in underwater and ground-surface pipelines [8].

By assuming that $\delta_c = \delta_{lc}^{(t)}$, condition (9) can be presented in the following form:

$$\delta_{lc}^{(t)} \geq 1.35 t \frac{\sigma_{0.2}}{E}. \quad (10)$$

As seen from Figure 3, the point of intersection of curves 2 and 3 almost coincides with the brittle-tough transition temperature, where the stable crack growth begins.

Allowing for dependence (7) and proceeding from expression (10), the requirement to impact toughness depending on the thickness of a structural element and yield stress of the material in this case can be written down as follows:

$$a_v^{(t)} \geq 0.27 t \frac{\sigma_{0.2} \sigma_{0.2}^{(t)}}{EA}, \quad (11)$$

where yield stresses $\sigma_{0.2}$ and $\sigma_{0.2}^{(t)}$, and elasticity modulus E are expressed in megapascals, and thickness t is expressed in millimeters in order to preserve dimensions and match formulae (7) and (10).

At low values of temperature shift ΔT , it can be assumed in the first approximation that $\sigma_{0.2} \approx \sigma_{0.2}^{(t)}$. Then expression (11) will have the following form:

$$a_v^{(t)} \geq 0.27 t \frac{\sigma_{0.2}^2}{EA}. \quad (11a)$$

Relationship (11a) between the values of impact toughness, thickness and standard strength properties differs substantially from the dependence given in study [8]

$$a_v [\text{J/cm}^2] \geq 0.125 \sigma_{0.2} [\text{MPa}]. \quad (12)$$

**Table 2.** Mechanical properties of welded joint ($T = 20^\circ\text{C}$)

Material	$\sigma_{0.2}$, MPa	σ_t , MPa	n^c acc. to (2)	δ , %	ψ , %
Base metal	407–424 415	585–592 588	0.13	23.6–24.6 24.3	67.9–69.8 69.1
Weld metal	416–450 433	540–561 550	0.10	23.6–24.6 24.3	66.0–67.9 66.9

It can be seen from expression (11a) that the requirement to impact toughness should be directly proportional to the square of yield stress of the material and thickness of the structural element, in contrast to the linear dependence from formula (12).

To illustrate, Figure 4 shows a three-dimensional plot of the required value of impact toughness $a_v^{(t)}$ depending on the thickness of the structural element and yield stress of the investigated welded joint made with electrodes ANO-TM in the brittle-tough transition range.

Fracture toughness of heat-affected zone of welded joint. To minimise heterogeneity of the welded joint and decrease error in evaluation of strength properties of the HAZ metal, mechanical properties of the weld metal were chosen to be close to those of the base metal. For this purpose, and to provide a straighter embrittlement zone parallel to the plate thickness, the welded joint was made with the K-groove by using electrodes UONI-13/55, the base metal being 25 mm thick steel 10KhSND.

Mechanical properties of the weld and base metals are given in Table 2.

Investigation results on evaluation of the characteristic of fracture toughness δ_c and value of impact toughness a_v within the studied temperature range are presented in Table 3 and in Figures 5 and 6.

It should be noted that the given investigation results characterise crack resistance of the welded joint

in the HAZ metal only at a distance of 1 mm from the fusion line.

Like for the weld, the temperature corresponding to a value of 35 J/cm^2 (-25°C in this case) is found from the minimal temperature curve of impact toughness shown in Figure 5.

We take values corresponding to the mean values of the base metal and weld equal to 424 and 569 MPa, respectively, as yield stress $\sigma_{0.2}$ and tensile strength σ_t in HAZ.

Using formulae (2) and (5), we determine values of n^c and $f(\beta)$ ($n^c = 0.115$; $f(\beta) = 2.02$). Then, according to expression (6), $a_v^{T_{28J} + \Delta T} \approx 70 \text{ J/cm}^2$.

As seen in the curve in Figure 5, the value of impact toughness of the Charpy specimen equal to 70 J/cm^2 corresponds to a temperature of -5°C . Therefore, temperature shift ΔT is 20°C .

In turn, this allows deformation curve δ_{1c} shown in Figure 6 to be shifted to the same value. Curve 1 in Figure 6 was plotted by using the minimal experimental values of impact toughness of the Charpy specimens from the investigated zone of the welded joint.

Calculated theoretical deformation curve $\delta_{1c}^{(t)}$ corresponding to a temperature shift of 20°C is shown in Figure 6. As seen from the Figure, the obtained point of intersection of curves 2 and 3 almost coincides with the brittle-tough transition temperature, where the stable crack growth begins.

Fracture toughness of low-alloy structural steels.

Consider investigation results on fracture characteristics δ_c (δ_{1c}) in the plane of rolled structural steels 09G2S, 10KhSND and 14G2AF.

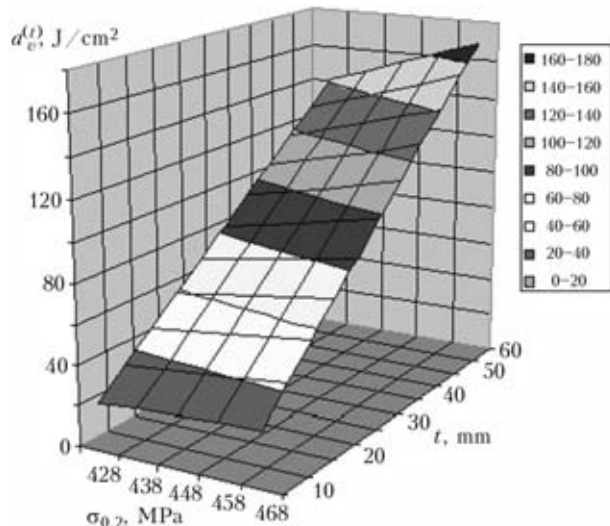


Figure 4. Values of impact toughness from formula (11a) for the welded joint made with electrodes ANO-TM in the brittle-tough transition range depending on thickness of a structural element and its strength properties

Table 3. Characteristics of crack resistance δ_c and impact toughness of welded joint in the HAZ metal on the three-point bend test specimen 25 mm thick

T_{test} , $^\circ\text{C}$	δ_c , mm	δ_c^{\max} , mm	$f(\beta(t))$ acc. to (5)	a_v , J/cm^2
+20	—	—	2.02	122; 120; 130
-25	0.245	—	—	—
-25	—	0.670	—	—
-30	—	—	—	27; 31; 32
-40	0.045	—	—	—
-55	0.100	—	—	—
-60	0.065	—	—	16; 22; 27

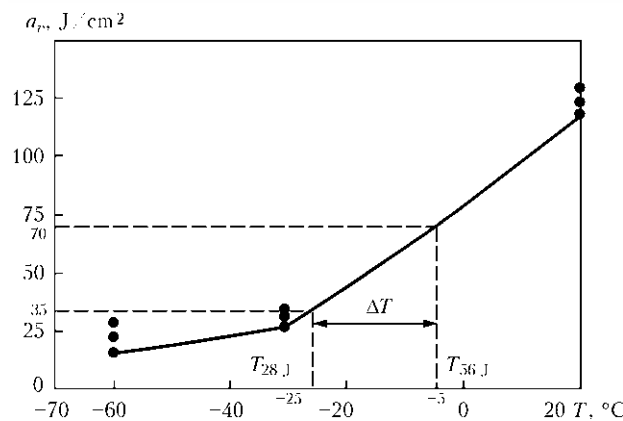


Figure 5. Temperature dependence of impact toughness of the near-weld zone: points — experimental values (the curve was plotted using the minimal experimental values)

Mechanical properties and strain hardening factor n^c calculated from formula (2) for the investigated structural steels in the rolling plane are given in Table 4.

Chemical composition of the investigated steels is given in Table 5.

To determine crack resistance characteristics and impact toughness values of steel 10KhSND in rolling plane (with plate thicknesses of 40 and 25 mm), the 37 and 25 mm thick specimens were made for evaluation of characteristic δ_c according to the recommen-

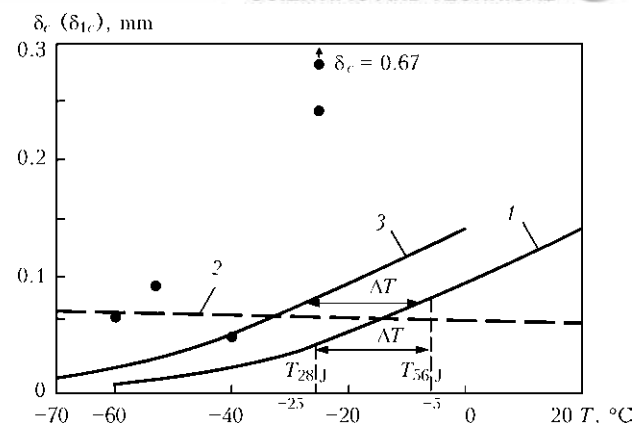


Figure 6. Temperature dependence of crack resistance characteristics: 1 — theoretical curve δ_{lc} calculated from formula (1); 2 — condition from formula (10); 3 — theoretical deformation curve $\delta_{lc}^{(t)}$ at $\Delta T = 20^\circ\text{C}$ calculated from formula (7); points — experimental values of δ_c

dations of GOST 25.506-85 (type 4). Similarly, for evaluation of characteristic δ_c of structural steels 09G2S, 09G2S-Sh and 14G2AF, the 19, 70 and 36 mm thick specimens, respectively, were made from them. The Charpy specimens for the above materials were cut from the central part of the rolled metal through thickness with a notch oriented in the same direction as for evaluation of characteristic δ_c .

Table 4. Mechanical properties and strain hardening factor n^c of structural steels

Steel grade	t , mm	T_{test} , °C	σ_y , MPa	σ_t , MPa	n^c	δ , %	ψ , %
10KhSND	25	+20	353.4	<u>523–530</u> 526	0.147	<u>32.7–33.0</u> 32.6	67.9
		-30	422.7	<u>627–630</u> 526	0.147	<u>33.7–36.6</u> 35.1	73.3
		-60	<u>453.5–488.2</u> 470.8	<u>633–682</u> 668	0.133	<u>28.7–36.6</u> 31.6	<u>67.9–71.6</u> 69.7
	37	+20	350.0	<u>544–551</u> 545	0.162	32.0	75.0
		-30	<u>346.5–381.6</u> 363.8	<u>561–566</u> 564	0.161	<u>30.0–36.0</u> 33.6	72.0
		-60	380.2	590	0.161	<u>32.3–34.0</u> 33.0	<u>71.6–73.3</u> 72.0
09G2S	19	+20	<u>294.8–315.6</u> 306.1	<u>503–517</u> 508	0.185	<u>36.6–38.6</u> 37.4	78.2
		-30	<u>336.1–329.1</u> 332.6	<u>544–551</u> 547	0.182	38.3	78.2
		-60	<u>347.0–353.4</u> 350.2	589	0.190	40.0	75.0
09G2S-Sh	70	+20	275.0	450	0.180	39.1	
		-60	332.0	530	0.171	40.0	
		-70	384.0	556	0.139	39.0	
14G2AF	40	+20	<u>400.0–415.0</u> 406.0	<u>576–586</u> 581	0.135	<u>32.0–33.3</u> 32.6	<u>67.2–67.7</u> 67.5
		-60	430.0	612	0.133	32.0	67.0

**Table 5.** Actual chemical composition of investigated structural steels, wt.-%

Steel grade	Specimen thickness, mm	C	Mn	Si	Ni	Cu	S	P	Cr
10KhSND	25	0.079	0.73	0.944	0.61	0.40	0.027	0.022	0.74
10KhSND	37	0.073	0.55	0.844	0.59	0.42	0.023	0.014	0.73
09G2S	19	0.050	1.13	0.670	0.02	0.05	0.045	0.017	0.10
14G2AF	40	0.200	1.67	0.458	0.09	0.35	0.036	0.030	0.17

Table 6. Results of three-point bend tests of Charpy specimens (orientation of specimens — across the rolling direction)

Steel grade	<i>t</i> , mm	<i>T</i> _{test} , °C	<i>a_v</i> , J/cm ²	<i>a_v^{max}</i> , J/cm ²	ΔT , °C
10KhSND	25	+20	82; 80; 68	82	24
		0	63; 59		
		-30	30; 28; 26		
		-60	21; 18		
10KhSND	37	+20	210; 192; 181	210	17
		0	175; 150; 131		
		-20	106; 85; 78		
		-40	72; 58; 51		
		-60	52; 47; 35		
09G2S	19	+20	315; 198; 196	315	20
		-20	155; 87; 75		
		-40	92; 55; 52		
		-60	72; 14; 7		
		-70	22; 16; 15		
09G2S-Sh	70	+20	>375	>375	1
		0	>375		
		-20	>375		
		-30	>375; 300; 314		
		-40	234; 285; 282		
14G2AF	36	-60	212; 207; 229	256	6
		-80	20; 15; 9		
		+20	256; 256		
		0	205; 196; 161		
		-40	150; 97; 92		
		-70	61; 51; 15		

Table 7. Results of evaluation of crack resistance characteristics δ_c (δ_{1c})

Steel grade	t , mm	$f(\beta)$ acc. to (5)	T_{28J} , °C	$a_c^{T_{28J} + \Delta T}$, J/cm ²	T_{test} , °C	δ_c (δ_{1c}), mm
10KhSND	25	1.73	-22	60	-20	0.365
					-40	0.040
					-53	0.115
					-60	0.038
10KhSND	37	1.36	-60	48	-25	0.227
					-40	0.099
					-60	0.117
09G2S	19	1.90	-48	66	+20	(0.500)
					+20	(0.480)
					+20	(0.480)
					-37	0.475
					-40	0.515
					-40	0.545
					-51	0.305
					-53	0.190
					-60	0.125
					-63	0.480
					-63	0.510
					-67	0.085
					-75	0.202
09G2S-Sh	70	1.16	-77	40	-65	0.950
					-73	0.373
					-74	0.133
					-75	0.202
14G2AF	36	1.44	-62	50	+20	(0.305)
					-40	0.300
					-53	0.190

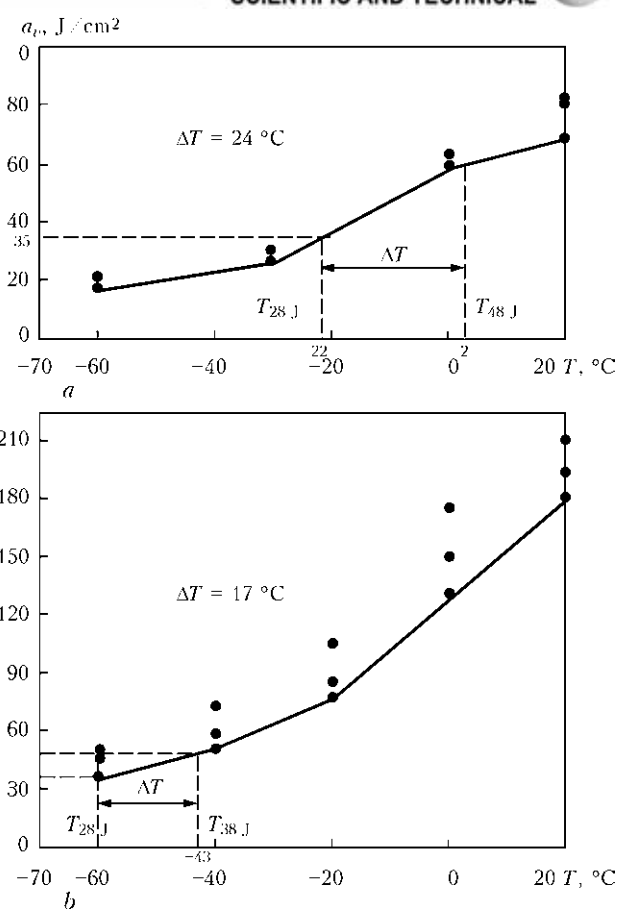


Figure 7. Temperature dependence of impact toughness of rolled steel 10KhSND 25 (a) and 37 (b) mm thick (see designations in Figure 5)

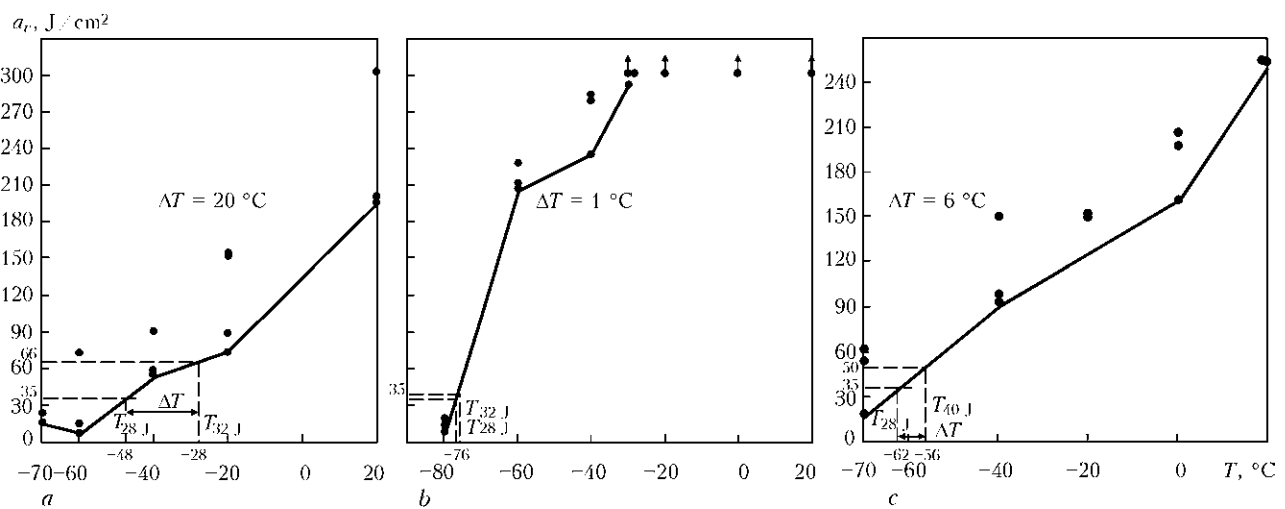


Figure 8. Temperature dependencies of impact toughness of 19 mm thick rolled steel 09G2S (a), 70 mm thick rolled steel 09G2S-Sh (b), and 36 mm thick rolled steel 14G2AF (c) (see designations in Figure 5)

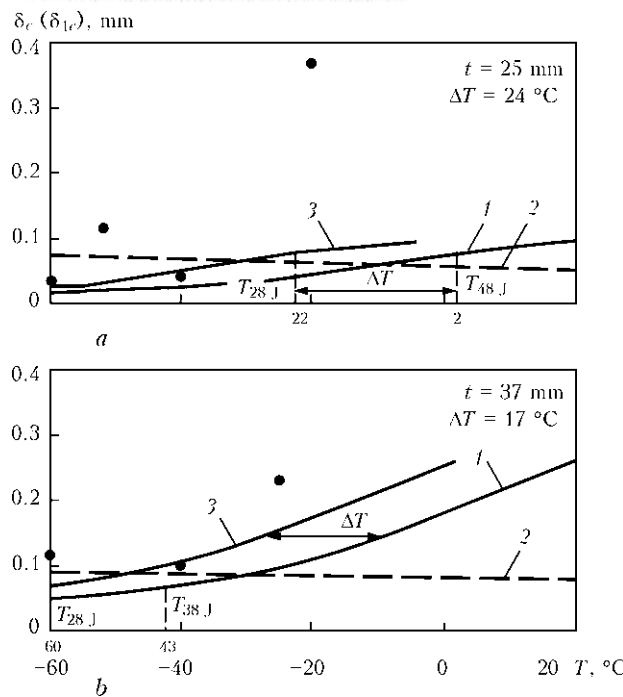


Figure 9. Temperature dependence of crack resistance characteristics of rolled steel 10KhSND: 1 — theoretical curve δ_{1c} calculated from formula (1); 2 — condition from formula (10); 3 — curve $\delta_{1c}^{(t)}$ calculated from formula (7)

The impact bend test results are presented in Table 6 and in Figures 7 and 8.

As seen from Table 6 and Figure 7, the investigated 25 mm thick rolled steel 10KhSND is characterised by too low values of fracture energy a_v^{\max} and increased temperature to meet the requirement of 28 J.

The value of δ_c was determined under static loading of the specimens at three-point bending within a temperature range of -75 to $+20$ $^{\circ}\text{C}$. Displacement of the crack edges was measured by using two displacement sensors. The test results are presented in Table 7 and in Figures 9 and 10. Also, it should be noted that toughness characteristic δ_c at temperatures below -20 $^{\circ}\text{C}$ were determined under the maximal load.

To determine δ_i in tough fracture of steels 09G2S and 14G2AF, stable crack growth Δl was fixed during the tests conducted at room temperature, after that the value of critical crack opening displacement corresponding to the beginning of tough fracture was evaluated from the results of tests of several specimens [9, 10].

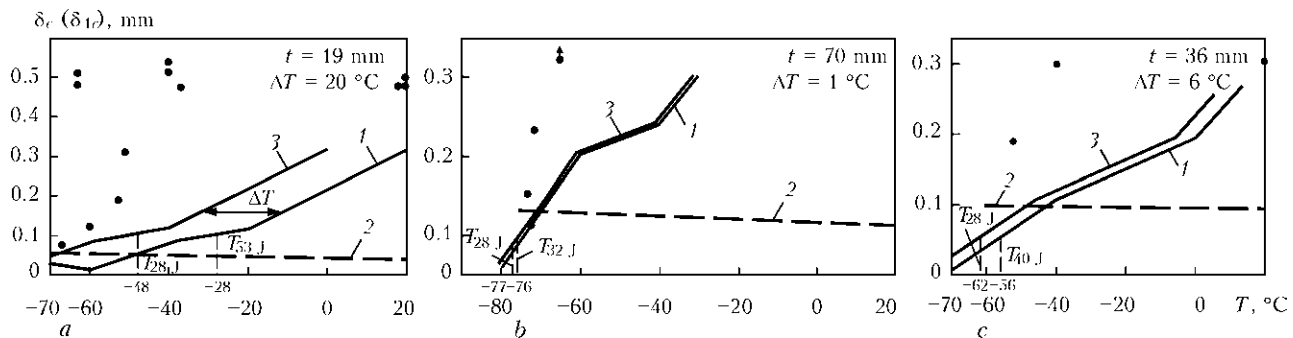


Figure 10. Temperature dependence of crack resistance characteristics of rolled metal: a — steel 09G2S; b — steel 09G2S-Sh; c — steel 14G2AF; 1–3 — same as in Figure 9

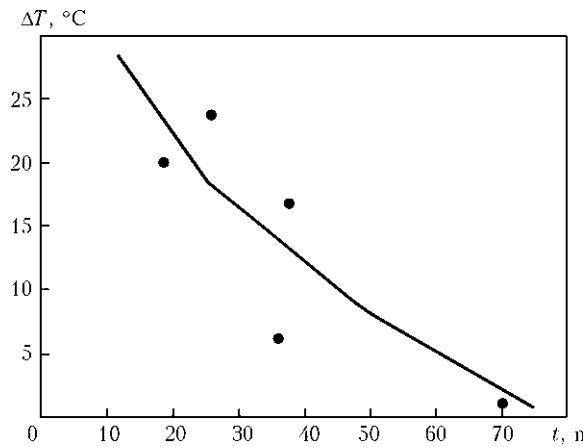


Figure 11. Dependence of temperature shift ΔT on thickness of specimens tested to three-point bending under static loading: curve — recommended temperature shift C according to standard ASTM E 1921-97; points — experimental values of ΔT

Corrected calculated fracture toughness characteristic $\delta_{1c}^{(t)}$ obtained with a temperature shift of curve 1 to the ΔT value, according to Table 7, is shown in Figures 9 and 10.

As seen from the data presented, the proposed calculated values of $\delta_{1c}^{(t)}$ describe well enough the experimental values of deformation characteristic δ_c at the lower bound of their scatter depending on the specimen thickness. This is indicative of the fact that the selected characteristics affecting the plane strain to plane stressed state transition condition depending on the specimen thickness are correct.

As far as a change in temperature shift C according to standard ASTM E 1921-97 is concerned, despite the general tendency to decrease in the ΔT value with increase in thickness of the specimens investigated, no direct relationship was observed between these two characteristics. The obtained experimental values of ΔT depending on thickness of the specimens tested to three-point bending are shown in Figure 11. As seen from the Figure, the recommended temperature shift C according to standard ASTM E 1921-97 only limits the temperature range of search for the values that correspond to $K_{jc} = 100 \text{ MPa}\cdot\text{m}^{0.5}$, as it describes only the mean values of the experimental data.

In general, it should be noted that, according to the results of experimental verification, when determining the temperature shift by using the approach



suggested in study [1] it is necessary to take into account both deformation and strength characteristics of the material. This makes it possible to more reasonably approach both selection of the temperature shift and determination of the temperature transition allowing for thickness of a structural element.

1. Dyadin, V.P. (2010) Evaluation of temperature shift depending upon the specimen thickness by the force and deformation criteria of fracture mechanics. *The Paton Welding J.*, 4, 14–21.
2. Gireenko, V.S., Dyadin, V.P. (1990) Correlation of characteristics of crack resistance of materials and welded joints with results of standard mechanical tests. *Avtomatisch. Svarka*, 6, 1–4.
3. Dyadin, V.P. (2004) Comparison of impact toughness values of Charpy and Mesnager specimens at tough fracture. *The Paton Welding J.*, 4, 21–26.
4. Malinin, N.N. (1975) *Applied theory of plasticity and creep*. Moscow: Mashinostroenie.

5. Kawano, S., Tada, M., Yajima, H. et al. (1987) Thickness effects on brittle fracture toughness of weld metal of high tensile strength steel. *Transact. of JWS*, 18(1), 68–76.
6. CAN/CSA-S473-92: Canadian standard association. Steel structures. Pt 3: Of the code for the design, construction and installation of fixed offshore structures. 1992.
7. (2006) *Rules for classification and construction of floating drilling units and off-shore stationary platforms*: Russian Maritime Register of Shipping. St-Petersburg: RMPS.
8. Gorynin, I.V., Illiin, A.V. (2008) Theoretical and experimental investigations of brittle fracture resistance of metal of welded structures for the Arctic shelf. *The Paton Welding J.*, 11, 20–24.
9. Musiyachenko, V.F., Mikhoduj, L.I., Kirian, V.I. et al. (1988) Fracture toughness of weld metal with yield stress of 600 to 800 MPa made in shielding gases. *Avtomatisch. Svarka*, 6, 39–44.
10. Serensen, S.V., Gireenko, V.S., Kirian, V.I. et al. (1975) Crack opening displacement in quasi-brittle and brittle fracture. *Ibid.*, 2, 1–6.

QUATTROJET™ — INNOVATION OXY-FUEL TORCH



ESAB offers QUATTROJET™ — oxy-fuel cutting system of an absolutely new type, which makes the process even more efficient and clears the way to complete automation.

The new oxy-fuel torch equipped with an automatic flame control senses any potential violation of the cutting process and automatically stops gas feeding. Therefore, in contrast to traditional systems, the cutting machine requires no continuous monitoring by an operator, as any leakage of fuel gas and oxygen is efficiently prevented. The flame control device reacts to any defect in the material treated, and to any malfunction of the cutting tool.

This control system improves safety of operators and workers, environment and machines, thus improving quality of automatic cutting.

To ensure the correct distance between the cutting nozzle and workpiece, QUATTROJET is fitted with a height determining device. Thus, there is no need to install an additional, separate sensor on the torch.

Conventional control systems, such as rings, wear out very quickly and require regular replacement. Other functions of compact oxy-fuel torch QUATTROJET include internal ignition system protected from dirt and damage, and device for quick replacement of the nozzle using no tools.





DETACHABILITY OF SLAG CRUST IN ARC WELDING (Review)

Part 2. Character of the effect of main factors on detachability of slag crust*

S.I. MORAVETSKY

E.O. Paton Electric Welding Institute, NASU, Kiev, Ukraine

The effect of various particular factors on detachability of slag crust in automatic arc welding is analysed. It has been established that the flux being developed for narrow-gap automatic arc welding of thick joints should ensure formation of the slag crust with the minimum possible strength and maximum possible linear thermal expansion coefficient. Brief characterisation of the currently available methods for experimental evaluation of detachability of the slag crust is given.

Keywords: submerged arc welding, multipass welding, narrow gap, alloyed steels, slag crust, detachability, chemical adhesion, phase composition of slag, oxidation potential

Problems associated with removal of slag crust in narrow-gap welding of thick-walled butt joints on alloyed steels are caused by chemical adhesion of slag to the weld metal and mechanical fixation of the crust. The mechanism of chemical adhesion was formulated in Part 1 of this study [1].

Mechanical fixation of the crust on the surface of a welded joint may take place independently of the presence or absence of chemical adhesion. In some cases such geometric peculiarities of the metal surface as depressions may be filled up with a liquid slag, which solidifies in cooling, thus leading to mechanical jamming of the crust when it is removed. This can be caused by violations of the welding technology resulting in formation of such defects as lacks of fusion, undercuts, and coarse ripples on the weld surface. However, in many cases the conditions that cause mechanical fixation of the crust may result from edge preparation even with a strict adherence to the welding technology. During groove filling, the edges of the pieces welded approach each other (the groove becomes narrower), this causing fixation and compression of the slag crust in the groove. The latter is likely to take place if approaching of the edges exceeds the value of transverse reduction of the slag crust.

The welding process is characterised by many particular factors that affect completeness of occurrence of both mechanisms causing deterioration of detachability of the slag crust (chemical adhesion and mechanical fixation). Knowledge of the role and character of the effect of the above factors on detachability of the slag crust is very important for development of a flux for multipass narrow-gap welding of alloyed

steels. In this connection, it is of interest to analyse the available applied research results on the effect of the most important factors on detachability of the slag crust.

Detachability of the slag crust can be affected to a substantial degree by varying the welding process parameters. Increase in heat input during welding of low-carbon steel leads to increase in time of contact of the softened slag and solidified weld metal. This results in growth of thickness of the oxide interlayer and deterioration of detachability of the slag crust. Decrease in arc voltage causes decrease in the amount of the molten slag and favours improvement of detachability of the slag crust [2]. However, the technology for welding of low-alloy limited-weldability steels stipulates for a wide-range variation of the process parameters, as well as for concurrent heating. In this connection, in welding of the given steels the above regularities are of low practical significance.

Correlation was revealed between the character of detachability of the slag crust, adhesion W and surface tension σ_{m-s} at the metal–slag interface [3]. It was experimentally proved that deterioration of detachability of the slag crust is accompanied by decrease in inter-phase tension at the interface between the slag and metal, which corresponds to increase in wettability of metal with the slag and intensification of the oxidation-reduction processes at the metal–slag interface [4]. In this case, the value of adhesion calculated from the Dupre formula increases:

$$W = \sigma_m + \sigma_s - \sigma_{m-s},$$

where σ_m (σ_s) is the surface tension of metal (slag) at the interface with the environment.

It was established that detachability of the slag crust at $W > 9 \cdot 10^{-3}$ N/cm is unsatisfactory independently of the proportion of the slag and deposited metal, and at $W < 9 \cdot 10^{-3}$ N/cm the lower the value of W , the better is the detachability.

* Beginning of the article is given in TPWJ, 2011, No. 1.



Much experimental data on the relationship of linear thermal expansion coefficient (LTEC) of slag α_s and metal α_m have been accumulated, but the conclusions made by different researchers are contradictory.

For instance, the authors of studies [5, 6] are of the opinion that the slag crust can be most readily removed from the groove at $\alpha_s > \alpha_m$. At $\alpha_s = \alpha_m$ the crust is not jammed, but some deterioration of its detachability might be expected. At $\alpha_s < \alpha_m$, the higher the difference of $\alpha_s - \alpha_m$, the more difficult it is to remove the crust from the groove. LTEC of slags, like of other oxide systems, depends on the chemical composition and may vary over very wide ranges [5, 6]. However, there is an opposite opinion that an easy detachability of the slag crust can be achieved if $\alpha_s < \alpha_m$. This statement can be found in many papers with a reference to study [7], where detachability of the slag crust formed in manual deposition of beads on steel plates by using electrodes VSR-50 manufactured by several factories was determined experimentally. In each case the volume thermal expansion coefficients (VTEC) of the slag crust were measured, among other parameters. And it was established that the electrodes with a better detachability of the slag crust had a lower value of VTEC than the electrodes with a worse detachability.

Proceeding from the simplified mechanism of fixation of the slag crust in the groove on the basis of the α_s and α_m relationship, study [6] expresses doubts about the results obtained in [7]. Moreover, it ignores the substantial differences in the procedure used by the authors of study [7] to determine detachability of the slag crust. Nevertheless, investigation of the combined cooling of the slag crust and plate with the deposited bead suggests that the conclusion of study [7] is correct.

Also, there is an opinion that in terms of detachability of the slag crust the absolute difference of $\alpha_s - \alpha_m$ is important, rather than the relationships of the type of $\alpha_s \geq \alpha_m$ or $\alpha_s < \alpha_m$. The higher the value of $|\alpha_s - \alpha_m|$, the better is the detachability of the slag crust, other conditions being equal. Based on the hypothesis of a local fixation of slag, the authors of study [8] see this effect of LTEC in the presence of chemical adhesion of the slag to metal «rooted» into the grain boundaries. Increase in $|\alpha_s - \alpha_m|$ leads to growth of tangential stresses at the slag to metal interface in cooling, which promotes fracture of the grain-boundary connecting «links» between the slag and metal.

Investigations were conducted to closely study polymorphic transformation of dicalcium silicate, and its realisation with a positive result was tested in practice of manufacture of covered electrodes [9–11]. It is a known fact that in cooling of dicalcium silicate $2\text{CaO}\cdot\text{SiO}_2$ its high-temperature β -modification with a density of $3.10\text{--}3.28\text{ g/cm}^3$ transforms into a low-temperature γ -modification with a density of 2.80--

2.97 g/cm^3 . The transformation has no definite starting temperature. It may occur at a temperature from 1000°C to room temperature, depending on the conditions. The resulting increase of up to 12 % in the specific volume of slag and internal stresses in them leads to self-grinding (self-spilling) of the slag, which has a very favourable effect on its removal from the groove.

Based on the stoichiometric proportion of oxides in structure of $2\text{CaO}\cdot\text{SiO}_2$, the authors of studies [9, 12] believe that the necessary condition for formation of this silicate in slag is the proportion of the $\text{CaO}:\text{SiO}_2$ molar fractions close to 2, or the weight fraction proportion close to 1.87, or $\text{CaCO}_3:\text{SiO}_2 = 3.33$. In practice, the lower limit of the $\text{CaO}:\text{SiO}_2$ proportion, at which $2\text{CaO}\cdot\text{SiO}_2$ can be detected in slag by X-ray diffraction analysis and improvement of detachability of the slag crust is observed, can amount to 0.5.

Study [13] describes the polymorphic transformation occurring at $T = 800\text{--}650^\circ\text{C}$ in slags of the $\text{MgO}\cdot\text{SiO}_2\text{-BaO-Al}_2\text{O}_3$ system, which is accompanied by increase in the specific volume without self-spilling of the slag. In this case, the polymorphic transformation plays a negative role in detachability of the slag crust.

An addition of 15 wt.% ZrO_2 to the oxide-fluoride slag system allows a substantial improvement of detachability of the slag crust in welding with self-shielding flux-cored wires [14]. Zirconium dioxide forms an independent crystalline phase of ZrO_2 in slag, in addition to calcium zirconate $\text{CaO}\cdot\text{ZrO}_2$. Cooling involves a number of polymorphic transformations of ZrO_2 with a marked change in the specific volume of the newly formed phases, this positively affecting detachability of the slag crust.

Therefore, the polymorphic transformations of slag accompanied by a change in the specific volume may have both positive and negative effect on detachability of the slag crust.

An important factor of detachability of the slag crust is its strength. As follows from the above regularities, it plays an ambiguous role, and its role depends on the type of a welded joint and presence of chemical adhesion between the slag and metal. Low mechanical strength of the slag promotes an easier removal of the slag crust jammed in the groove at the presence or absence of chemical adhesion, as well as from the surface of the bead deposited on a plate at the absence of chemical adhesion. High mechanical strength of the slag crust, as believed by the authors of study [8], provides its easier removal from the surface of the deposited bead at the presence of chemical adhesion.

The factors of strength of multi-phase systems of partially solidified or mainly crystalline slags are proportions of crystalline and amorphous components [2], as well as types and sizes of crystals. It might be expected that decrease in strength of the slag crust



will be favoured primarily by the phenomena that lead to formation of structural stresses and microdefects in it, such as anisotropy of thermal expansion of crystals, difference in LTEC between the glass phase and adjacent crystals and between separate crystals, susceptibility of crystals to polymorphic transformations with a change in their specific volume, etc. The degree of compactness of the slag crust also has a marked effect on its strength [15]. A spherical pore formed in a material acts as a mechanical stress raiser, and the smaller the radius of the pore, the stronger is its effect. According to the calculations [16], the 10 % porosity decreases strength of the material approximately two times, compared to the solid material.

Detachability of the slag crust is a very complicated process, the character of which depends on many phenomena of a physical-chemical and physical-mechanical nature. In this connection, the general physical investigation methods are applied to study problems of detachability of the slag crust. For example, to investigate slag in terms of its structural-size correspondence to the weld metal and oxides, in a general case it is necessary to determine chemical composition of metal, identify crystalline phases in the metal, its oxides and slags, and determine type and parameters of their crystalline lattice. The chemical, spectral, X-ray diffraction and X-ray microprobe analysis methods are employed for these purposes. Phase (mineralogical) composition of slags is also investigated by the crystal optics and petrography methods. The presence and temperature of occurrence of polymorphic transformations in slags with a change in their specific volume are established, and LTEC values of the slags are determined by using the dilatometry methods.

As noted above, strength of the slag crust is an important factor in terms of its effect on detachability. Strength of the slag crust can be predicted from the results of identification of the slag phases. However, of a higher interest is its direct quantitative evaluation. The procedure of determination of strength of the slag crust is used for this purpose [14].

Methods for direct experimental determination of detachability of the slag crust have the following sequence: realisation (simulation) of the investigated variant of welding with participation of the metal and slag phases; removal of the slag crust by the procedure that involves the force impacts on it as a physical experiment with a simultaneous measurement of parameters and results of these impacts, or as a technological test with a statement of qualitative attributes. These methods allow a direct determination of detachability of the slag crust as a result of the additive effect of a set of factors characteristic of the selected technological variant of welding.

As the manual slag crust removal method is most widely applied in the welding industry, the first notions of the character of detachability of the slag crust were, undoubtedly, of the organoleptic origin, and

specialists considered this property of the slags to be qualitative. The qualitative (point-rank) method for evaluation of detachability of the slag crust in welding consists in the fact that performer of the slag crust removal operation forms its own opinion on the detachability proceeding from the results of his direct actions. Determination of the detachability at the qualitative level is more preferable for production, as it is not time-consuming and requires no special tools. Also, this method is very often used in theoretical studies [1, 2, 6, 12–15, 17].

When solving the problems of detachability of the slag crust, it is desirable to have the possibility of quantifying it at the scientific-and-technical level. One of such methods [18] is based on the fact that V-groove welding is performed on a plate of the investigated base metal by using the investigated welding consumables. Upon cooling a sample to room temperature, the angle between the groove edges is gradually increased by three-point bending under static loading until the slag is detached. The authors of study [18] take angle γ of bending of the plate equal to increase in an angle between the V-groove edges at which the slag is detached as a measure of detachability of the slag crust.

Other methods were suggested later on, where the energy of various dynamic loads transferred to the welded joint or slag crust to remove it from a unit surface of metal was used as a measure of detachability of the slag crust. Detachability of the slag crust in this case is measured in Joules per square meter or square meters per Joule.

Such a method was first proposed by I.N. Voronovitsky and co-authors [19, 20]. Thereafter it received acceptance in practical studies [9, 21, 22]. According to this method, an experimental sample with a deposited bead in the V-groove and non-removed slag was put on supports of the impact pendulum-type testing machine. The rear plane of the sample was impacted by a weight suspended on the pendulum. Energy E transferred to the experimental sample as a whole was metered by varying mass and height of lifting of the weight. The E/F ratio was calculated by measuring area F of the weld metal cleared from the slag as a result of the impact.

The method described in study [23] is based on the principle of removal of the slag crust by the inertia force. According to this method, a stop of the sample moving at speed v because of impact collision with a fixed arrester causes removal of the slag with mass M from some surface of a spot weld with area S under the slag inertia forces. Division of its kinetic energy accumulated before the stop by surface area S gives the value of the specific energy of detachability of the slag crust. A drawback of the method is that preparation of the sample is not related to the welding technology. This makes it necessary to study the issue of the effect by the weld deposition conditions on



detachability of the slag crust, as this property may depend, in particular, on the heat input, time of existence of the slag pool, etc. [1].

The common drawback of the methods for determination of detachability of the slag crust [20, 23] and method for evaluation of strength of the slag crust [5] is that it is necessary to establish the minimal value of the force effect sufficient for obtaining the planned experimental result. The minimal value of the energy can be correctly determined by the said methods only by way of multiple reiteration of the experiment, where the energy of the force effect gradually changes, the other factors remaining unchanged. For this it is necessary to prepare several, nominally identical experimental samples, which makes the investigations more time- and materials-consuming.

Therefore, development of the new methods for quantitative evaluation of detachability of the slag crust (as well as for improvement of the available ones) should be regarded as a topical problem for specialists in the field of welding.

CONCLUSIONS

1. In welding of alloyed steels, the possibilities of improvement of detachability of the slag crust through varying the welding process parameters are limited.

2. To improve detachability of the slag crust, the composition of flux for welding of thick-walled joints on alloyed steels should be selected so that it could provide the slag crust with a maximum possible LTEC and minimum possible strength.

3. Strength of the slag crust can be changed, and its detachability can be improved by providing a target effect on peculiarities of its micro- and macrostructure, in particular, due to the presence of the phases susceptible to polymorphic transformations, which leads to self-spilling of the slag.

4. The majority of the available methods for direct experimental determination of detachability of the slag crust are characterised by increased time and materials intensity, this hampering their wide application. Development of the methods for quantitative determination of detachability of the slag crust in welding is still a topical problem. At present, the qualitative method for evaluating it on bead-on-plate samples is most common.

1. Moravetsky, S.I (2011) Detachability of slag crust in arc welding (Review). Part 1: Mechanism of chemical adhesion of slag crust to weld metal. *The Paton Welding J.*, **1**, 28–31.
2. Rabkin, D.M., Gotsalsky, Yu.N., Kudelya, E.S. et al. (1950) About detachability of slag crust in automatic submerged-arc welding. *Avtomatich. Svarka*, **3**, 10–27.
3. Yakobashvili, S.B. (1962) Interfacial tension of welding fluxes and its influence on detachability of slag crust. *Ibid.*, **9**, 37–39.
4. Yakobashvili, S.B. (1970) *Surface properties of welding fluxes and slags*. Kiev: Tekhnika.
5. Podgaetsky, V.V. (1950) Mechanical fixation of slag on weld in automatic welding. *Avtomatich. Svarka*, **6**, 30–40.
6. Vornovitsky, I.N., Medvedev, A.Z., Cherkassky, A.L. (1973) Influence of coefficient of thermal expansion of slag on its detachability from weld metal. *Svarochn. Proizvodstvo*, **3**, 35–37.
7. Grinberg, N.A., Rogova, E.M. (1960) Factors influencing the detachability of slag crust from weld. *Ibid.*, **11**, 18–20.
8. Volobuev, O.S., Potapov, N.N., Volobuev, Yu.S. et al. (1989) To the problem of influence of linear thermal expansion coefficient on slag crust detachability. *Ibid.*, **8**, 37–39.
9. Pokhodnya, I.K., Karmanov, V.I., Upyr, V.N. (1980) Detachability of slag crust of electrodes with basic coating. *Avtomatich. Svarka*, **11**, 33–34.
10. Vornovitsky, I.N., Saveliev, V.G., Sidlin, Z.A. (1997) Re-alization of silicate decomposition in welding slags. *Svarochn. Proizvodstvo*, **5**, 11–12.
11. Vornovitsky, I.N., Saveliev, V.G. (2001) Peculiarities of manufacture of electrodes with self-spilling flux. *Ibid.*, **5**, 46–49.
12. Lazarev, B.I., Timofeev, M.M., Potapov, N.N. et al. (1979) Peculiarities of development of flux for narrow-gap welding. *Ibid.*, **5**, 21–23.
13. Hirai, Yu., Tokuhisa, M., Yamashita, I. et al. (1982) Development of the narrow gap submerged arc welding process – NSA process. *Kawasaki Steel Techn. Rep.*, **5**, 81–83.
14. Mojsov, L.P., Mityashin, L.L., Burylev, B.P. (1990) Study of phase composition of oxide-fluoride slags and their detachability from metal. *Adgeziya Rasplavov i Pajka Materialov*, Issue 24, 82–85.
15. Wittung, L. (1980) Some physical and chemical properties of welding slags and their influence on slag detachability. In: *Proc. of Int. Conf. on Weld Pool Chemistry and Metallurgy* (London, Apr. 15–17, 1980), Vol. 1, 83–92.
16. Pavlushkin, N.M. (1972) *Principles of the technology of pyroceramics*. Moscow: Stroyizdat.
17. Pavlov, I.V., Kosenko, A.A., Gurevich, V.I. et al. (1986) Detachability of slag crust from austenitic weld metal. *Svarochn. Proizvodstvo*, **7**, 37–38.
18. Lipodaev, V.N., Bojko, V.A., Kakhovsky, Yu.N. et al. *Method for evaluation of detachability of slag coating*. USSR author's cert. 407686. Int. Cl. B 23 K 29/00. Publ. 10.12.73.
19. Vornovitsky, I.N., Medvedev, A.Z., Cherkassky, A.L. *Method for evaluation of detachability of slag coating from weld metal surface*. USSR author's cert. 407685. Int. Cl. B 23 K 29/00. Publ. 10.12.73.
20. Vornovitsky, I.N., Malashonok, V.A., Cherkassky, A.L. (1975) Procedure for quantitative evaluation of slag detachability. *Svarochn. Proizvodstvo*, **2**, 47–48.
21. Shono, S.A., Kassov, D.S., Karpenko, V.M. (1976) Evaluation of slag systems of flux-cored wire by slag detachability. *Avtomatich. Svarka*, **3**, 22–24.
22. Grin, A.G., Bogutsky, A.A. (1996) Procedure for evaluation of slag crust detachability. *Ibid.*, **3**, 58–59.
23. Kurlanov, S.A., Potapov, N.N., Bazhenov, A.V. et al. (1986) Procedure for quantitative evaluation of slag detachability. *Svarochn. Proizvodstvo*, **7**, 39–40.



CAUSE OF SECONDARY HARDENING IN Cr-Mo-V WELD METAL DURING LONG-TERM HEAT EXPOSURE

P. MOHYLA, I. HLAVATY and P. TOMCIK

Technical University of Ostrava, Czech Republic

Results of microstructural analysis quantified changes in the dispersion phase in Cr-Mo-V weld metal during exposure in the sub-creep range are presented. The hypothesis that changes in the dispersion of MX particles during long-term heat exposure are significant has been confirmed by presented results.

Key words: CrMoV steel welds, sub-creep range, secondary hardening, vanadium carbides and carbonitrides, microstructural analysis, image analysis

Low-alloy creep-resistant steels of 0.5 % Cr–0.5 % Mo–0.3 % V type are used in power industry for fabrication pipes and tubes. Their long-term creep resistance, expressed as creep rupture strength (CRS) after 105 h, is significantly higher in comparison with 2.25 % Cr–1 % Mo steels. The other significant property of creep-resistant steels containing vanadium is their demanding technological processing, which stems from the dominant affect of the dispersion phase on their mechanical properties. Parameters of dispersion phase are very sensitive on heat treatment. Vanadium carbides and carbonitrides (MX particles), which precipitate mainly during tempering, play the key role in Cr-Mo-V steels.

However, during long-term heat exposure the number, mean size and mean spacing of particles are changed. These changes significant influence mechanical properties and thereby even the durability and operating reliability of power equipment. Operation of the tested steel 14MoV6-3 in the sub-creep temperature range (maximum 480 °C) causes secondary hardening, accompanied by a decrease of impact toughness. The mentioned secondary hardening is especially pronounced in welded joints tempered at temperatures lower than those required by the material specification, i.e. temperatures lower than 720 °C.

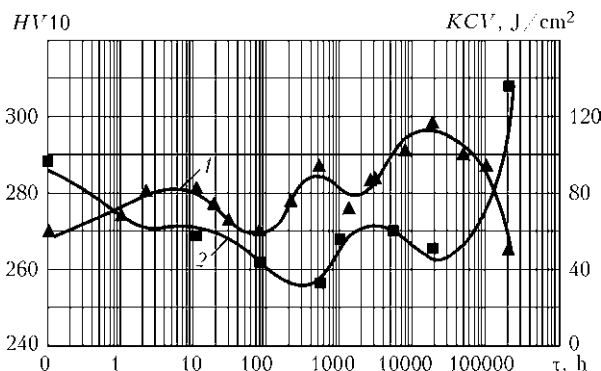


Figure 1. Hardness (1) and impact toughness (2) of weld metal at operating temperature of 450 °C (tempering at 680 °C for 2 h)

Figure 1 shows the changes in hardness and impact toughness of weld metal tempered at 680 °C. Mechanical properties were measured according to relevant standards [1]. Microanalysis using an electron microscope was performed to confirm additional precipitation of MX particles in weld metal of 14MoV6-3 steel.

Electron microstructural analysis. Weld metal samples tempered to 680 °C and after subsequent heat exposure served as material to be studied. Parameters of simulated heat exposure were as follows: for sample 1.0 – initial condition; for sample 1.11 – after annealing at 500 °C for 23.4 h; for sample 1.1 – after annealing at 550 °C for 50.4 h; and for sample 1.20 – after annealing at 550 °C for 546.5 h

These samples are highlighted in Figure 2. Parameters of simulated heat exposure are recalculated to operating temperature of 450 °C.

Structure-phase analysis of weld metal. The weld metal microstructure contains a mixture of ferrite and bainite. The electron-microscope study was conducted using transmission electron microscope (TEM) of JEM 200CX type, equipped with an energy dispersion analyser. Identification of minority phases was performed using a combination of electron diffraction and qualitative energy dispersion analysis of particles on extraction carbon replicas. Thin metal foils were prepared by jet polishing in the electrolyte (95 % CH₃COOH and 5 % HClO₄) at room temperature and voltage $U = 80$ V.

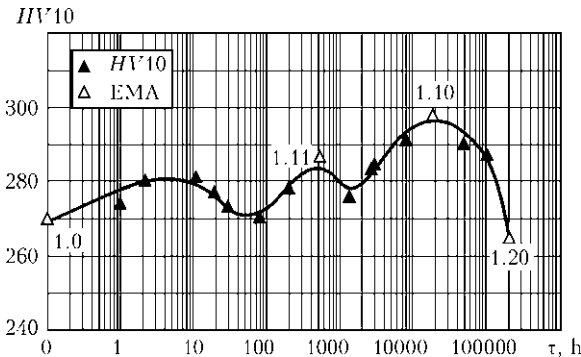


Figure 2. Selection of samples for electron microstructural analysis (EMA), operating temperature of 450 °C, tempering at 680 °C for 2 h

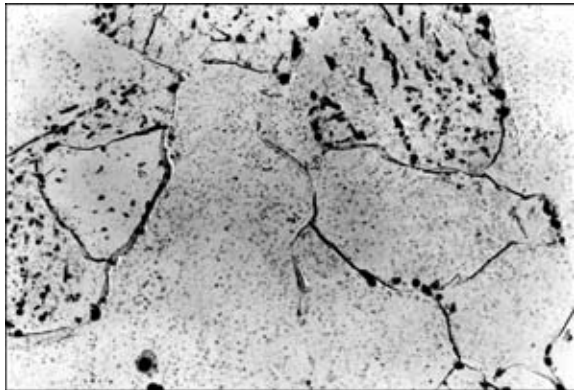


Figure 3. Distribution of precipitate on extraction carbon replica for sample 1.0 ($\times 9000$)

Results of minority phase study in the samples were as follows: MX, M_3C in sample 1.0; MX, M_3C in sample 1.11; MX, M_3C in sample 1.1; and MX, M_3C in sample 1.20. It is evident that all samples contained particles of cementite and MX, where $M = V$, and $X = C$ and N . A typical example of precipitate distribution in extraction carbon replicas is presented in Figure 3. Fine MX particles precipitated inside ferrite and bainite-ferrite grains, while the relatively coarse cementite grains usually lined the bainite-ferrite boundary. The fibrous morphology of MX particles observed in works [2, 3] was not seen in studied samples. Furthermore, weld metal included numerous globular particles of complex silicon, manganese and titanium oxides.

Dislocation density was determined in bainite-ferrite plates. Dislocation density was calculated using the Ham's method:

$$\rho = \left(\left(\frac{N_1}{L_1} \right) + \left(\frac{N_2}{L_2} \right) \frac{1}{t} X \right) (\text{m}^{-2}), \quad (1)$$

where N_1, N_2 is the number of intersections of two parallel lines with dislocations; L_1, L_2 is the total length of lines; $t = 125 \text{ nm}$ is the foil thickness selected; X is the factor considering the share of non-visible dislocations for the selected imaging diffraction conditions.

The density of dislocations in individual samples was assessed on photographs with a total magnifica-

tion of 109,000 (Figure 4). Measurement results (arithmetic mean and standard deviation) were as follows, $\rho \cdot 10^{-14} \text{ m}^{-2}$: in sample 1.0 — 4.91 ± 0.94 ; in sample 1.11 — 4.26 ± 0.97 ; in sample 1.1 — 4.50 ± 0.66 ; and in sample 1.20 — 3.60 ± 0.95 . It is evident that the differences in dislocation density in bainite-ferrite are insignificant in measured samples.

Image analysis. Image analysis methods enable determination of important parameters characterising the dispersion phase, such as mean particle size or number of particles per unit area, and subsequently the calculation of the number of particles per unit volume or mean inter-particle spacing. Our objective was the determination of these parameters for MX particles in the case of individual samples, i.e. during different stages of long-term heat exposure of weld metal in the sub-creep region. Three samples were selected for these purposes, namely 1.0, 1.1 and 1.20 (see Figure 2). Extraction carbon replicas were made from these samples and photographed subsequently with a magnification of 151,000. The photograph of sample 1.20 is presented in Figure 5. All the photos were converted into electronic images. These images were subject to image analysis using Micro Image 4 software. The result is a set of output values, namely particle area A_x , maximum diameter D_{\max} , mean diameter D_{mean} , minimum diameter D_{\min} , equivalent particle diameter D_{eq} and the particle area — total photograph area ratio P_A , as well as the number of particles n_0 , number of photographs, and total monitored area A_0 .

The image analysis for each sample was performed on several photos, therefore the total monitored area A_0 is the sum of the individual photograph areas.

The number of particles per unit area n_s was calculated as a proportion of the number of monitored particles n_0 and monitored area A_0 :

$$n_s = \frac{n_0}{A_0}. \quad (2)$$

Calculation of the number of particles per unit volume was performed using a formula from the Ashby and Ebeling paper [4], which deals with the determi-

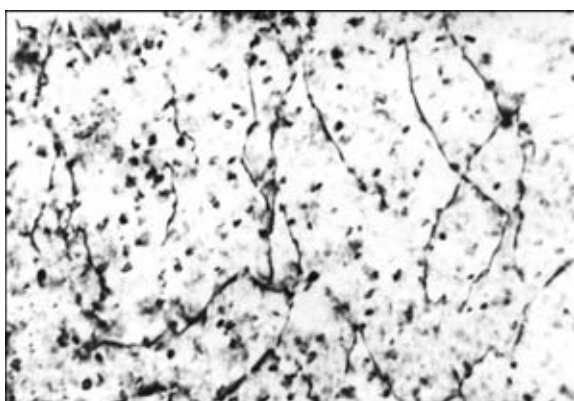


Figure 4. Dislocation substructure ($\times 109,000$) of weld metal (thin foil, sample 1.20)

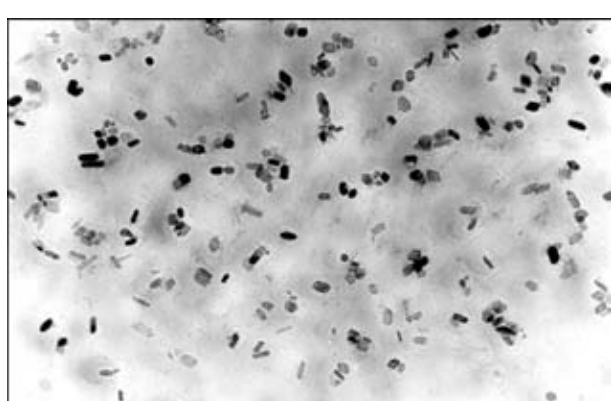


Figure 5. Dispersion of MX particles ($\times 151,000$) in the weld metal microstructure (bainite, extraction carbon replica, sample 1.20)



Calculation results for n_s , n_v and λ

Sample No.	A_x , nm ²	d_{eq} , nm	$n_s \cdot 10^{-14}$, m ⁻²	$n_v \cdot 10^{-22}$, m ⁻³	λ , nm, acc. [7]	λ , nm, acc. [8]
1.0	168.24 ± 10.59	13.65 ± 0.33	2.13037	1.79595	52.72	32.92
1.1	124.01 ± 3.24	12.10 ± 0.15	7.96117	7.08676	24.26	13.68
1.20	246.10 ± 8.04	16.91 ± 0.29	2.81644	1.82597	43.10	25.46

nation of number, size and spacing of secondary phase particles in extraction replicas:

$$\frac{n_v}{n_s} = \frac{1}{d_{eq}} \left\{ 1 + \left(\frac{\sigma}{d_{eq}} \right)^2 \right\}, \quad (3)$$

where n_v is the number of particles per unit volume; n_s is the number of particles per unit area; d_{eq} is the equivalent spherical particle diameter (arithmetic mean); σ is the standard deviation of equivalent diameter

The equivalent particle diameter d_{eq} is the diameter of the projection of an equivalent spherical particle (circle) into a section plane of the same area as is the area of the real particle (general shape). The d_{eq} value was determined from a measured particle area A_x according to the following formula:

$$d_{eq} = \sqrt{\frac{4A_x}{\pi}}. \quad (4)$$

Particle spacing was determined according to the plane square particle arrangement model, which is suitable for assessing dispersion hardening of low-alloy steel [5]. The calculation was performed in two alternatives as per paper [6]. According to Kelly and Nicolson [7] the mean distance of particle edges is determined from

$$\lambda = (n_v d_{eq})^{-1/2} - \sqrt{\frac{2}{3}} d_{eq}. \quad (5)$$

According to Ashby [8], equation (5) is rectified, due to mutual interaction of dislocation sections after overcoming a particle, as follows:

$$\lambda = 0.69(h_v d_{eq})^{-1/2} - \sqrt{\frac{2}{3}} d_{eq}, \quad (6)$$

where d_{eq} is the equivalent particle diameter; λ is the mean particle spacing; n_v is the number of particles per unit volume

Calculation results are summarised in the Table.

So, dominant observed processes are the additional precipitation and coarsening of MX particles. Sample 1.1 with the highest hardness during heat exposure (see Figure 2) represents an area of additional precipitation of MX particles. This is indicated by the highest number of particles per unit volume, smallest size and smallest mean inter-particle spacing in comparison to the other samples. In comparison with the

initial condition (sample 1.0), the number of particles increased almost 4 times and the mean inter-particle spacing dropped more than 2 times. In comparison, sample 1.20 represents an area of coarsening of secondary particles. This is confirmed by the largest mean particle area, significant decrease in number of particles (approximately by 4) and almost a doubled increase in mean inter-particle spacing compared to sample 1.1. The significant influence of the secondary phases on mechanical properties of 14MoV6-3 steel is also confirmed by the fact that the dislocation density remained almost unchanged during observed heat exposure.

CONCLUSION

The dispersion of MX particles of 0.5 % Cr–0.5 % Mo–0.3 % V steels changes its parameters during steel tempering and subsequent long-term heat exposure. These changes significantly influence the material mechanical properties. Operation of 0.5 % Cr–0.5 % Mo–0.3 % V weld metals in the sub-creep range causes secondary hardening accompanied by a degradation of plastic properties. This hardening is pronounced especially in welded joints tempered at lower tempering temperatures (of about 680 °C). Proper post-weld heat treatment at temperature of about 720 °C can be recommended for 14MoV6-3 steel.

Acknowledgements. This result of project LN00B029 was supported by the Ministry of Education of Czech Republic.

1. Krejci, L. (2006) Mechanical testing of welded joints. In: *Proc. of Seminar «Svarovaci den 2006»*. Ostrava: TU, 40–47.
2. Schmidova, E., Svanda, P., Vesely, D. et al. (2009). Mechanism of degradation of stabilised corrosion-resistant steel during the welding cycle. *Anti-Corrosion Methods and Materials*, 56(4), 206–217.
3. Bosela, M., Vinas, J., Varga, V. (2001) The analysis of welds-on with resistance against of high area pressure. In: *Proc. of 9th Int. Sci. Conf.* (Trnava, 25–26.10.2001). Bratislava: STU, 186–191.
4. Ashby, M.F., Ebeling, R. (1966) On the determination of the number, size, spacing and volume fraction of spherical second-phase particles from extraction replicas. *Transact. of Metallurgical Society of AIME*, 236.
5. Prnka, T. (1975) *Diss. for Technical University of Ostrava*.
6. Purmensky, J. (1978) *Diss. for Technical University of Ostrava*.
7. Kelly, A., Nicholson, R.B. (1963) Precipitation hardening. *Progress in Material Sci.*, 10.
8. Ashby, M.F. (1969) *Physics of strength and plasticity*. MIT Press, 113.



EFFECT OF LOW-FREQUENCY RESONANCE OSCILLATIONS ON STRUCTURE AND CRACK RESISTANCE OF DEPOSITED HIGH-CHROMIUM CAST IRON

Yu.N. TYURIN, Yu.M. KUSKOV, L.I. MARKASHOVA, Ya.P. CHERNYAK, E.N. BERDNIKOVA, V.I. POPKO,
O.S. KASHNARYOVA and T.A. ALEKSEENKO
E.O. Paton Electric Welding Institute, NASU, Kiev, Ukraine

An experiment was carried out on cladding with high-chromium cast iron. The probability of impact on formation of structure of the deposited metal by low-frequency oscillations, the frequency of which coincided with that of natural oscillations of a workpiece (under resonance conditions), was established, the deposited metal having higher hardness and being characterised by a uniform distribution of chromium between dendrites and eutectic, and by smaller sizes of dendrites near the fusion line. A higher crack resistance of the deposited metal was noted.

Key words: *arc cladding, low-frequency oscillations, resonance condition, structure of deposited metal, cold cracks*

Strains and stresses formed in cladding of workpieces may lead to cold cracking of metal. The most common methods for preventing cold cracking is preliminary and concurrent heating, as well as delayed cooling. These methods are energy-consuming, and they do not improve the quality of cladding. For example, cladding with high-chromium cast irons is accompanied by formation of transverse cracks in the deposited bead immediately behind the zone of movement of the welding arc, and heating of a workpiece does not guarantee their absence.

Study [1] proposed methods for improving cold crack resistance of alloys by using a rational system of alloying of the materials welded or composition of the weld metal, selecting an initial structure of steel before welding, etc. However, these recommendations are hard to use for cladding.

One of the ways of improving crack resistance of alloys is to externally affect the metal that solidifies. Electromagnetic, ultrasonic, low-frequency and other types of oscillations are used as sources of external effects [2–5]. They provide metal with a microcrystalline structure and improved mechanical properties, which reduces the probability of cracking [6].

Available are welding, cladding and stress relief methods, where workpieces are affected by elastic sound-range oscillations. Statements on the efficiency of welding methods, which meet the conditions of resonance of frequencies of an exciting force and frequencies of natural oscillations of a workpiece, can be found in other publications as well [7–9]. However, in practical application of this technology, the frequency of affecting a piece being welded is chosen arbitrarily, as a rule. The efficiency of welding is assessed from structure of the deposited metal. Study

[10] gives the following characterisation of this approach: «it is likely that the problem of an optimal frequency and amplitude of oscillations of the melt in terms of achieving maximal refining of the primary structure has to be solved empirically so far, by allowing for practical results of the previous studies».

The purpose of the present study is to assess the efficiency of low-frequency resonance oscillations (LRO) and their impact on cracking of the deposited high-chromium cast iron. This assessment was performed visually from the quantity of cracks in the deposited metal, as well as by comparative analysis of its structure.

The flow diagram of cladding of samples by involving the external effect by LRO is shown in Figure 1. Samples of steel St3 measuring $50 \times 60 \times 180$ mm and 6 kg in weight were prepared for cladding. The cladding process was performed with device AD-231 by using 2.6 mm diameter flux-cored wire PP-AN197, which provided chromium cast iron as a deposited metal. Length of the deposited bead was 140–150 mm. The cladding process parameters were as follows: current $I = 500$ A, arc voltage $U_a = 28$ V,

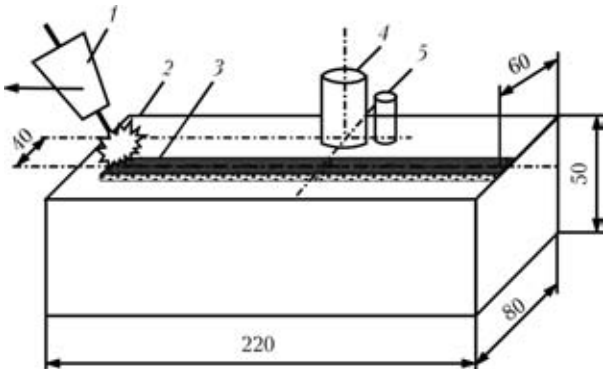


Figure 1. Flow diagram of cladding of samples by involving the external effect by LRO: 1 – welding head; 2 – sample; 3 – deposited cast iron bead; 4 – oscillations exciter; 5 – sensor

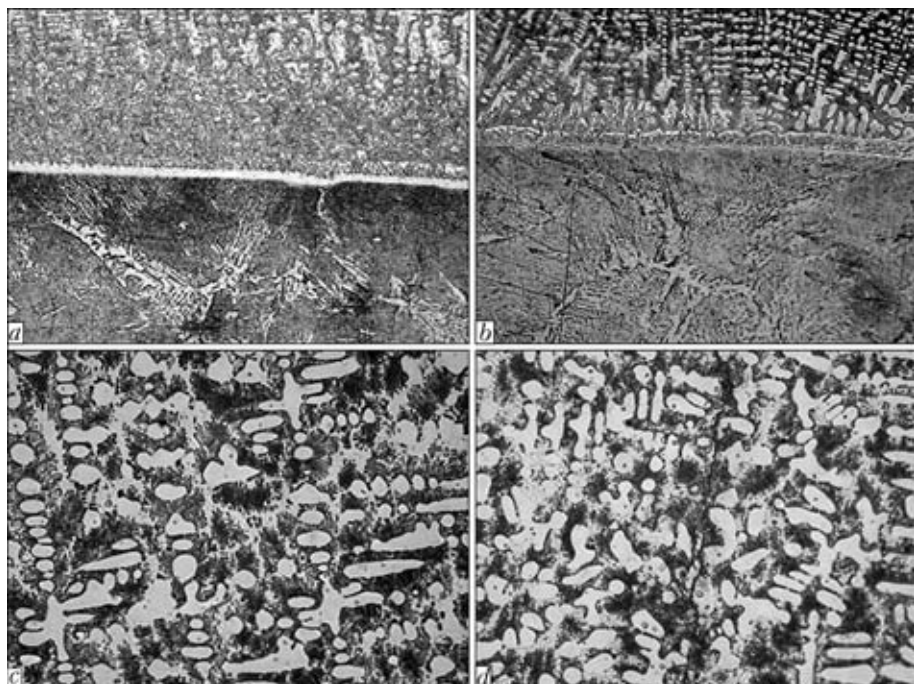


Figure 2. Microstructures of fusion zone between steel St3 (*a, b* – $\times 400$) and deposited high-chromium cast iron (*c, d* – $\times 1000$) obtained without (*a, c*) and with LRO (*b, d*)

cladding speed $v_c = 20$ m/h. The samples were not subjected to preheating, and after cladding they were cooled in air. While performing cladding, the exciting force frequency was varied according to readings of a sensor to meet the condition at which the sensor showed the maximal amplitude of oscillations of a sample, which corresponded to the coincidence of frequencies of external and natural oscillations of the sample (resonance). The external oscillations frequency was 136 Hz, and power was 20 W.

It was found out that cladding by involving LRO provided improvement of crack resistance of the deposited metal. For example, during the experiments a transverse crack initiated only in one out of five samples. Cladding with LRO at frequencies other than the resonance ones (higher or lower than 136 Hz) did not give the expected result: up to 7–8 transverse cracks were detected on the bead surfaces, like in the case of cladding without LRO.

Results of metallographic examinations with an optical microscope showed that in both cases a transition layer 8–20 μm thick formed in the base to deposited (high-chromium cast iron) metal fusion zone, this layer having an austenitic-martensitic structure with clearly defined needles, and hardness of about HV 7400–7900 MPa (Figure 2, *a, b*).

Structure of the deposited metal consisted of dendrites (alloyed austenite–carbides) and eutectic of the rosette type, composed of austenite and carbides (Cr_7C_3 or FeCr_7C_3), as well as austenite decomposition products (troostite) (Figure 2, *c, d*).

The use of LRO provided decrease in sizes of dendrites in the deposited layer. Their sizes decreased two times with distance to the fusion zone. For instance, the mean size of dendrites with the application of LRO was 5–7 μm , and that without LRO was 13–15 μm (Figure 3). Owing to the LRO effect the sizes of dendrites, D_d , decreased approximately to 1–2 μm .

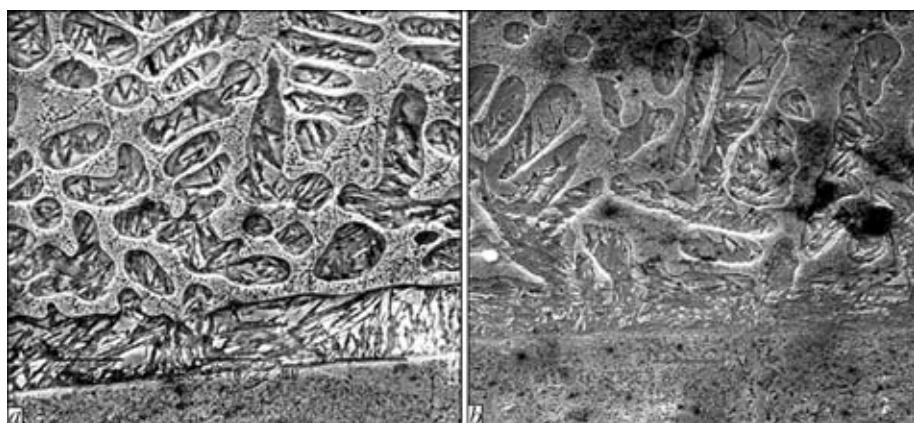


Figure 3. Microstructures ($\times 2300$) of high-chromium cast iron fusion zone obtained without (*a*) and with LRO (*b*) under scanning electron microscope

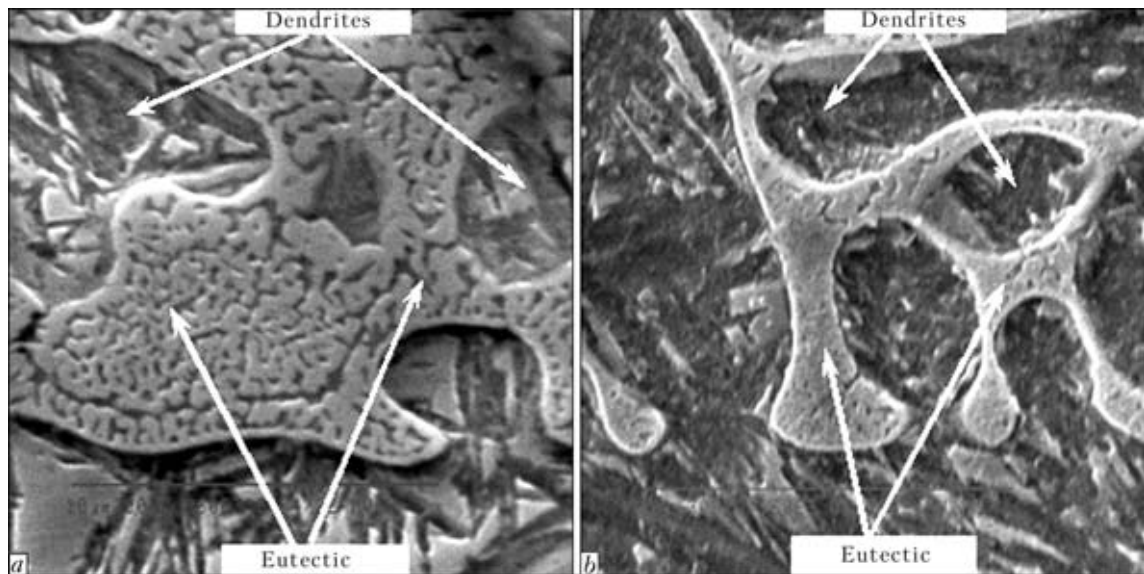


Figure 4. Microstructures ($\times 9600$) of fusion zone between steel St3 and high-chromium cast iron illustrating dendritic-eutectic structure produced without (a) and with LRO (b)

(minimum) and $5 \mu\text{m}$ (maximum) directly at the fusion line with thickness $\delta \approx 100-200 \mu\text{m}$. The similar trend to change in sizes of dendrites took place in the eutectic components of structure with size $D_{\text{eut}} \approx 15 \mu\text{m}$ (without LRO) and $D_{\text{eut}} \leq 8 \mu\text{m}$ (with LRO) (Figure 4).

In addition to differences in size, dendrites also exhibited differences in morphology of the phase components. Thus, dendrites had a characteristic non-equiaxed shape (e.g. sizes 15×10 , $15 \times 13 \mu\text{m}$, etc.) in structure of the deposited metal produced without LRO (Figure 4, a). In case of the application of LRO the shape of dendrites became more globular (e.g. $5-7 \mu\text{m}$) (Figure 4, b). In cladding without LRO, dendrites had a clearly defined orientation, i.e. mostly normal to the fusion line (columnar crystals) (see Figure 2, c).

The use of LRO promoted disorientation of crystal boundaries relative to the fusion line, the disorientation angle changing from 20° or more (see Figure 2, d). In case of LRO, the dendrites, especially of a small size, were characterised by higher hardness (approximately by 13–40 %). Hardness of the eutectic also increased approximately by 22–48 %.

The averaged values (5–10 measurements) of weight content of the main alloying element, i.e. chro-

mium, in dendrites and eutectic indicate to the fact that its content in the eutectic was higher than in the dendrites (Table). Chemical heterogeneity of chromium in the deposited metal produced with LRO was 1–5 %, whereas without LRO it amounted to 5–8 %. This is indicative of homogenisation of the content of chromium in the deposited metal when using LRO. Furthermore, increase in the chromium content (Figure 5) led to strengthening of the fusion zone and decrease in the probability of cracking.

Analysis of the results obtained allows a conclusion that the use of LRO in cladding with high-chromium cast iron leads to formation of more dispersed dendrites and eutectics in structure of the deposited metal, the degree of their dispersion increasing with distance to the fusion zone (Figure 6). The application of LRO promotes morphological changes in structural components of metal. They acquire the globular shape with disoriented crystal boundaries, this causing decrease in size of the dendrite spacings in crack initiation regions, i.e. in the base to deposited metal transition zone (Figure 6, b). The metal deposited with LRO has high hardness.

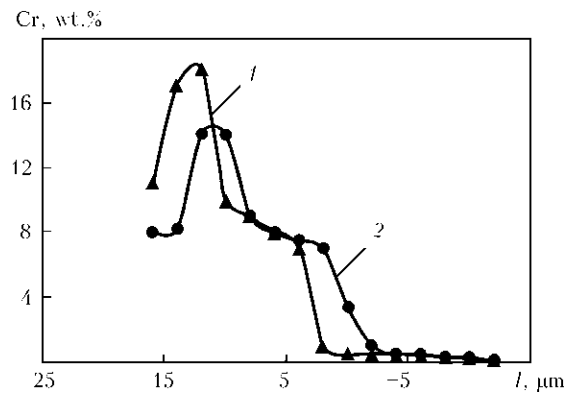


Figure 5. Dependence of content of chromium in fusion zone upon cladding parameters: 1 – without LRO; 2 – with LRO; l – distance from fusion line

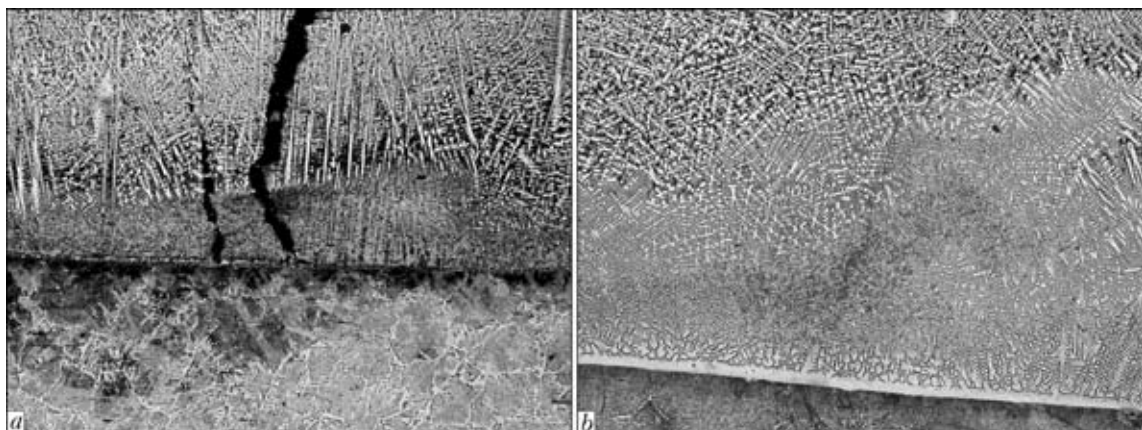


Figure 6. Microstructures ($\times 300$) of typical sites of initiation of cracks in deposited high-chromium cast iron produced without (a) and with LRO (b)

Structure of the deposited metal produced without LRO is characterised by the presence of columnar dendrites near the fusion zone (Figure 6, a). As a rule, cold cracks forming in the deposited metal have a clearly oriented character, i.e. they are arranged along the dendrites. The width of COD ranges approximately from 10–20 μm (near the origin of a crack) to 35–85 μm (as it propagates deep into the deposited metal). Formation of cracks occurs primarily along the interfaces between the dendrites and eutectic. The cracks initiate mostly within the fusion zone. It should be noted that the deposited metal near the fusion line about 10–20 μm wide has a pronounced acicular structure, consisting mostly of the martensitic component, this being confirmed by very high values of hardness (about HV 7400 MPa). At the same time, the deposited metal adjoining the fusion line is characterised by a coarse-grained structure and low hardness of the dendrites (about HV 2970–3300 MPa). The eutectic has low hardness (approximately HV 1400–1430 MPa).

Therefore, hardness in the fusion zone varies from HV 1400 to 7400 MPa. It seems that it is this fact that creates favourable conditions for initiation of cracks.

In a number of cases the cracks may also initiate in the cast iron deposited by using LRO. But in this case the cracks differ in size, character of propagation and COD, compared to the cracks that initiated without LRO (Figure 6, b).

Firstly, with LRO the cracks initiate not near the fusion line, but at a substantial distance from it (approximately 125–150 μm), i.e. in depth (in bulk) of the deposited metal. Secondly, the width of COD is about 2–8 μm , which is 10–15 times smaller than in cladding without LRO. Thirdly, the crack propagation path is of a wavy character. It is indicative of the presence of considerable barriers the crack collides with, the barriers being dispersed disoriented structural increased-hardness components of cast iron.

CONCLUSIONS

1. Low-frequency resonance oscillations applied to a workpiece, the frequency of which coincides with the frequency of natural oscillations of the workpiece (resonance conditions), affect the structure and mechanism of formation of cracks in cladding with high-chromium cast iron.

2. High-chromium cast iron deposited by involving LRO is characterised by an increased hardness, more uniform distribution of the main alloying element, i.e. chromium, between dendrites and eutectic, as well as by smaller sizes of the forming dendrites.

3. The metal deposited with LRO is much less sensitive to formation of cold cracks, which are characteristic of high-chromium cast iron.

4. To achieve the maximal efficiency of impact by LRO on the solidifying metal, it is necessary to build an upgraded automated equipment capable of controlling the frequency of external oscillations depending on the variable cladding conditions, weight of the deposited metal and temperature of a piece being clad.

1. Makarov, E.L. (1981) *Cold cracks in welding of alloyed steels*. Moscow: Mashinostroenie.
2. Pogodin-Alekseev, G.I., Gavrilov, V.I. (1966) Influence of elastic oscillations on solidification of metals and alloys. *Izvestiya AN SSSR. Metallofizika*, **1**, 80–101.
3. Boldyrev, A.M. (1976) On the mechanism of formation of structure of the weld metal with introduction of low-frequency oscillations into the weld pool. *Svarochn. Proizvodstvo*, **2**, 53–54.
4. Ryzhov, R.N. (2007) Influence of pulse electromagnetic actions on formation and solidification of welds. *The Paton Welding J.*, **2**, 49–50.
5. Russo, V.L. (1958) Study of the effect of elastic oscillations of different frequencies on solidification of the weld pool. In: *Welding*. Leningrad: Sudpromgiz.
6. Korytov, V.A., Gosteava, I.I., Butakov, B.I. (1995) Vibropulse treatment of steel in a pouring ladle — the effective method for increasing crack resistance of cast metal. *Stal*, **5**, 38–42.
7. Matyukhin, Yu.E. *Method for relieving residual stresses in welded joints on vessels and apparatuses, as well as on their elements*. Pat. appl. 2003136226/02 RF. Int. Cl. C 21 D 1/30. Publ. 20.05.2005.
8. Buryshhev, B.I. *Method for welding of metal parts*. Pat. appl. 2002125911/02 RF. Int. Cl. B 23 K 9/16. Publ. 27.02.2005.
9. Buryshhev, B.I. *Method for welding of metal parts*. Pat. appl. 2002125910/02 RF. Int. Cl. B 23 K 9/16. Publ. 27.02.2005.
10. Aristov, S.V., Russo, V.L. (1982) Solidification of weld metal at low-frequency oscillations of the melt. *Svarochn. Proizvodstvo*, **11**, 42–44.

LASER BASED GIRTH WELDING TECHNOLOGIES FOR PIPELINE CONSTRUCTION

S. KEITEL and J. NEUBERT

SLV Halle (Saale), Germany

To increase efficiency in pipeline construction, examinations on new welding processes for joining of pipes are indispensable. To this end, increasing productivity of the welding process but also requirements on the material are of immediate importance. Hence, a possible alternative is laser-GMA hybrid welding. The technological approach is the use of the laser typical deep penetration effect for the generation of a high quality free root pass or a complete weld in one step. The results of the technology and equipment developments and their performance under construction site similar conditions are given by this presentation. A high laser power and the advantages of its guidance via fiber optics allow the use of orbital welding.

Keywords: *arc welding, hybrid laser-arc welding, pipelines, welding technology, equipment, productivity of welding, construction site conditions*

For years well tested and proven arc welding processes have been applied for welding of large pipes of oil and gas pipelines. Depending on the length of the pipeline to be produced, the wall thickness of the individual pipes and the material they are made of, versatile variations of these processes are used, with a scope extending from manual arc welding with stick electrodes (Figure 1) up to the application of so-called orbital welding units using the MAG process. In this case the welding movement is not performed manually by the welder but fully mechanised using motor-driven systems and clamping rings across the entire circumference of the pipe. If permitted by the length of the pipeline and the profile of the ground, a number of these orbital units are used at the same time with every single station having been designed for welding of one or two passes and then being displaced to the next pipe joint to produce the same weld seam there. Such production aggregates often rely on several welding heads per unit [1] thus representing a high state-of-the art, both in relation to equipment and welding. This, however is connected with a high expenditure on personnel and plant engineering (Figure 2).



Figure 1. Cover pass of weld on a pipe in manual arc welding

Particularly with regard to the increasing focus on the supply of energy in Germany and Europe in the future the question of new and high-performance technologies in pipeline construction has arisen, in order to substantially meet the demand in the future.

A further increase of the performance in this area bears some problems, since the arc processes applied have obtained their physical limits concerning deposition efficiency and welding speed. Here, no essential increases can be achieved by optimizing the arc welding technology.

The development of welding processes of increased performance must be carried out under the following aspects:

- reduction of the number of passes at constant and improved seam quality, respectively;
- reduction of the number of welding stations and thus the expenditure on equipment and personnel.

Welding processes based on laser beam, on the one hand, offer the technology and, on the other hand, the equipment needed to fulfill this demand. In the following the proof of this shall be given.

Point of origin of technology and equipment. The application of laser-GMA hybrid welding is a promising technology for the future.

In laser-GMA hybrid welding both processes are combined, such that both the laser beam and the arc



Figure 2. Building site in pipeline construction

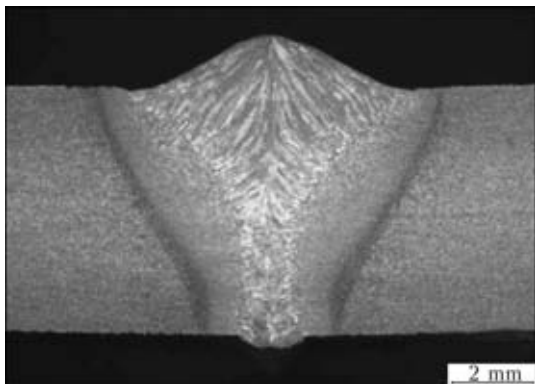


Figure 3. Formation of the weld in hybrid welding

act in a common melting pool. The result is more than simply adding both of the energy sources and the filler metal put in; it is rather that the resulting synergistic effects combine and enhance the advantages of the single processes. Thus, a joint profile is generated that is similarly deep as that obtained by laser welding, but has a considerably better gap bridging capability. Hence, on the field of thin sheets very high welding speeds can be obtained, which partly are many times the amount of the state-of-the-art of welding with shielding gases. With larger plate thicknesses the advantages are not within the area of welding speed, but there is rather the possibility of reducing the number of layers by single pass layers, often without additional joint preparation.

A typical formation of the seam for a sheet plate thickness of 8 mm using GMA, laser beam and hybrid welding are shown in Figure 3.

The fact that today the application of laser beam sources under construction site conditions is possible, is based on the rapid development in this field. Thus, beam sources of the latest generation, the so called fiber lasers, do not only cover the two-digit kilowatt range but also distinguish themselves by a sturdy and compact structure. In connection with a very high efficiency and an excellent beam quality the preconditions for a mobile application are given, which could not be executed using state-of-the-art conventional



Figure 4. Gulco orbital system for welding pipes

laser beam sources (CO_2 - or Nd:YAG lasers). In the last five years fiber lasers have been used as a mobile application in shipbuilding and in the production of pipes [2].

Laser-GMA hybrid welding of pipe connections under conditions similar to those on construction sites. *Objectives and technological approach.* The objective of the examinations on technology and equipment described in the following was the transfer of the state of knowledge of laser-GMA hybrid welding for the production of pipe joints, incorporating all necessary aspects such as tolerances, environmental influences, mobility of the entire equipment and welding out-of-position.

The focus of examinations was laid on the use of the laser typical deep welding effect for the production of a high quality free root pass at root faces of 6–10 mm. To this end, the different arrangements of the laser beam and the arc possible for hybrid welding of butt joints were compared to the different types of joint preparation.

The approach for the production of pipe joints was welding of two vertical-down seams being a common practice in pipeline construction and considerably reducing the types of freedom in the arrangement of laser beam and arc required for the technological optimum of the seam formation.

For the generation of a closed seam profile the weld head was extended by a further arc torch, thus enabling to weld the first pass using hybrid welding and the cover pass using GMA welding during one welding run. The objective was to produce a closed seam profile up to a plate thickness of 12 mm in one rotation. Further, this trailing process is a good opportunity to have a positive influence on the mechanical-technological properties of the weld seam.

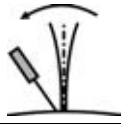
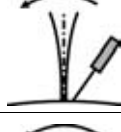
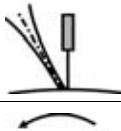
Equipment. In order to verify the principal feasibility of the laser-GMA process during girth welding the proven techniques were used.

The equipment for the examinations was a commercially available system for pipe welding by the Company Gulco (Figure 4). This system was equipped with a tractor on a ring guide for the generation of girth welding as well as with a contact seam tracking and weld scanning system based on two control axes for the transverse and height positioning of the process components to the weld groove. The arrangement of the contact sensor forwarding the welding process was executed in direction of movement.

Equipped with various stiffening elements, the adaptation of the weld head to the control axles for height control was executed. For transferring the possible serial types of arrangement of laser beam and GMA arc shown in Table 1, the hybrid welding head was equipped with additional degrees of freedom (Figure 5).

As shown in Table 1, either the laser or the arc was considered at neutral position each, for reasons of simplification. No intermediate levels were used.

Table 1. Serial arrangements of laser beam and welding arcs

Variation	Neutral process	Arrangement of the 2nd process	Schematic representation
1	Laser beam	Arc forward travelling	
2		Arc trailing	
3	Arc	Laser beam forward travelling	
4		Laser beam trailing	

Two different fibre lasers were used as laser beam sources. In the first phase, with the focus of investigation on root faces up to 6 mm, a system with an output of 4.5 kW (Figure 6, a) was used, and for phase 2 at a root face of 8 mm, a mobile 10 kW laser from the SLV Mecklenburg-Vorpommern was integrated to the test built-up (Figure 6, b). The 4.5 kW fiber laser from the year 2003 was one of the first sources of fiber lasers for welding within this performance class, having proven its long standing stability in many applications.

Figure 7 shows the completed welding head with the equipment for hybrid welding and the integrated second arc torch for welding the cover pass during one vertical-down weld movement.

Welding was performed on pipe pieces at lengths of up to 6 m. In this case larger tolerance results compared to a pipe with calibrated ends, in particular with regard to quality and misalignment of edges.

Through the integration of the components described, the entire test set-up shown in Figure 8 was realized.

Execution and results of the technological examinations. As already described in the previous section,



Figure 6. Overview of the laser systems used in the test: a – 4.5 kW fiber laser; b – 10 kW

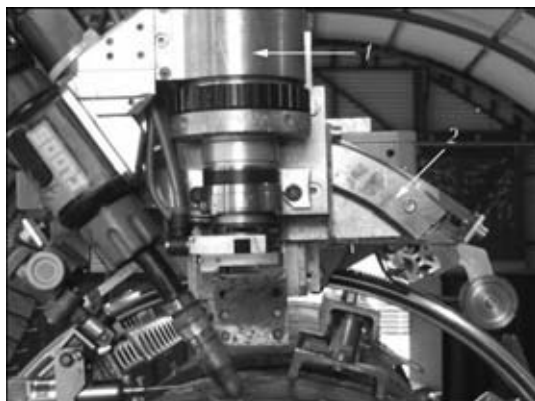


Figure 5. Mechanical realization of the degrees of freedom for changing the arrangement of laser and arc in series: 1 – hinge with holding device for swiveling the arc around the optic; 2 – curved guide for changes of angle of the process axes for joining

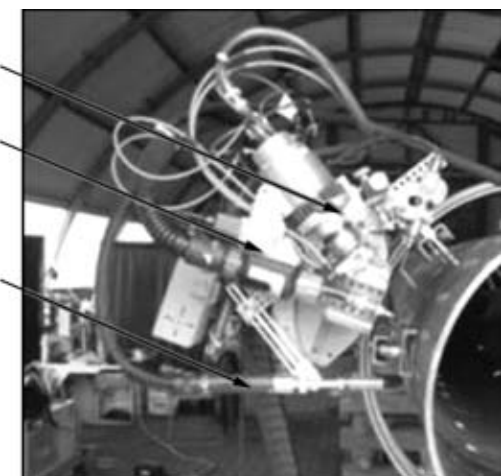


Figure 7. Welding head with hybrid equipment for root pass welding and arc torch for filler pass welding: 1 – laser optics; 2 – hybrid arc; 3 – arc torch for filler pass welding



Figure 8. Entire test set-up on the pipe

the test was performed using two laser beam sources of different output. In doing so, first the principal test series for determining the basic parameters for the hybrid arc and for determining the tolerance susceptibility of the hybrid process at continuously changing welding positions across the pipe circumference was performed in phase 1 using a 4.5 kW fibre laser. Test phase 2 served to estimate the potential of the hybrid process at higher laser performance at a simultaneous increase of the root faces for the root pass from 6 to 8 mm. To this end, a 10 kW fibre laser system was used.

For the execution of all test welds the following specifications were given:

- removing the internal coating from all edges;
- measuring the wall thickness, height and width of the root face of each edge;
- tacking of the joint with outside centering under the following parameter: longitudinal seam of the pipe to be joined abutting the longitudinal seam of the fixed pipe (increased conditions of tolerance);
- measuring the edge offset and air gap at tacked joint;

Table 2. Seam preparation and macrosections of hybrid-welded joints

Seam preparation	First pass	Closed seam profile
4.6 kW laser, root face of 6 mm		
6.5 kW laser, root face of 8 mm		

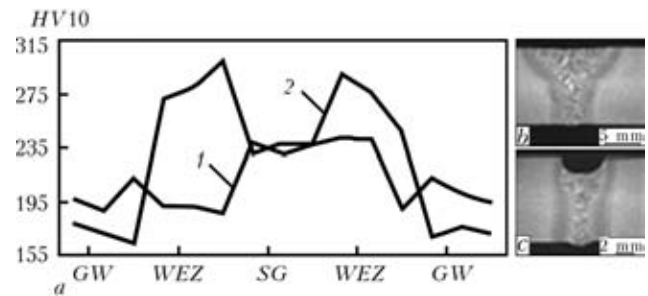


Figure 9. Influence of the trailing arc on distribution of hardness in the root area [3] (a), and macrosections obtained with (b) and without (c) backing: GW, WEZ, SG — spatial positions of the welding head

- adjusting the focus position and geometrical parameters is carried out for each joint again;
- guide edge for contact seam tracking is the fixed pipe;
- welding was performed in two vertical-down weld;
- aimed preparation of macrosections at 45, 90 and 150°, and at 315, 270 and 210° respectively.

In the following the results are shown in the form of macrosections both for the first hybrid welded pass and the closed seam profile by the trailing arc at a different variation of seam preparation at a laser output of 4.6 and 6.5 kW (Table 2).

Through the tolerances measured at the pipe joints and the welding parameters assigned today, there are considerable results on the different tolerances of the process.

The examinations were concluded by the determination of the distribution of hardness in particular in the root area of the weld seams, since this laser beam dominated area in the heat-affected zones could be susceptible to increased hardening. During these examinations, pure root welding without cover pass was compared to welding with closed seam profile through the trailing arc with the results being shown in Figure 9.

A decisive object of investigation was the determination of typical tolerances in pipeline construction and the examination of the influence of these tolerances on the hybrid welding process. During the trials

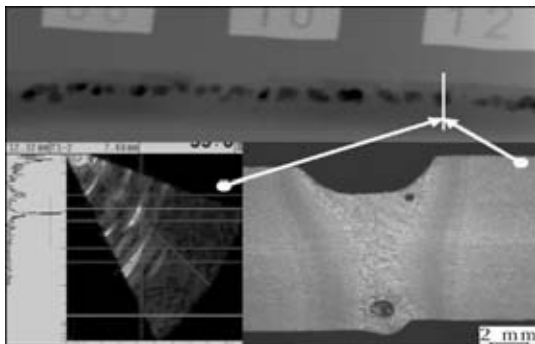


Figure 10. Correlation between cross section of weld and non-destructive methods

the pipe joints were positioned and fixed using typical tools and methods resulting in tolerances typical of pipeline construction. In order to draw conclusions from these tolerances during the future evaluations, the joining edges and the welded joints were measured.

The evaluation and interpretation of the weld quality took place on the basis of methods of non-destructive and destructive testing. First the welded pipe segments were investigated by phased-array (ultrasonic) and X-ray testing. Objective was to verify the detectability of imperfections by non-destructive methods and to establish the correlation to the cross section of the weld regarding dimension and location of these imperfections. The result of these investigations is shown as an example in Figure 10 [4].

The data recorded in such a way served both for developing different diagrams to show peak positions and directly comparing them to the welding result and with regard to the tolerances.

Further development of equipment and technology. The major objective of the investigations shown was to prove the principal suitability of hybrid welding for pipeline construction with regard to the more rough climatic conditions in this field of application. Here, important information with a great influence on the structural design of the equipment was obtained.

The following deficiencies could be summarized:

- the welding speeds to be obtained were too low;
- the objective is to obtain 3 m/min;

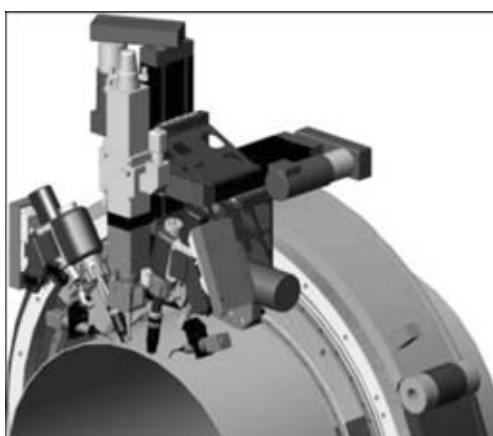


Figure 11. Design for the further development of equipment for hybrid welding of pipe joints

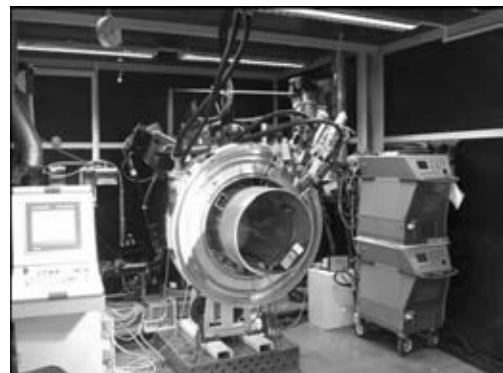


Figure 12. Specialized prototype of equipment for hybrid welding

- a position depending adaptation of the laser performance is necessary;
- the modification of direction and orientation, respectively, requires much time and is a source of failure due to the high number of adjustment steps;
- the existing technology does not comply with the requirements of the process as far as the mechanical properties are concerned.

The objective of the further development of the equipment was to increase the stability of the rotational movement along the pipe and to adapt it to the conditions of the hybrid process. Figure 11 shows the design of the more specialized prototype for hybrid girth welding.

The specialized prototype developed on the basis of this (Figure 12) for the realization of a girth welding movement for laser-GMA hybrid welding has the following technical data: traveling speeds in positioning – up to 6 m/min, in welding – up to 3 m/min; pipe diameters processed – 500–700 mm; change of the parameters depending on position; and seam tracking and guidance system.

The integrated laser working head allows coupling with all fiber guided solid-state lasers of outputs of up to 20 kW.

A further focus of the current examinations has been laid on the optimization of the process for pipe wall thicknesses starting from 10 mm at different root faces for the first pass to be welded using a laser, namely the 12 kW fiber laser system available at the SLV Halle since January 2009 (Figure 13).



Figure 13. Fiber laser system YLS-12000



Figure 14. Radioscopic exposure of overlapping of the weld starts (12 o'clock position)

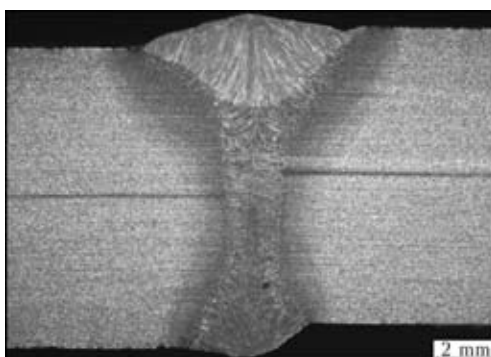


Figure 15. Macrosection of welded joint at misalignment of edges of 1 mm

The focus of the examinations, on the one hand, was directed to investigate the possibilities of the formation of the seam and the root with the laser output available and, on the other hand, on the overlapped areas at the weld start obligatory when welding two vertical-down seams at the circumference of the pipe. Figure 14 is showing the result of the radiographic testing in the overlapping area of the start areas for a pipe wall thickness of 10 mm.

The weld areas were tested on internal imperfections metallographically. To this end, pipe typical tolerances were considered in order to make statements about the influences of higher laser power and increased welding speeds on the weld formation with regard to different tolerances. Figure 15 is showing the formation of the seam at 3 o'clock position for a pipe wall thickness of 10 mm, for higher laser outputs too.

This phase of examinations was concluded by performing material tests for determining the mechanical-technological characteristic values for the test material L360NB. The results of the tensile test are shown in Table 3, while the notched bar impact work at a temperature of 0 °C is shown in Table 4.

Summary and outlook. In order to increase efficiency in pipe line construction, examinations of new welding processes for joining of pipes are indispensable with the focus on increasing the welding speed at a reduced number of passes. A possible alternative is the laser-GMA hybrid welding process, since due to the development of the fiber laser a beam source with new fields of application is available [3].

The objective of the investigations presented was to prove the principal suitability of hybrid welding for pipeline construction as well as the behaviour of

Table 3. Results of the tensile test*

Yield strength $\sigma_{0.5}$, MPa	Tensile strength σ_t , MPa	Elongation of fracture δ , %	Contraction of fracture ψ , %
345	532	42	71
368	539	39	69

* Position of fracture — base metal.

Table 4. Results of the V-notched bar impact test

T , °C	Dimensions, mm		Impact toughness, J/mm ² , at impact work, J			
	a	b	1	2	3	M
0	7.5	8.0	201	128	77	136
	7.5	8.0	180	181	169	177

this process in out-of-position welding which is required for its application.

Furthermore, both closed seam profiles were produced and hardening increase of the heat-affected zones of the root area were reduced for a pipe wall thickness of 10 mm for an arc process trailing the hybrid welding.

The results distinctively show the potential of the hybrid process at high laser output and with brilliant beam qualities. In a next step of the examinations the results are to be transferred to larger pipe wall thicknesses.

As an alternative of the existing approaches [5] there is the idea of using the hybrid process for the production of a high quality root pass at root faces of 12–15 mm. This approach is the basis of the examinations currently performed.

Acknowledgements. The authors gratefully acknowledge funding of the Federal Ministry of Economics and Technology. We express our further thanks to the industrial partners Verbundnetz Gas AG, Friedrich Vorwerk Rohrleitungsbau GmbH & Co. KG, Carl Cloos Schweißtechnik GmbH, Gullco International Ltd. and Bergrohr GmbH participating in the project for their support in transferring the tests into practice as well as Mr. Stuch, Stuch GmbH & Co. KG for advising us.

- Blackman, D., Dorling, V., Howard, R. (2002) High-speed tandem GMAW for pipeline welding. In: *Proc. of 4th Int. Pipeline Conf.* (Calgary, Alberta, Canada, 2002), 517–523.
- Keitel, S., Jasnau, U., Neubert, J. (2008) Applications of fiber laser based deep penetration welding in shipbuilding, rail car industries and pipe welding. In: *Proc. of 4th Int. Symp. on High-Power Laser and their Applications* (St. Petersburg, 24–26 June 2008).
- Keitel, S., Neubert, J., Stroufer, M. (2009) Laser based girth welding technologies for pipelines — GMAW gets support. In: *IIW-Tagung* (Singapore, 12–17 July 2009).
- Schwalenberg, C. (2008) *Technologieentwicklung fuer das MSG-Laserstrahlhybridschweissen in Zwangslagen an hochwertigen Rohrleitungswerkstoffen:* Diplomarbeit. Hochschule Merseburg.
- Gumennyuk, A., Gook, S., Lammers, M. et al. (2009) High power fibre laser welding for pipeline applications. In: *Proc. of 5th Int. Congress on Laser Advanced Materials Processing*.

EXPERIENCE OF MANUFACTURE AND APPLICATION OF SEAMLESS FLUX-CORED WIRE FOR ELECTRIC ARC WELDING*

V.N. SHLEPAKOV and A.S. KOTELCHUK

E.O. Paton Electric Welding Institute, NASU, Kiev, Ukraine

Design features of seamless flux-cored wires designed for electric arc welding are considered. Their technical and economic advantages and disadvantages have been analyzed. Process flowsheets of manufacturing seamless flux-cored wires with filling of the pre-welded tubular billet, as well as with continuous filling of U-shaped profile of tube billet with subsequent welding of wire sheath longitudinal butt are described.

Keywords: *electric arc welding, seamless flux-cored wire, flux-cored wire manufacturing technology, its advantages and disadvantages*

Wire with a powder or flux core, which is enclosed into a metal sheath, is called flux-cored wire (Figure 1). Wires, in which the core consists of a mixture of metal powders or just the metal powder, are also included into the flux-cored wires. Such wire is called metal-core, i.e. wire with a metallic core. A metal billet capable of withstanding considerable plastic deformation (forming, reduction) is used as the sheath in flux-cored wire manufacture [1].

Among the flux-cored wires designed for electric-arc welding of steels, so-called seamless flux-cored wires in which the core is enclosed into a monolithic sheath, have a special place. Owing to the sealed structure, such flux-cored wires have a number of specific properties, which it is difficult or often practically impossible to ensure in rolled flux-cored wires, having a butt joint in the sheath.

Technical solutions on flux-cored wire manufacture. Method of flux-cored wire manufacture from large castings or forgings was one of the first to be tried out. Technology of manufacturing solid wire is quite well-established in metallurgical and hardware production. However, filling of a large billet with powder filler runs into serious technical difficulties already at the stage of primary processing – hot rolling. At traditional rolling methods by the forming sequence of ring–square–ring billet fracture occurs even at their slight filling. Change of the sequence of rolled stock forming or inclusion of the operation of swaging leads to a significant increase of processing operation cost. Nonetheless, this technology is still finding limited application. It has the advantages of the use of known technical means and methods of metal processing to achieve a sufficiently moisture-

proof wire, as its core is reliably protected from moisture. Complexity of solving the metallurgical problems at multiple heating of the billet, need for a large quantity of equipment and energy consumption in manufacture can be regarded as the disadvantages of the above technology.

Manufacturing moisture-proof wire and possibility of application of known technologies for its processing, form the base of the process of flux-cored wire manufacturing from a tubular billet. An extended welded tube with a longitudinal seam is used, with high requirements made of the seam quality.

Over the recent decades production technologies have been developed for manufacturing seamless flux-cored wire from thick-walled strips in one process line: forming, filling with flux, welding of the sheath butt, reduction and achievement of the requirement diameter.

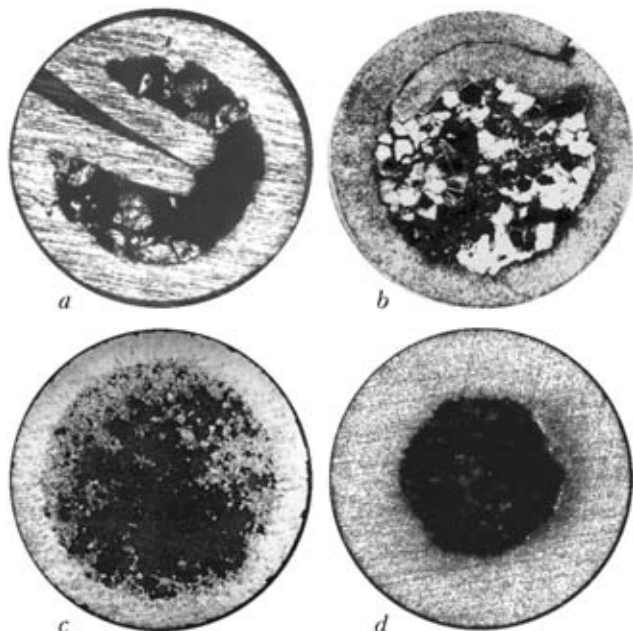


Figure 1. Different designs of flux-cored wire sheathes: *a* – rolled with double bending of edges; *b* – rolled with edge overlapping; *c* – seamless wire manufactured by continuous filling of U-shaped profile of tube billet with flux with subsequent welding of the longitudinal butt of the wire sheath; *d* – seamless wire manufactured by filling pre-welded tubular billet

* Based on a presentation made at the V International Conference «Welding consumables. Technologies. Manufacture. Quality. Competitiveness» (Artyomovsk, June 7–11, 2010).

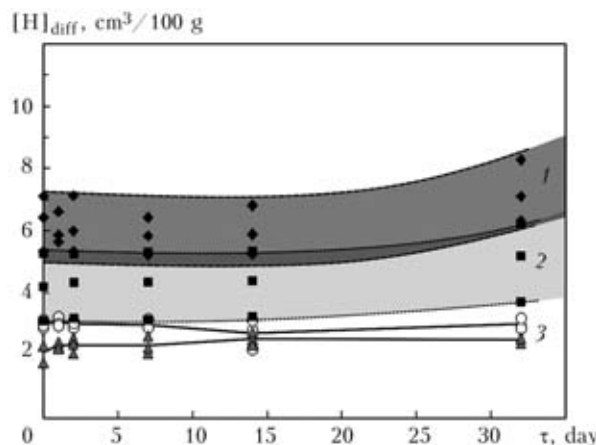


Figure 2. Content of diffusible hydrogen $[H]_{\text{diff}}$ in the metal deposited with flux-cored wires of different types: 1 – seamless [3]; 2 – rolled but with treated charge and surface; 3 – conventional rolled wire after storage in the shop [3]; τ – soaking time

ter. Positive results were obtained in welding of a tubular sheath by high-frequency resistance welding and recently – by the laser.

The advantages of the above technology are absence of hot rolling, moisture-proofness of the manufactured wire, applicability of traditional processes of reduction, heat treatment and protective coating application, and the disadvantages are the need to solve metallurgical problems in development of the core compositions and heat treatment of wire billet, apply high-quality agglomerated flux produced by special formulas, as well as considerable power consumption. Nonetheless, this process is applied commercially in a number of countries (Air Liquid Welding Group-Oerlikon, France-Switzerland; Drahtzug Stein, Germany; Nippon Steel, Japan).

Main features of seamless flux-cored wires are as follows:

- core is not humidified, so that diffusion hydrogen content in the deposited metal of less than $5 \text{ cm}^3/100 \text{ g}$ is guaranteed;

- copper coating of the surface provides certain protection from surface corrosion and ensures better electric contact, promotes reliable fusion of the edges;
- alloying and microalloying elements can be used to give special properties to the weld metal;
- stability of wire shape along its entire length is ensured, allowing application of feed mechanisms with one roller pair;
- welding efficiency increases approximately 1.5 times compared to solid wire.

Main technological advantages of seamless flux-cored wires are achieved owing to ultra-low hydrogen content in the weld metal that allows preventing cold cracking in welding of high-strength steels or lowering the temperature of preheating required before welding [2].

Owing to an absence of a slot in the flux-cored wire sheath and protective coating on its surface, a low content of diffusible hydrogen in the deposited metal is guaranteed even at long-term storage of the wire (Figure 2).

Accuracy of feeding flux-cored wire to the welding point by the data of [3] is much higher than that of rolled flux-cored wires in most of the cases (Figure 3). Small longitudinal depressions on the wire surface are the possible defects resulting from excessive pressure of the feed rollers on the seamless wire [4].

Seamless wires have certain disadvantages of technical and economic nature: practical absence of the possibility of manufacturing self-shielded wires; limitations on addition of low-melting materials to the core; need to apply liquid glasses for agglomerated flux; capital costs for seamless wire manufacture are by an order of magnitude higher than for rolled flux-cored wire; considerable power consumption in manufacture; high finished product prices (for instance, for seamless flux-cored wire they are 1.5–2 times higher than for rolled wire).

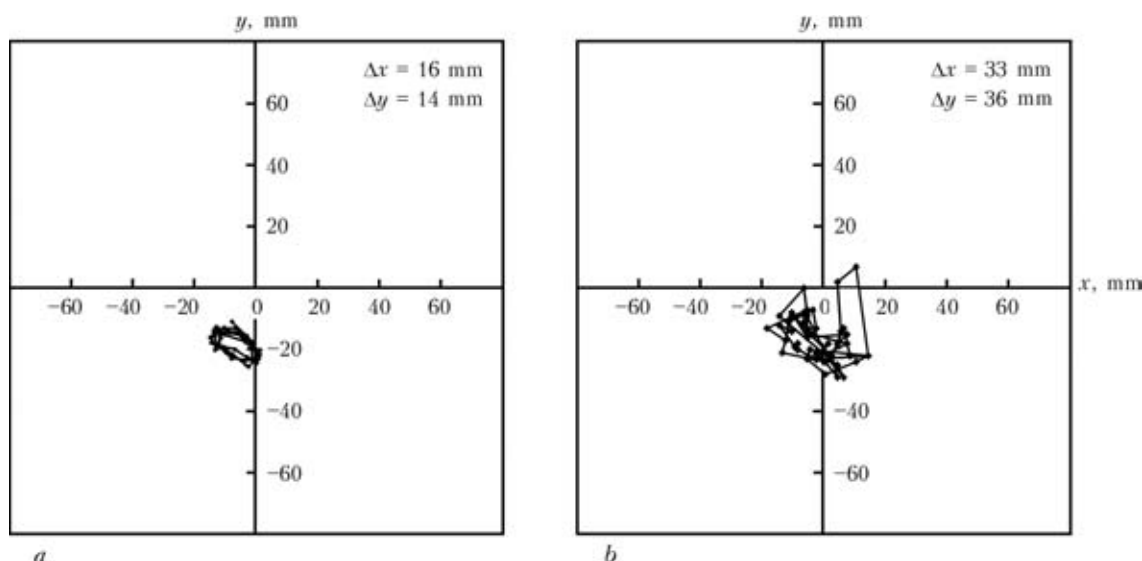


Figure 3. Accuracy of feeding seamless (a) and rolled (b) flux-cored wires of 1.2 mm diameter by a straight welding torch at 150 mm extension to the point of welding [3] (top view of welding plane, ordinate axis indicates the direction of welding torch motion): Δx , Δy – average deviation of wire hitting point from the aiming point across and along the welding direction, respectively

Advantages and disadvantages of flux-cored wires compared to solid wires

Welding flux-cored wires	Disadvantages	Advantages
<i>General</i>		
Seamless tubular	No possibility of manufacturing self-shielded wires Significant limitations on addition of low-melting substances Need for application of liquid glass for production of filler – agglomerated flux	Possibility of achievement of high properties (in particular, impact toughness) at low temperature Low susceptibility to cracking, particularly hydrogen-induced cracking, in the metal of weld and welded joint High technological properties in welding in shielding gases Possibility of microalloying to ensure special properties of weld metal
Rolled	Difficulty of ensuring a low hydrogen content (need for drying, baking) High fume level in welding with self-shielded wires	Possibility of achievement of high values of strength and viscoplastic characteristics in welding low-alloyed and alloyed steels High welding technological properties Possibility of welding performance without additional shielding High welding process efficiency (particularly with wires of metal-core type)
Solid	Need to ensure complex alloying Electrode metal loss for spattering Need to apply additional shielding of molten metal	High stability of ensuring the specified composition and properties at low alloying level Reliability of feeding through hoses of semi-automatic welding machines Convenience of application in robotic process Absence of slag crust on weld surface
<i>Technico-economic</i>		
Seamless tubular flux-cored	High manufacturing costs, considerable power consumption High finished product prices Slag removal costs	Possibility of copper coating or application of other coating types on the wire surface Application at different methods of mechanized and automatic welding Longer storage life with preservation of welding properties Application in welding of alloyed steels
Rolled flux-cored	Difficulties of feeding wires with a thin sheath Slag removal costs (except for wires of metal-core type)	Application for all the processes of automatic and robotic electric arc welding and surfacing Possibility of cleaning and treatment of the surface with special coatings Adaptation to welding conditions (application in mounting) Low manufacturing cost, particularly of wires of alloyed types
Solid	Cost of spatter removal and weld shape finishing High cost of wires of alloyed types	Possibility of application of any coating types on the surface Suitability for all the mechanized and robotic welding processes Longer storage life with preservation of welding properties Low manufacturing cost, particularly of wires of low-alloyed types

Most of the world manufacturers of flux-cored wires apply the technology of its production from cold-rolled strip. The wire is made in one process line, which includes a unit for forming wire of different designs with a built-in operation of continuous filling by a mixture of powders and multi-die machine, where the wire is reduced to the required size.

The advantages of such a technology of flux-cored wire manufacturing are a small number of equipment and personnel, low power consumption, possibility of manufacturing wires in a wide range with fast rearrangement of production. This technology uses roller reduction, various methods of producing the wire billet and treatment of the finished wire surface for coating deposition, thus giving it special properties.

Flux-cored wire is supplied only with application of standardized methods of winding and packing. So, plastic reels or wire frames are packed into film or foil, and then into cardboard, metal or plastic containers of Marathon type. According to ISO standards,

application of continuous inspection with strict documenting of the procedures is envisaged. Up-to-date equipment of production process control is widely used, and qualified personnel are involved, ensuring a stable product quality.

Generalized data on production and application of flux-cored wires for electric-arc welding, compared to solid wires, is given in the Table.

Technology of seamless flux-cored wire manufacturing. Among the currently available technological processes of seamless flux-cored wire manufacturing, the process envisaging filling of the finished (pre-welded) tube with flux, differs essentially from the process of continuous filling of the tube with flux (charge) with subsequent welding of the butt of wire sheath by high-frequency current or laser.

PWI conducted research and pilot-production work for a number of methods to manufacture seamless flux-cored wires, starting with producing various billets by hot rolling and including the above-given proc-



esses. Work on specific problems of the technology of manufacturing seamless flux-cored wires and specialized equipment is carried on at present.

In these subjects let us single out those aspects, which, in the opinion of our specialists, are essential for achievement of the desired results.

Seamless flux-cored wire with filling of a pre-welded tubular billet [4]. Initial billet is a strip from low-carbon steel of hot (after etching and neutralization) or cold rolling, which is unwound through accumulator-regulator and is fed into a forming driving machine for forming into a tube with a slot (clearance) with a high accuracy of edge straightening. The next technological stage in the flow chart is making the butt joint by high-frequency resistance welding with a controlled thermal cycle, as well as reduction and calibration of the tubular billet. Tubular billet is wound into bundles and cleaned, which is followed by quality inspection. The next stage is intermediate annealing and drawing of the tube for the design size for filling with flux. Annealing is performed at the temperature of 600–700 °C in shaft furnaces heated by gas or electricity, and even though annealing is incomplete, it allows eliminating the consequences of cold deformation and relieving internal stresses.

The main specialized stage of flux-cored wire manufacturing includes two operations – winding of the tubular billet on a frame (reel) and vibration filling with agglomerated flux. Winding is performed in rows turn-to-turn with rigid fixation. As a rule, from 500 to 1000 m of the tubular billet is wound on the reel. Initial pipe dimensions are from 9 up to 15 mm in diameter (on the outside), and pipe wall thickness is from 1.8 up to 2.0 mm.

Depending on the drive power, one or two reels with the tubular billet are fastened on the vibration feeder. Vibrating table is brought into the working mode by a powerful electric motor with a short-circuited rotor (three-phase). Vibrating conveyor makes fast sinusoidal motions, controlled by unbalanced mass. Owing to symmetrical oblique motions of the carrier, flux particles are brought into motion to both

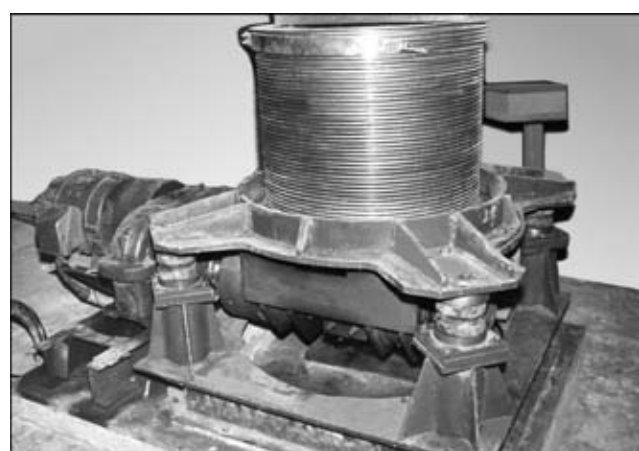


Figure 4. Spiral-vibration unbalanced conveyor for filling tubular billets with charge developed at PWI

sides by an elliptical trajectory along a circumferential guide. In the steady-state mode the powder filler moves smoothly in the tubular billet up to its complete filling (Figure 4).

Powder can be fed into the tubular billet from a hopper through a connecting hose. A transparent hose is put onto the free end of the tubular billet to monitor the full flowing of powder. Following the procedure developed at PWI, flux-powder is fed at a controllable rate into the tubular billet by special narrow-jet feeder, which prevents formation of «plugs» and powder ejection by the air flow pressed out of the tube. The outgoing end of the tubular billet ends in a throttle insert [5]. The unit of PWI design is also fitted with a device for continuous recording of vibration trajectory, which is important both in setting up of the working mode and in billet filling, considering that the mass of the filled flux-cored wire billet increases by 15–20 % by the moment of process completion.

Agglomerated flux for flux-cored wire is manufactured by the traditional procedure. Its drying-baking is performed at the temperature of 250–300 °C. It is taken into account here that high-temperature baking will be continued at intermediate annealing of the semi-finished product of the seamless flux-cored wire.

Flux-cored wire manufacturing from flux-filled semi-finished product includes the following operations: intermediate dry drawing and annealing, finishing drawing to the specified size and application of a copper coating.

Intermediate drawing is mainly performed using drawing mills (five- or six-fold) with drawing drum diameter of 600 mm and drawing speed of 5–6 m/s. Intermediate annealing is performed at wire diameter of 5.4–5.5 mm (initial billet diameter of 11–12 mm) and 4.7–4.8 mm (initial billet diameter of 9–10 mm). If it is required to manufacture wire of 1.0–1.2 mm diameter, then it is desirable to perform annealing at wire intermediate diameter of 3.6 mm.

Fine drawing, copper coating and winding on product carriers (reels and bobbins) and wire forming into bundles in case of supplying in Marathon type containers are well-known operations in manufacture of the majority of flux-cored wire types.

A special feature of the technology of seamless flux-cored wire manufacture is monitoring wire filling with charge (flux) before copper coating [4].

An instrument of FKG type of Oerlikon design envisages application of slot-type sensor, and KZP type instrument developed by G.V. Karpenko Physico-Mechanical Institute of the NAS of Ukraine (Lvov) – application of a double-loop sensor [6]. Both instruments include a system of measurement of saturation magnetic flux of metal section. A differential method (comparison of the checked tube with the reference one) is used to increase measurement accuracy. Unfilled wire regions are registered. However,

recording the vibrations during wire filling requires individual setting up of the measurement modules at control of each wire type.

Seamless wire in flow-line production. The most often used for seamless flux-cored wire manufacturing are two processes similar in their sequence, in which filling of the formed tube, subsequent closing of the profile and welding are performed successively in a flow with forming and reduction of the tube filled with flux. Continuous flow of the performed operations allows avoiding shifting of the powder filler before its compacting at reduction.

Essentially similar to the earlier considered technology is the technology of agglomerated flux manufacturing, which includes a number of known operations, namely dry mixture preparation by a specified formula, dry mix mixing with liquid glass, granule balling, flux baking, its sieving, followed by crushing of coarse particles. The difference consists in higher temperature of drying-baking (usually 350 °C) and soaking to cooling in tight steel containers before flux sieving to lower hydrogen content. Such a technological operation can be sufficient for manufacturing rutile-type flux-cored wires and insufficient for wires of low-hydrogen type, if subsequent degassing (baking) is not envisaged here.

Seamless flux-cored wire with continuous filling of the tube with flux and laser welding of the tube butt. Technology is designed for relatively small production. Depending on fitting of one process line, production output from 1000 (at two-shift operation) up to 2000 t/year (at three-shift operation) can be achieved.

The technology is based on forming U-shaped tubular billet, pouring dosed powder into its profile, roller closure and laser welding of the tube butt with subsequent cooling and reduction of the wire billet by cold rolling to manufacture the semi-finished product. Reduction of the semi-finished product is performed in two stages by cold rolling, using four- or eight-stand rolling-on machines up to producing wire of the specified diameter (1.2, 1.4 and 1.6 mm). Reduction can be followed by intermediate low-temperature annealing of the semi-finished product. The following final operations (final calibration, cleaning, copper coating and winding on product carriers) are typical for all the processes of seamless flux-cored wire manufacturing.

The main part of the process up to producing a wire billet from cold-rolled strip is performed in one process line, fitted with a unit for strip unwinding from the reels. Such process reels take up to 1 t of the strip. The strip is fed to edge preparation device through tension regulator, and then to the unit for liquid degreasing of the strip. Prepared strip comes to the forming machine with a built-in flux metering device. Closed tubular billet with a fixed position of the tube sheath butt is fed to laser welding section.

Acceptable welding quality is achieved at CO₂-laser power from 6 up to 10 kW and up to 15 m/min welding speed. After the cooling chamber the welded billet is fed to the billet reduction section of the five-stand roller mill. The result of the flow process is semi-finished flux-cored wire product of 7.0 to 7.5 mm diameter, which is wound on the process reel.

The next stage includes two- or four-stage cold rolling of the semi-finished product to the specified size. Proceeding from wire diameter, this process stages are arranged in such a sequence: in the first mill at the inlet – 7.0–7.5 mm, at the outlet – up to 3.0 mm, with intermediate diameter of 4.6 mm; in the second mill at the inlet – 3.0 mm, at the outlet – 1.2 mm, with 1.9 mm intermediate diameter.

Technico-economic parameters of production indicate that this technology is not a high-cost one, owing to a rational application of the equipment and small capital investments into automation and measuring instrumentation (in particular, filling of the strip U-shaped profile is monitored by the instrument measuring the level of flux layer in the profile). Use of small process cans of unified dimensions favours cost reduction, but requires additional reloading and respective setting up of the equipment, which results in the coefficient of main equipment utilization not higher than 0.80–0.85.

PWI studied the main processes of the technology and provided solutions on sound cleaning of the strip and the wire, continuous control and monitoring of the wire filling with flux. Work on improvement of laser welding technology, the realization of which is insufficiently reliable in modern production, is carried on now.

Seamless wire with continuous filling of the tube with flux and high-quality resistance welding. The technology is designed for continuous mass production with a high quality and level of automated system control. Block-diagram of the main technological process (up to manufacturing of the semi-finished seamless flux-cored wire product) is similar to that described above. The main difference consists in the process of tube butt welding. This technology uses induction-resistance high-frequency welding with controlled parameters. The main components of the process flowchart are sound (as to accuracy) forming of the tubular profile with edge closing, billet filling with flux using an automated feeder, closing of profile edges, welding of the tube longitudinal butt, controlled cooling, reduction of flux-filled tube up to compaction of the core and calibration (with preliminary flash removal, if required) [3].

Stable welding quality is ensured by a system of automatic control, maintaining the specified level of heat input at variation of tube movement speed. If at application of standard equipment for high-frequency welding temperature fluctuations in the butt center reach 150–170 °C, the control system allows keeping



temperature fluctuations within $\pm 12^\circ\text{C}$ of the specified value (about 1250°C).

After welding the flux-filled tube cools down. The rate of air cooling to the temperature below 500°C (martensite transformation temperature) is controlled.

Reduction of the filled tube up to core compaction and calibration by shape and size are performed in a flow in a forming device (4×4 roller stands). This operation additionally includes a block of tube welding quality control by various NDT techniques (using ultrasound, eddy currents).

After passing the main manufacturing stage, the seamless wire billet is subjected to annealing in flow units using induction heating. This operation is particularly important when manufacturing flux-cored wires with stainless steel sheath.

Further technological process follows the typical technology, including roller cold rolling, drawing through standard or roller dies. The final operations of cleaning, copper coating and winding on product carriers are performed in typical equipment for wire manufacture.

It should be taken into account that equipment power inputs essentially depend on the diameter and wall thickness of the tubular billet, as well as forming and reduction rate. Electric power of the unit for high-frequency welding at increase of working speeds of forming-reduction from 50 up to 120 m/min increases from 100 up to 150 kW. Power of the unit for semi-finished product annealing increases accordingly. Despite the applied engineering solutions and automation of operations, capital costs for production by this technological scheme, as well as energy carrier costs are not high. Such production will only be effi-

cient with large product outputs (more than 10,000 t/year) and quite high wire prices.

CONCLUSION

Presented technologies of manufacturing seamless flux-cored wire require a rather considerable volume of investments for their implementation, feature high power consumption and require involvement of highly-qualified personnel (particularly, for ensuring sound forming and welding).

Technical characteristics of the produced product have certain advantages compared to solid wires and rolled flux-cored wires. The main of these advantages is a low level of hydrogen content in the weld metal. Market prices for seamless flux-cored wires are 1.5–2 times higher than the prices of rolled flux-cored wires. In this connection, a specific sector of welding consumables market should be found, where the achieved advantages will justify the costs.

1. Pokhodnya, I.K., Shlepakov, V.N., Alter, V.F. et al. (1980) *Manufacturing of flux-cored wire*. Kiev: Vyshcha Shkola.
2. Nobutaka, Yu., Tadashi, K. (1995) A chart method to determine necessary preheat temperature in steel welding. *Quarterly J. JWS*, 13(3), 347–357.
3. Shimura, K. (2008) *Seamless flux-cored wire*: Presentation of Nippon Steel & Sumikin Welding Co. at Japan Int. Welding Show 2008 (Tokyo, Apr. 9–12, 2008).
4. Samorodov, I.G. (2007) Specifics of manufacturing and application of seamless flux-cored wires. In: *Proc. of Int. Sci.-Pract. Conf. on Welding and Related Technologies in Construction, Reconstruction and Repair of Gas Pipelines* (Moscow, 22–23 Nov. 2007).
5. Pokhodnya, I.K., Poturaev, V.N., Chervonenko, A.G. et al. (1983) Solution of problems of vibration filling of pre-welded tubular billets of flux-cored wires by loose charge. In: *Abstr. of Papers of All-Union Conf. on Welding Consumables* (Cherepovets, 10–14 Oct. 1983). Kiev.
6. Panasyuk, V.V., Teterko, A.Ya., Pokhodnya, I.K. et al. (1975) Continuous control of flux-cored wire filling with charge during its manufacturing. *Avtomatich. Svarka*, 5, 48–49.

DEVELOPMENT AND PUTTING INTO PRODUCTION OF TECHNOLOGIES AND EQUIPMENT FOR ELECTRIC WELDING OF LIVE TISSUES (Innovation project of the NAS of Ukraine fulfilled by PWI)

A new generation power source and its operation algorithm were developed for HF welding of live tissues at 440 kHz frequency, which have passed full-scale testing on animals at PWI. A new concept of electrosurgical tool designed for mass application has been developed and verified in practice. A study with recording of electrical parameters in HF welding of live tissues and analysis of the influence of parameters and process control algorithms on welded joint quality have been performed, in particular directly in the clinical conditions. Obtained results form the base for further development of new equipment and process control systems.

CAPABILITIES OF APPLICATION OF HIGH-STRENGTH LOW-ALLOY PIPE STEELS FOR MANUFACTURE OF HIGH-PRESSURE VESSELS

V.M. KULIK, M.M. SAVITSKY, V.P. ELAGIN and E.L. DEMCHENKO
E.O. Paton Electric Welding Institute, NASU, Kiev, Ukraine

Technical capabilities and rationality of manufacturing mobile combined high pressure vessels of small specific weight are considered. Low-alloy low-carbon steels of higher and high strength and large diameter pipes can be used for shell billets. Butt joints acceptable in terms of properties and cyclic fatigue life are produced by multilayer submerged-arc welding, and they can be improved by arc treatment with a partial melting. Welded case is subjected to annealing without performing high-temperature strengthening and is reinforced along the cylindrical part by a composite material of a high specific strength.

Key words: *submerged-arc welding, high-strength low-alloy steels, high-pressure vessels, welded joints, argon arc treatment, thermal cycle, structure, mechanical properties, cyclic life, specific weight*

As international experience shows the operative gas supply of such small enterprises as farms and other is reasonably to perform using mobile high pressure vessels of a small specific weight M/V , the designs and technologies of manufacture of which are developed by a number of companies. For the sea supply of liquefied natural gas it is offered to manufacture of cylinders-storages of $V = 16 \text{ m}^3$ ($M/V = 1.7 \text{ t/m}^3 (\text{kg/l})$) capacity and to use them at low frequency and number of loading cycles.

Reduction of specific weight and increase of cyclic life of high-pressure vessels is achieved by their reinforcement with materials of a high specific strength [1, 2]. The earlier developed technological process of manufacturing combined vessels (cylinders) of 219–360 mm diameter for using natural gas in capacity of automobile fuel includes A-TIG + TIG welding (without edge bevel) of longitudinal and circumferential welds of a shell and bottoms produced of sheet steel 30KhGSA of 3.5–6.0 mm thickness, high postweld tempering, forging of longitudinal weld, hardening and tempering to provide necessary level of strength ($\sigma_t = 950\text{--}1000 \text{ MPa}$) [3]. The automobile cylinders are characterized by required serviceability under the conditions of everyday filling and using energy carrier and by small specific weight $M/V = 0.65\text{--}0.75 \text{ kg/l}$. However small capacity (30–60 l) causes limitation of practical possibility of gas supply by such cylinders. For considerable increase of their capacity it is necessary to increase diameter up to 600–1000 mm and thickness of wall (using alloyed steel) up to 10–17 mm. The preparation and assembly of edges for welding becomes more complicated, the need in pre-heating arises, duration of welding process is 3.5–25 times increased ($v_w = 3.0\text{--}4.5 \text{ m/h}$), consumption of

electric power energy and argon, and formation of burnt spot on the surface of steel body during quenching in oil complicates its dressing.

In this paper the improvement of technological efficiency of manufacture of the combined high-pressure vessels of a small specific weight for operative gas supply of single consumers is considered. This can be achieved using large-diameter pipes of low-alloyed steels of higher strength and applying more efficient welding using consumable electrode.

The optimal combination of service and weight characteristics of combined welded automobile cylinders and high-pressure vessels is provided at $K = 1.60\text{--}1.65$ safety factor of welded body. To manufacture high pressure vessels the steels of different chemical composition, structure and mechanical properties and pipes of them including those welded with relation of $\sigma_{0.2}/\sigma_t$ within the limits of 0.48–0.87 are applied [4]. The increase of σ_t of steel body from 500 to 1000 MPa allows decreasing M/V of combined vessel for working pressure down to 19.6 MPa from 1.33 to 0.65 kg/l due to increase of D/S relation (diameter to wall thickness) from 31 to 63 (Figure 1). In combined vessels of steels $\sigma_t \geq 550 \text{ MPa}$, $M/V \leq 1.18\text{--}1.22 \text{ kg/l}$, which is lower than $M/V = 1.25\text{--}2.0 \text{ kg/l}$ of produced steel automobile cylinders. Keeping the relation $D/S = 0.016\text{--}0.032 > 0.010$ causes necessity in conductance heat treatment of the welded body, and proportional decrease of D and S results in simplification and reduction of duration of performance of welding-technological works.

Welds should have the tensile strength at the temperature of 20 °C corresponding to σ_t of base metal and KCU of not lower than 50 and 30 J/cm² respectively for the temperature of 20 and lower than –20 °C, and welded joints of low-alloy manganese and silicon-manganese steels should withstand tests at static bending for the angle of not lower than 80° [4]. The life of vessels of $N = 5500$ cycles can be considered as sufficient for everyday filling and consumption of gas

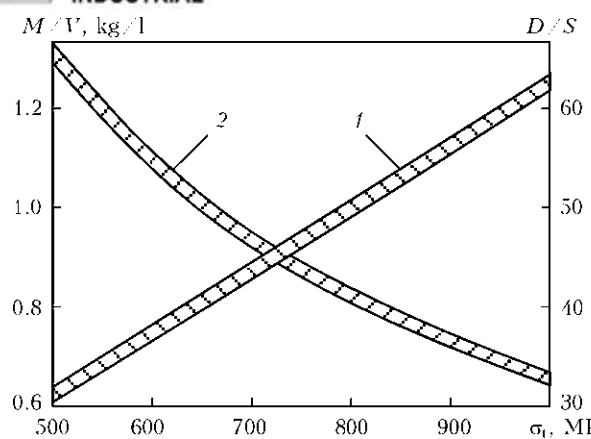


Figure 1. Influence of strength of steel on the size parameter D/S (1) and specific weight M/V (2) of combined high-pressure vessel during 15 years of operation similar to automobile cylinders.

As is known, the high strength of low-alloy steels, including pipe steels, is provided by increase of manganese content of up to 2 %, by micro-alloying with niobium, vanadium, titanium, chromium, copper, nickel, boron, by transfer from hot rolling (normalization) to controllable rolling, thermomechanical and new kinds of treatment. Here, with decrease of content of carbon (from 0.20 to 0.03 %) and sulphur (from

0.035–0.040 to 0.010 %) and lower the considerable increase of ductility (deformability) and toughness, improvement of their weldability as compared to carbon alloyed steel is achieved [5–7]. Thus, the premises are created for rejection of heating and postweld tempering and also applying welding using consumable electrode instead of argon arc welding using non-consumable electrode. In Ukraine and abroad the pipes of large diameter are produced applying longitudinal submerged-arc welding of low-alloy pipe steels of strength class X65, X70, X80 and X100 with $\sigma_t \geq 550$, 560, 620 and 760 MPa, $\sigma_{0.2} \geq 450$, 480, 550 and 690 MPa, $\delta \geq 18\%$. The main gas pipelines welded by circumferential welds are operated under changing pressure and temperature including the conditions of the Far North. It is obvious that welded vessels manufactured of mentioned steels and pipes are acceptable for operation under less extreme conditions as well.

The analysis of data of Table 1 evidences that safety factor K of welded body of vessel can change within wide limits from 0.96 to 2.10. When $K = 1.60$ –1.65 the specific weight of combined vessels manufactured applying steels of strength class X65, X70, X80 and X100 can be 1.08–1.11; 1.03–1.06; 0.85–0.89 and 0.76–0.77 kg/1. The prospective is the application of

Table 1. Calculation characteristics of high-pressure vessels of welded pipes for main pipelines

No.	Class of steel strength	σ_t , MPa	Pipe		Body	M/V , kg/1
			D , mm	S , mm		
1	X65	590	762	19.1	1.51	1.02
2		590	762	20.2	1.60	1.08
3		670	1220	18.9	1.06	0.63
4		590	914.4	25.0	1.65	1.11
5	X70	600	914.4	19.1	1.34	0.85
6		620	914.4	28.6	2.10	1.28
7		620	914.4	23.0	1.59	1.03
8*		620	914.4	24.0	1.66	1.07
9	X80	752	610	12.7	1.60	0.85
10		722	762	15.6	1.51	0.84
11		734	1016	17.5	1.29	0.70
12		750	1020	21.5	1.61	0.86
13		750	720	15.5	1.65	0.89
14		750	610	13.0	1.63	0.90
15		801	1219	14.3	0.96	<0.60
16		838	1219	14.3	1.00	<0.60
17	X100	816	914.4	13.2	1.20	0.65
18		858	914.4	13.2	1.26	0.65
19		858	914.4	17.0	1.63	0.80
20		890	914.4	15.0	1.49	0.72
21		890	914.4	16.5	1.64	0.77
22		890	1020	18.5	1.65	0.77
23		890	762	13.5	1.61	0.76
24		890	610	11.0	1.64	0.77

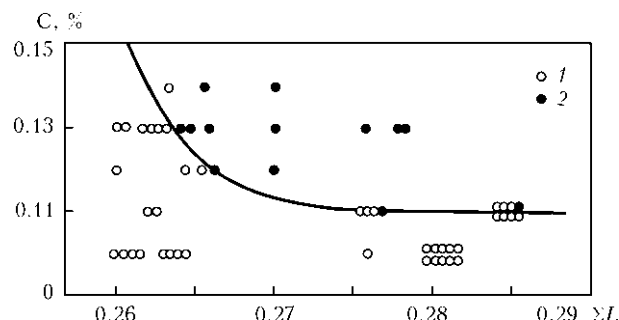


Figure 2. Influence of carbon and alloying elements on cold cracks formation in the submerged-arc welded joint of high-strength steel [9]: 1 – no cracks; 2 – cracks present

pipes of steel of grade X80, the production of which is mastered in Ukraine. Therefore further our investigations were directed to the evaluation of possibility of use of tubular billets of mentioned steel as applied to manufacture of the mobile high-pressure vessels.

As the object of investigations the butt joints according to the GOST 8713-79 and 14771-76 were selected with multilayer welds of steel of grade X80 of 20 mm thickness of the following chemical composition, %: 0.094 C; 1.97 Mn; 0.362 Si; 0.03 Mo; 0.02 Nb; 0.014 Ti; 0.02 P and 0.03 S, which is characterized by the following mechanical properties: $\sigma_t = 650$ MPa, $\sigma_{0.2} = 547$ MPa, $\delta = 21.6\%$, $KCV^{+20} = 327$ J/cm² and $KCV^{-40} = 245.5$ J/cm². The carbon equivalent $C_{eq} = 0.20-0.44 < 0.45\%$ calculated according to different formulae allows referring it to those not susceptible to cold cracking [8]. It corresponds also to such combination of carbon content and parameter of alloying

$$\Sigma L = (\text{Mn} + \text{Cr})/20 + \text{Si}/30 + (\text{Ni} + \text{Cu})/60 + \text{Mo}/15 + \text{V}/10 = 0.22\%,$$

at which cold cracks in welded joints of high strength steels welded by submerged-arc welding are absent (Figure 2) [9]. Therefore, the submerged-arc welding of such joints is performed without preheating however preheating is recommended during welding in shielding gases and its temperature depends on carbon equivalent, thickness of steel and temperature of environment. The crack formation is prevented by auto-preheating, delayed cooling, thermocycling in multi-pass welding.

The automatic welding of mentioned joints was performed under flux AN-47 using wires Sv-10Kh2M and Sv-08KhM and mechanized welding in carbon dioxide was performed using wire Sv-08G2S. A part of welded joints was subjected to argon arc treatment with partial melting in the middle of a weld in the areas of transition from a weld to base metal and furnace tempering at the temperature of 600 °C during 1 h. The thermal cycles of welding (Figure 3) and argon arc treatment were recorded using thermal couple VR-20/5, fastened on the opposite side of a butt, and potentiometer KSP-4. Welded joints were investigated by metallographic, durametric methods, tested

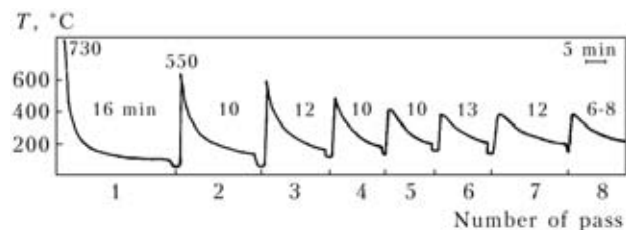


Figure 3. Characteristic thermal cycle of multilayer submerged-arc welding

for static rupture, static bending at angle 90°, impact bending of specimens with a circular notch along the weld, fusion zone and HAZ (at the distance of 2 mm from a weld), and also for fatigue at tension with frequency of 5 Hz up to $\sigma_{max} = 300-350$ MPa of a cycle, keeping the relation $\sigma_{max}/\sigma_t = 0.48-0.56$ (the same as at cyclic tests by inner pressure of combined cylinders with welded body of steel 30KhGSA).

As was shown by analysis of thermal cycles, during deposition of the first beads of weld of joints produced both under flux, as well as in carbon dioxide at heat input of 21.6 and 9 kJ/cm², their cooling occurs at the speed of $w_{6/5} = 8-12$ and 14–18 °C/s which corresponds to rational interval $w_{6/5} = 5-35$ °C/s at $q/v_w = 9-35$ kJ/cm [10]. At the next passes which were performed after cooling of welded joints down to the temperatures of 90–180 and 80–120 °C (during 5–16 min), weld root is heated up to the temperatures of 680–350 and 540–290 °C. With the increase of succession and removal of beads being performed, the temperature of heating metal of the lower part of welded joints is decreased and metal is subjected to multiple short-time tempers which promote the absence of cold cracks in welded joints (Figure 4, a).

In the process of argon arc treatments from $v_{tr} = 7.5$ m/h ($q/v_{tr} = 12.5$ kJ/cm) and $v_{tr} = 4.8$ m/h ($q/v_{tr} = 19.5$ kJ/cm) with a partial melting of 7–10 and 13–14 mm width respectively at the places of

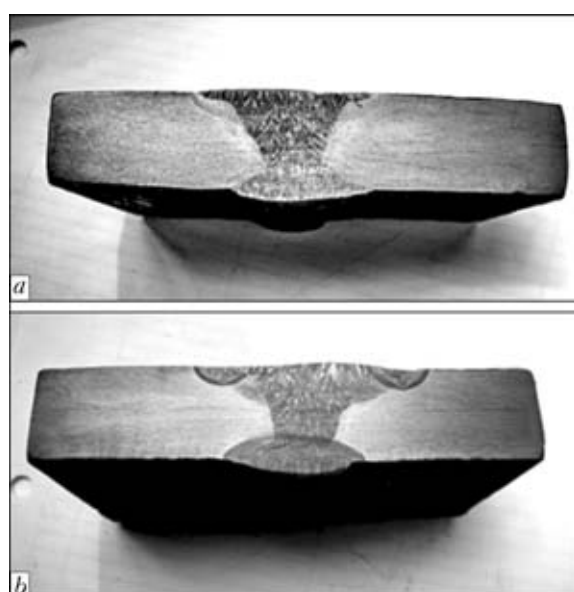


Figure 4. Macrostructures of butt joints produced by submerged-arc welding before (a) and after (b) argon arc treatment

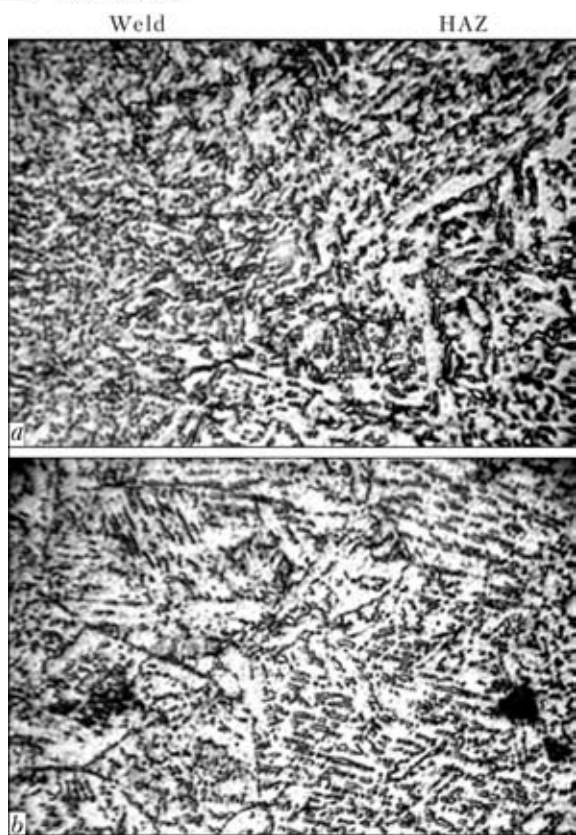


Figure 5. Microstructures ($\times 320$) of metal of fusion zone (a) and HAZ (b) of submerged-arc welded steel of grade X80

transition of a weld to a base metal and also of 25–27 mm width at the middle of a weld the undercuts were removed, sharp transitions to a base metal (Figure 5, b) and indentations among beads were smoothed. A welded joint is heated across the whole thickness. A metal of upper part of a joint at the depth of up to 8–12 mm undergoes phase and structural transforma-

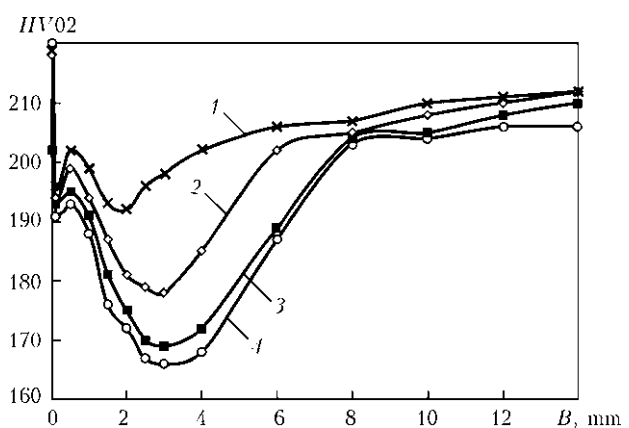


Figure 6. Distribution of hardness across the width B of HAZ metal on steel X80 welded under flux (2–4) and in carbon dioxide (1) in the state after welding (1, 2), argon arc treatment (3) and high tempering (4)

tions. In the lower part it is exposed to short-time tempering.

As the results of metallographic investigations show, the ferrite-bainite structure with inclusions of MAC-phase is formed in HAZ metal of joints produced using submerged-arc welding (Figure 5). Its hardness is gradually decreased at the distance of 0.1–0.3 mm up to HV0.2–193 and at the distance of 3 mm from a weld to HV0.2–178 relatively to HV0.2–215 of a base metal (Figure 6, curve 2). The lower weakening of HAZ metal (at the distance of 0.1–0.3 mm from a weld) up to HV0.2–195 and 2 mm from a weld of up to HV0.2–192 is observed after welding in carbon dioxide (Figure 6, curve 1). After argon arc treatment and furnace tempering the character of distribution of hardness across the width of HAZ is not changed (Figure 6, curves 3, 4), and its values are decreased. The zonal reductions of hardness in HAZ metal ac-

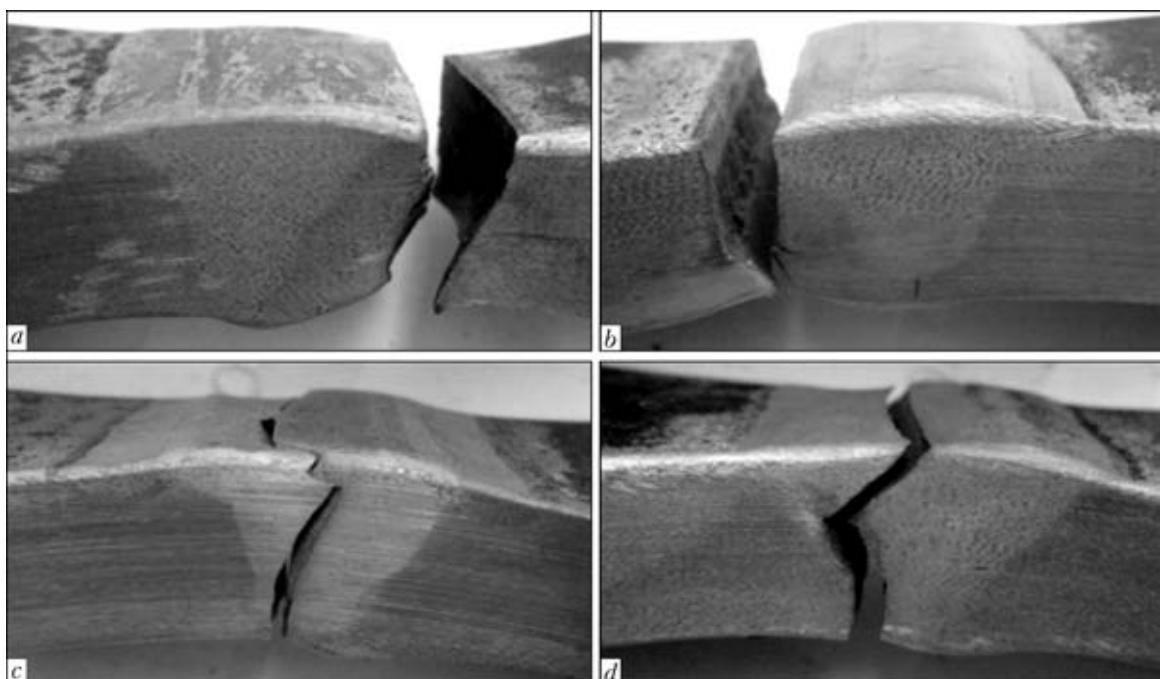


Figure 7. Character of fracture at fatigue test of joints of submerged-arc welded steel of grade X80 in the state after welding (a), argon treatment with partial melting of a weld (b), transition places from weld to base metal (c) and high tempering (d)

cording to our assumption is the demonstration of a localized decarburization of metal in the fusion zone and at the areas which were heated in welding up to the temperatures of transformation.

After argon arc treatments of joints with a partial melting of a weld of 10Kh2M type and transition from it to a base metal the hardness of these areas is increased up to $HV0.2-(243-262; 230-245$ and $145-163$). Near the partial melts of a weld it is decreased down to $HV0.2-(225-237)$ and is not almost changed on the joint reverse side. The furnace tempering causes the decrease in hardness down to $HV0.2-(233-247)$. The increased hardness of chromium-molybdenum weld metal in different states proves its higher strength than that of the base metal.

The tensile strength of welded joints produced by submerged-arc welding is 610 MPa. Their fracture occurs beyond the weld. The bend angle of such joints is not lower than 90° . The impact toughness of HAZ metal is $KCU^{+20} = 286 \text{ J/cm}^2$ and $KCU^{-40} = 144 \text{ J/cm}^2$ after submerged-arc welding, and $KCU^{+20} = 321 \text{ J/cm}^2$ after welding in carbon dioxide. In weld metal of the type 10Kh2M and 08KhM produced by submerged-arc welding $KCU^{+20} = 86$ and 139 J/cm^2 and $KCU^{-40} = 38$ and 52 J/cm^2 , respectively. After arc treatments and furnace tempering the impact toughness of these areas is changed negligibly ($KCU^{+20} = 279-305 \text{ J/cm}^2$ of HAZ metal and $KCU^{+20} = 87-95 \text{ J/cm}^2$ of weld of type 10Kh2M). As is seen, the impact toughness of welded joints of the steel of grade X80, welded under flux, exceeds standard requirements.

At fatigue test of flat specimens it was established that fracture of welded joint (Figure 7) begins from formation of cracks in the places of concentration of stresses, in particular in transitions from weld to base metal on the front or both sides, and develops along the weld, fusion zone or HAZ metal. If fracture of welded joints in postweld conditions and argon arc treatment with a partial melting in the middle of a weld begins on the front side and their life is 58,100–86,100 and 49,300–104,900 loading cycles, then the fracture is initiated at the later stage from the root part after arc partial melting of transition places from weld to base metal (the angle and radius of conjugation between weld and base metal is increased). The life of these joints is increased up to 86,300–106,400 cycles (Table 2). After high tempering, increasing the equilibrium of structure and decreasing the level of residual stresses, it is increased up to 114,100–312,400 cycles. In combination of two latter technological operations one can expect even more intensive increase of cyclic life. The established cyclic life at uniaxial tension of welded joints of low-alloyed steel in different states exceeds the life of hydraulically tested combined cylinders with a thermostrengthened body of alloyed steel (15,000–24,000 cycles [3]) 3.3–13 times.

Table 2. Cyclic life of butt joints of steel of strength class X80 produced by multilayer submerged-arc welding using wire Sv-10Kh2M

Postweld treatment	σ , MPa	N , cycle
Without treatment	300	58,100
	350	86,100
Arc partial melting of a weld	300	104,900
	350	49,300
Arc partial melting of transition places	300	106,400
	350	86,300
High tempering	300	312,400
	350	114,100

The carried out investigations prove that mobile high pressure vessels for operative supply of liquified gases are reasonable to be manufactured using pipes of large diameter in capacity of billets of shells and sheet rolled metal to form bottoms of low-alloyed steels of increased strength with a low carbon content. Circumferential welds of shells and bottoms of wall thickness of 13–24 mm are reasonable to be made using multilayer submerged-arc butt welding without pre-heating. Proportional decrease of wall thickness and diameter of vessel promotes simplification and decrease of duration of welding-technological works. To improve serviceability it is reasonable to subject butt joints to arc treatment with a partial melting of transition places from weld to base metal. The welded body is subjected to an obligatory tempering. Its cylindrical part is strengthened by polymer composite material of a high specific strength.

Here, the formation and welding of shell, forging of longitudinal weld, furnace postweld tempering and high-temperature heating with further hardening are eliminated.

1. Paton, B.E., Savitsky, M.M., Kulyk, V.M. et al. *Cylinder*. Pat. 18874 Ukraine. Publ. 25.12.1997.
2. Paton, B.E., Savitsky, M.M., Kulyk, V.M. et al. *Pressure cylinder*. Pat. 61162 Ukraine. Publ. 17.11.2003.
3. Savitsky, M.M., Savichenko, A.A., Kulik, V.M. et al. (2007) Light-weight welded cylinders for motor transport. *The Paton Welding J.*, 1, 43.
4. (1998) *Rules of manufacturing and safe operation of pressure vessels*. Kyiv.
5. Tukhbatullin, F.B., Galiullin, Z.T., Karpov, S.V. et al. (2001) Low-alloy steels for main gas pipelines and their resistance to fracture. In: *Inform. Review on Transport and Overhead Gas Storing Series*. Moscow: IRTs Gazprom.
6. Bauer, D., Flus, P., Amoris, E. et al. (2006) Microstructure and characteristics of pipe steels after thermomechanical treatment. *Novosti Chyorn. Metallurgii za Rubezhom*, 4, 65–76.
7. Nabuki, I., Shigeri, E., Jos, K. (2006) Pipes UOE with high characteristics for main pipelines. *Ibid.*, 77–80.
8. Makarov, E.L. (1981) *Cold cracks in welding of alloy steels*. Moscow: Mashinostroenie.
9. Malyshevsky, V.A., Grishchenko, L.V., Baryshnikov, A.P. (1999) Welding consumables and technologies of low-alloy steels. *Voprosy Materialovedeniya*, 20(3), 46–62.
10. Zakharova, I.V., Chichkarev, E.A., Vasiliev, V.G. et al. (2001) Structure and properties of HAZ metal of low-alloyed pipe steels modified with calcium. *The Paton Welding J.*, 8, 14–17.



AUTOMATIC CONTROL DRIVE OF ELECTRODE MOVEMENT TRAJECTORY FOR THE ARC SURFACING MACHINES

S.V. GULAKOV and V.V. BURLAKA
Priazovsky State Technical University, Mariupol, Ukraine

Suggested is the design of the electrode movement mechanism for deposition of complex-configuration beads on working surfaces of machine parts and tools by using the automatic electron control system. The device is a modification of the connecting rod gear, in which the connecting rod is made with a possibility of automatic adjustment of its length.

Keywords: electric arc surfacing, drive of electrode oscillation, connecting rod gear, automatic control system

Control of a bead trajectory is necessary for providing quality formation of a deposited working layer with complex trajectory on a repairable part. In particular, a quick change of a movement trajectory, for example, in the apexes of zigzags (Figure 1), accompanied by possible distortion of a weld pool shape during change of electrode movement direction is to be taken into account [1].

The aim of the present work is to develop and investigate a simple and reliable device for electrode oscillation, allowing formation of the necessary trajectory of its movement.

A connecting rod gear (CRG) was used as a principle device for electrode oscillation. It provides the trajectory of movement of driven element close to sine. Change of the forming trajectory in it can be performed by means of control of a drive motor or change of geometric parameters of the CRG elements.

Formation of movement trajectory through control of the drive motor requires its frequent reverses and significant accelerations that results in overheating and reduction of system reliability.



Figure 1. Surface of the roll with deposited zigzag-shape beads

© S.V. GULAKOV and V.V. BURLAKA, 2011

The work proposes a drive based on the CRG in which the connecting rod is made with a possibility of program adjustment of its length in the process of mechanism operation [2] (Figure 2). At that, minimum and maximum length of the connecting rod determine the boundaries for resulting «corridor» of allowable positions of the driven element (Figure 3, curves L_{\max} , L_{\min}). The linear parameters of the connecting rod are changed with the help of additional drive, mounted on it. Thus, it is possible to form a deposited bead of any shape in the ranges of «corridor» of allowable positions, for example, rectangular (Figure 3, curve 1) or trapezoid (Figure 3, curve 2) ones.

It follows from Figure 2 that a coordinate $y(\varphi)$ of electrode holder for geometry reasons is determined as

$$y(\varphi_{\text{CRG}}) = R \sin \varphi_{\text{CRG}} + \sqrt{L(\varphi_{\text{CRG}})^2 - (R \cos \varphi_{\text{CRG}})^2}, \quad (1)$$

where R is the crank length, m; φ_{CRG} is the angle of rotation of the CRG, degree; $L(\varphi_{\text{CRG}})$ is the connecting rod length, m.

It can be seen from expression (1) that control of the connecting rod length L during the oscillation period (complete crank revolution) can significantly influence on a principle of electrode holder movement.

Automatic control system (ACS) provides a change of the connecting rod length $L = f(\varphi)$ (see Figure 2) in such a way that the trajectory of electrode movement $y(\varphi)$ meets the set one.

Thus, the function $y(\varphi)$ can have the following form for obtaining the electrode movement trajectory:

$$y(\varphi) = Y_0 + \frac{H}{2} \frac{2}{\pi} \arcsin (\sin (\varphi_{\text{CRG}})), \quad (2)$$

where Y_0 is the displacement, m; H is the oscillation range, m.

Coefficient $2/\pi$ before the arcsine function is a standard. It is convenient to select displacement Y_0 equal

$$Y_0 = \frac{\sqrt{L_{\min}^2 - R^2} + \sqrt{L_{\max}^2 - R^2}}{2}, \quad (3)$$

that provides centering in the «corridor» of allowable positions.

Thus, for realizing of the rectangular trajectory of electrode movement the length of connecting rod of the CRG should be changed in such a way that an equation is fulfilled

$$\begin{aligned} R \sin \varphi_{\text{CRG}} + \sqrt{L(\varphi_{\text{CRG}})^2 - (R \cos \varphi_{\text{CRG}})^2} = \\ = Y_0 + \frac{H}{2} \frac{2}{\pi} \arcsin (\sin \varphi_{\text{CRG}}). \end{aligned} \quad (4)$$

Solution of equitation (4) is the following:

$$\begin{aligned} L(\varphi_{\text{CRG}}) = \\ = \sqrt{[Y_0 + \frac{H}{2} \frac{2}{\pi} \arcsin (\sin \varphi_{\text{CRG}}) - R \sin \varphi_{\text{CRG}}]^2 + (R \cos \varphi_{\text{CRG}})^2}. \end{aligned} \quad (5)$$

The trapezoid trajectory can be obtained through modification of the rectangular oscillation in the following way:

$$y(\varphi) = Y_0 + \frac{H}{\pi} \arcsin \times \left(\begin{array}{l} \left\{ \begin{array}{l} \frac{\pi}{2} - \gamma, \text{ if } \varphi \in \left[\frac{\pi}{2} - \gamma; \frac{\pi}{2} + \gamma \right], \\ \frac{3\pi}{2} - \gamma, \text{ if } \varphi \in \left[\frac{3\pi}{2} - \gamma; \frac{3\pi}{2} + \gamma \right], \\ \varphi, \text{ if } \varphi \in \left(0; \frac{\pi}{2} - \gamma \right) \cup \left(\frac{\pi}{2} + \gamma; \frac{3\pi}{2} - \gamma \right) \cup \left(\frac{3\pi}{2} + \gamma; 2\pi \right), \end{array} \right. \end{array} \right) \quad (6)$$

where γ is the half angular width of trapezium vertex.

At that, a range of trapezoid oscillation H' and parameter γ are in the ratio

$$H' = H \left(1 - \frac{2\gamma}{\pi} \right). \quad (7)$$

The ACS with proposed compound drive of the electrode movement should provide reliable operation, error-free continuation of operation after disconnection and further renewal of power supply, and good quality parameters, such as time of adjustment and re-adjustment.

The compound drive of electrode movement as a control object, including the CRG with variable length of connecting rod and direct current motor controlling this length, is sufficiently complex linear system with internal feedbacks.

Armature voltage is a parameter of control object using which the latter can be influenced from the ACS side. It should change in such a way that the coordinate of electrode holder X_{out} is changed on specified principle. At that it is necessary to provide a current of the armature at a secure level due to frequent reverses and accelerations of motor of the additional drive. The system should also be stable to self-excitation.

Implementation of the ACS in a form of classic single-loop adjuster with total negative feedback on

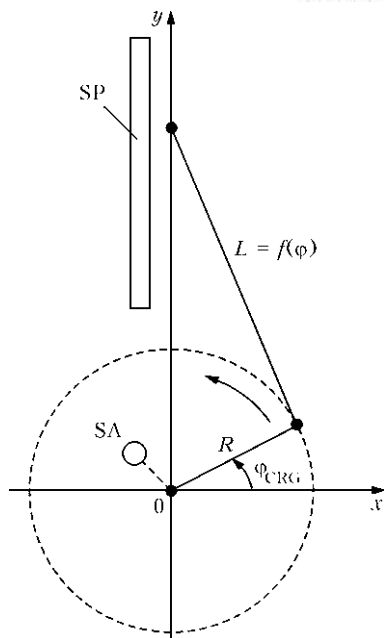


Figure 2. Kinematic scheme of the drive: SA — sensor of crank rotation angle; SP — sensor of electrode position

electrode position results in unsatisfactory parameters of adjustment quality since the control object is an inertial element of the second row that complicates stabilizing of a closed system.

Improvement of adjustment parameters in the single-circuit scheme of automatic control is seemed to be impossible due to absence of information about operation of internal feedbacks in the control object.

The whole control system was divided into the embedded loops in order to have the possibility of their series adjustment and optimization for simplifying synthesis of the ACS and providing better adjustment characteristics. At that, separate adjustment loops provide «uncoupling» of internal feedbacks in the control object that gives the possibility of maximum reduction of adjustment time, preserving at the same time physical limitations on voltage and current of the motor armature.

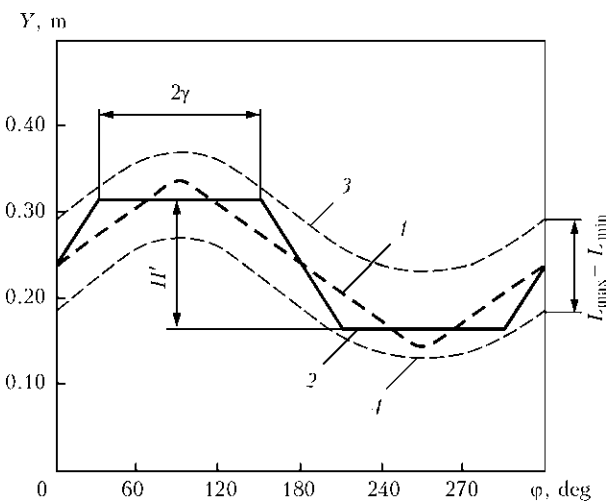


Figure 3. CRG trajectories: 1 — triangle; 2 — trapezoidal; 3, 4 — with proposed L_{\max} and L_{\min} , respectively



The control system has three adjustment loops: adjuster of current of armature, rate and position. The task of each adjuster in structural scheme of control system for electrode oscillation mechanism is maximum quick and accurate processing of corresponding task. At that, formation of the negative feedbacks is possible.

Pulse hysteresis adjuster provides a formation of current of motor armature of the additional drive that predetermines a high reaction rate of the system and small loss of power in the adjuster.

The ACS was realized in practice on the ATMEL single-chip microcontroller ATMega168-20. Combining of the most of adjustment functions in one chip allows obtaining a system with a possibility of flexible setting of virtually all adjuster parameters. Besides, application of a micromodulator allows easily providing diagnostics of the drive operation in real time and detecting its faulty operations at minimum time.

The main drive motor is a DC motor with independent excitation by 230 W power, nominal armature voltage 110 V, 2.9 A current and 2400 rpm nominal revolution rate.

Motor with excitation from constant magnets of DP-40-40 type was selected for the additional drive. It can be explained by simple control (adjustment of a rate of shaft revolution is carried out only through change of voltage on the armature), small response time (electromechanical time constant of around 300 ms), large limit moment (around $5 M_{\text{nom}}$), good weight-dimension indices and high power-to-weight ratio (40 W at 1.1 kg weight).

A mode of motor operation in the linear drive can be classified as an intermittent duty (S3 on GOST 183-74) since time of oscillation cycle (around 30 s) does not exceed the time constant of machine heating. Hence, the control system allows short-time fivefold overloads of the motor during reverses; at that, the root-mean-square current of the armature, taken as a

cycle time, does not exceed the nominal one that guarantees absence of the overheating.

Selsyn motor with balanced three-phase voltage system supplied on winding of its stator was used for determination of rotation angle of the crank of movement mechanism. The electromotive force of the rotor winding and voltage of one of the phases is supplied on control circuit. The rotation angle is determined programmatically on phase shift between the signals mentioned above.

Position of an oscillating platform with installed on it mechanism of electrode feeding is determined with the help of contact-free probe Micropulse, output signal of which has (-15 – +15) V change ranges and is renewed at 2 kHz frequency.

Liquid-crystal indicator of TIC154 type in standard connection scheme and four-button keyboard were used for the interactive adjustment of system parameters. The adjustment is carried out with the help of a hierarchical menu.

Supply voltage of both motors is formed by half-bridge inverters, controlled from a controller and manufactured using IRG4PC30UD transistors and IRS2113 drivers in the standard connection scheme. The possibilities of data exchange with personal computer through RS-232 interface and on-board re-programming of the controller are also considered in the scheme.

Application of the compound drive also allows changing of the oscillation amplitude during operation that provides the possibility of carrying out surfacing of a layer with predetermined distribution of properties, for example, surface of rolls with indentations [3].

A dependence of the optimum length of crank on the amplitude of required osculation trajectory at which additional drive requires minimum power [4] was derived by authors. This improves the dynamic characteristics of the system (reduction of moment of inertia) through a preliminary adjustment of the crank length before surfacing cycle.

Figure 4 shows the oscillograms of armature voltage U_a and current I_a of motor of the additional drive at execution of triangular trajectory of the electrode movement with optimum selected length of the crank. Proposed system for control of the drive of electrode movement has characteristics which allow formation of the movement trajectory optimum for surfacing.

Developed electromechanical device for control of the electrode movement trajectory, including the CRG, set in motion by powerful electric drive, and device for measurement of the connecting rod length, consisting of the direct current drive, installed directly on it, and the ACS adjusting geometric parameters of the connecting rod according to specified principle should be noted in conclusion. The system is realized using microprocessor technology and provides minimizing of power of the device for measurement of the

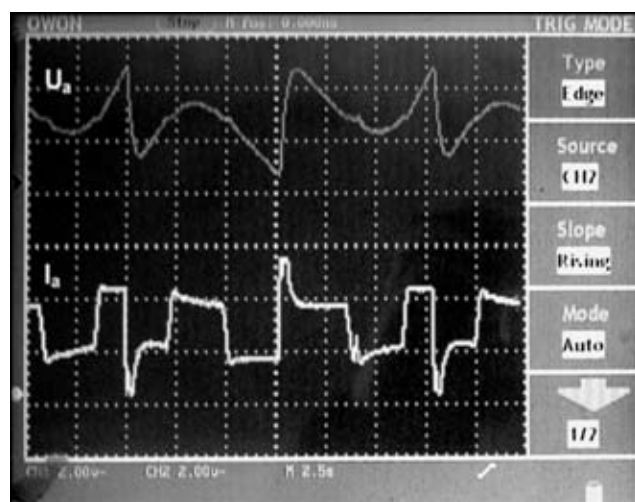


Figure 4. Oscillograms of armature voltage U_a and current I_a of motor of the additional drive at execution of triangular trajectory of the electrode movement

connecting rod length by means of preliminary selection of the optimum crank length. The inspection of the device under laboratory experimental-industrial conditions showed the high dynamic characteristics (override of around 10 %, time of adjustment 1.8 s at execution of step excitation) and sufficient (around 7 %) accuracy of operation of the oscillation mechanism.

The tests on stability of given system to influence of the external disturbances were carried out taking into account real mechanical characteristics of the device and limitations of the parameters (armature current and maximum speed). Optimization of the pa-

rameters of ACS control loops was carried out according to the results.

1. Gulakov, S.V., Nosovsky, B.I. (2005) *Surfacing of working layer with controlled distribution of properties*. Mariupol: PGTU.
2. Gulakov, S.V., Burlaka, V.V., Psareva, I.S. *Drive of electrode movement in surfacing unit*. Pat. 86294 Ukraine. Int. Cl. B23K 9/04. Publ. 10.04.2009.
3. Gulakov, S.V., Nosovsky, B.I. *Control device of deposition process of zigzag-shape weld*. USSR author's cert. 1403498. Publ. 15.04.88.
4. Gulakov, S.V., Burlaka, V.V., Psareva, I.S. et al. (2006) Control of arc surfacing process of working layer by zigzag-shaped beads. In: *Protection of metallurgical machines against failures*, Issue 9, 202–207.

DEVELOPMENT OF THE TECHNOLOGY FOR REPAIR OF THREADED HOLES IN AXLES OF RAILROAD CAR WHEELSETS (Innovation Project of the NAS of Ukraine accomplished by the E.O. Paton Electric Welding Institute)

The technology developed is intended to repair damaged threaded holes M20 in necks of axles of railroad cars RU1-Sh by the explosion cladding method. The technology is characterized by low costs (compared to fusion welding), full strength of welded joints, absence of cracks characteristic of the overlaying repair technology in them, and absence of pores, lacks of penetration, undercuts and slag inclusions, shrinkage, reduction and decrease in diameter of seats of the axle necks for roller bearings.

At the first stage of the work the investigation objects were damaged threaded holes M20-6N of 180 mm long fragments of the necks of axles RU1-Sh, and at the second stage — damaged threads on the full-scale 1450 mm long axles. Coatings were applied by the explosion cladding method to a preliminarily made 20.4 mm diameter bore in a cylindrical tube of steel 20. The ingenious procedure was developed in collaboration with State Enterprise «Ukrainian Research Institute of Railroad Car Construction» for mechanical tests of welded joints on the repaired threaded holes. Fatigue resistance tests of the welded joints conducted under minimal and maximal loads (49 and 98 t, and frequency of 50 Hz) showed the average values of fatigue life equal to 122,000 cycles, which are only 4 % lower than the basic values of fatigue life of new axles equal to 127,000 cycles.

The new technology was used to repair damaged holes in two full-scale axles RU1-Sh transferred to State Enterprise «Ukrspetsvagon» and included into structure of a car truck, which is being subjected to field tests at the Panyutino–Lozovaya Station during 2011. Upon completion of the tests, the technology proposed is to be applied at railroad car repair plants of State Enterprise «Ukrzaliznytsya».



INFORMATION-CALCULATION SYSTEM FOR HYGIENIC CHARACTERISTICS OF WELDING ELECTRODES

O.G. LEVCHENKO, V.V. SAVITSKY and A.O. LUKIANENKO

E.O. Paton Electric Welding Institute, NASU, Kiev, Ukraine

A computer system is presented comprising indicators of emission levels and chemical composition of fumes that pollute the work zone air in coated-electrode welding, as well as a system for calculation of the required ventilation air exchange. They can be applied to calculate the content of harmful substances in the work zone air when using different types of ventilation (local and general) and to select the type of the ventilation system for welding under different conditions.

Keywords: *arc welding, coated electrodes, hygienic characteristics, welding fumes, prediction, ventilation*

The main means of worker protection from welding fumes (WF) contaminating the air in production facilities in electric arc welding is exhaust system of ventilation. Effectiveness of WF removal from the work place depends on the correct selection of the kind of ventilation system and its efficiency, which is calculated on the basis of experimental data on intensity of WF component evolution.

This work considers the developed computer information-calculation system (ICS) which allows obtaining information about the characteristics of levels of WF harmful component emissions in manual arc welding in different modes, predicting concentration of WF and gases (carbon oxide and nitrogen dioxide) in the work zone air, as well as calculation of the required air exchange and selection of the kind of ventilation system.

Main functions of ICS «Welding hygiene» are as follows:

- entering and editing information on initial data and hygienic characteristics of welding electrodes;
- information storage and displaying;
- searching for the necessary information;
- predicting the concentration of WF, manganese, carbon oxide and nitrogen dioxide in the work zone air, depending on welding mode and distance to the welding arc;
- calculation of characteristics of ventilation air exchange, i.e. quantity of air, required for dilution of harmful substances in the work zone air to threshold limit concentrations (TLC);
- issuing recommendations on selection of a ventilation system or means of individual protection of respiratory organs.

ICS includes the following subsystems: selection of electrode grade; selection of welding mode; selection of welding conditions (without ventilation, with general or local ventilation).

Compared to the known information systems [1–4] ICS «Welding hygiene» developed by us gives more

complete information in a more understandable form about the initial characteristics of welding electrodes (purpose, coating type, kind of current, welding mode) and general characteristics of WF emission levels: intensity of formation (V_f , g/min), specific evolution (G_f , g/kg), coefficient of intensity of formation (β_f , g/(kW·h)) and coefficient of specific evolution (γ_f , g/(kW·kg)). The system gives the data on experimental and calculated WF concentrations in the working zone air at different distances to the welding arc in case of availability of general, local ventilation and without it, which are used to select the most effective ventilation system. ICS allows performing hygienic assessment of known coated-electrode grades for welding low-carbon and low-alloyed steels and eventually provide recommendations on selection of the respective ventilation system (local or general).

ICS «Welding hygiene» data base contains information on quality characteristics of WF emissions: their composition for low-carbon, low-alloyed, medium-alloyed and high-alloyed steels. On the other hand, it presents results of investigations of the dependencies of concentrations of WF, manganese as the determinant toxic component in welding of low-carbon and low-alloyed steels [5], as well as gases (carbon oxide and nitrogen oxides), characteristic for welding with electrodes not containing any fluorides in their coating. These dependencies are used by the computer system for selection of the kind of ventilation system, ensuring WF content in accordance with the standard requirements [6].

Searching for information in the data base is performed by the specified welding electrode grade. Search result is documented in the form of an output document (Figure 1).

Results of computer system functioning can provide hygienic parameters, characterizing the composition, level of WF emissions, and can allow calculation of the required air exchange of general ventilation taking into account the LTC of harmful substances. The air exchange is presented in the form of two characteristics: first – quantity of ventilated air per one kilogram of electrodes consumed in welding (Q_m , m³/kg), the second one is the same per a unit of



Figure 1. Output document of ICS «Welding hygiene»

welding time (Q_t , m^3/h). By the values of these characteristics ICS allows performing comparative hygienic assessment of welding electrodes of various grades, including local electrodes, against foreign electrodes, using Q_t value.

Manganese concentration in the work zone air can be derived by calculation by the data of its formation intensity, using graphic and analytical dependencies obtained in [5]. For this purpose graphic information (Figure 2) was included into the data base of «Welding hygiene» system. This information allows determination of manganese concentration (C_{Mn}) in the required point depending on ventilation conditions (general, local or no ventilation), welding mode and distance from the arc L .

In addition, the right-hand part of ICS window (see Figure 2) presents text information on recommendations for normalizing the content of harmful substances in the working zone air. These recommendations determine in which cases general ventilation and in which cases local ventilation should be used, which depends on electrode grade, welding mode parameters and distance from the welding arc to the required point. If there is no local ventilation device in the work place, ICS proposes application of an independent filter-ventilation unit. Now, if local ventilation does not ensure harmful substances content in this point below the TLC, it is proposed to use the means for individual protection of respiratory organs (filter respirator or welding face shield with a system of clean air feeding to the breathing zone).

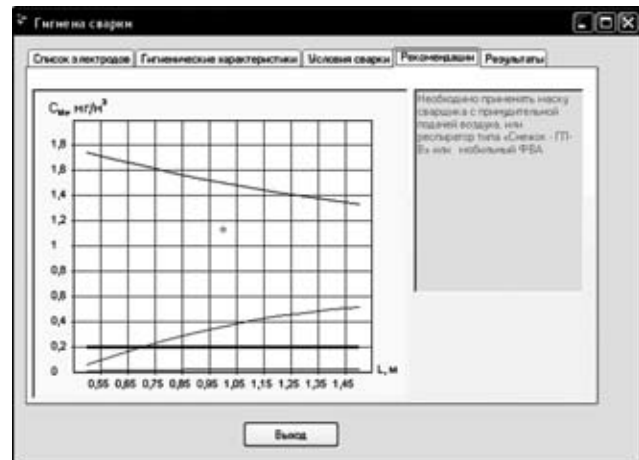


Figure 2. Graphic dependences of ICS and recommendations on selection of the kind of ventilation system and (or) means of individual protection of respiratory organs

Alternatively, the graphic dependencies given in ICS (see Figure 2) show how and to what extent WF impact on the body of workers being near the welding station can be reduced by changing the welding mode parameters and distance from these workers to the welding arc.

This system will be useful for welding fabrication specialists and labour safety units in enterprises applying arc welding. It will provide them with systematized information on hygienic characteristics of welding electrodes with the purpose of selection of the least hazardous grades, will enable adequate selection of systems of work place ventilation and individual protection of respiratory organs. As a result, it will enable increasing the level of protection of workers of welding professions and lowering the risk of development of their occupational diseases.

1. Demchenko, V.F., Levchenko, O.G., Metlitsky, V.A. et al. (2001) Data retrieval system of hygienic characteristics of welding aerosols. *Svarochn. Proizvodstvo*, **8**, 41–45.
2. Polukarov, O.I., Krushilko, O.E., Polukarov, Yu.O. (2006) Application of information-analysis system in planning of labor protection measures in welding production. *Svarshchik*, **2**, 42–44.
3. Machaczek, S., Matusiak, J. (1994) *Katalog charakterystyk materialow spawalniczych pod wzgledem emisji zanieczyszczen*. Gliwice: Instytut Spawalnictwa.
4. (1994) *Programy komputerowe dla potrzeb spawalnictwa*. Gliwice: Instytut Spawalnictwa.
5. Levchenko, O.G., Lukianenko, A.O., Polukarov, Yu.O. (2010) Experimental and calculation determination of the concentration of harmful materials in the work zone air in coated-electrode welding. *The Paton Welding J.*, **1**, 24–26.
6. GOST 12.1.005-88: SSBT. General sanitary-hygienic requirements to work zone air. Introd. 01.01.89.



THESES FOR A SCIENTIFIC DEGREE



E.O. Paton Electric Welding Institute of the NAS of Ukraine

A.N. Kislitsa (E.O. Paton Electric Welding Institute) defended thesis for a Candidate's degree on the subject «Microplasma spraying using wire electrodes» on December 22, 2010. It established the main technological peculiarities of microplasma spraying process from wire materials and defined the factors having the most significant influence on spraying process and properties of coatings.

The calculation-theoretical analysis of process of dispersion of melt of neutral wire material under the conditions of microplasma spraying (MPS) showed that the condition for melt droplet detachment from the end of a neutral wire is a required speed of a microplasma jet which depends on the properties of wire material, mainly on surface tension of its melt and for $\sigma = 0.914\text{--}2.3 \text{ J/m}^2$ it is $270\text{--}430 \text{ m/s}$. It corresponds to the consumption of plasma gas in the limits of $100\text{--}300 \text{ l/h}$ being established. The data of consumption of plasma gas lead to the turbulent character of plasma jet expiration ($Re = 5000\text{--}9000$).

The diameter of wire and its feed rate to the arc zone during MPS depend on thermophysical properties of its material which determine its stable melting in the arc zone. In case of using W, NiCr, Ti wires the diameter of wire is $0.2\text{--}0.4 \text{ mm}$, and feed speed is $3\text{--}6 \text{ m/min}$.

The volt-ampere characteristics of microplasmatron with a remote anode and protective nozzle for the conditions of MPS from wire materials are determined. The influence of technological parameters on

efficiency factor of plasmatron was investigated which reached 73 %, and the temperature of plasma here was 17,700 K.

The level of influence of different factors of wire spraying process on the average size of particles for different materials during dispersion of wire melt by plasma jet as well as on material utilization factor is determined applying the method of design of the multifactor experiment. The mathematical processing of obtained data allowed obtaining linear regressive models showing the influence of the most considerable parameters of the process (current strength, consumption of plasma gas, distance of spraying, wire feed speed) on formation of jet of particles of sprayed material and complex of characteristics of W, NiCr and Ti coatings under the conditions of MPS using wire materials.

For the conditions of MPS of wire materials the rate of particles of sprayed material is determined which depends on current strength and consumption of plasma gas and inversely proportional to the specific weight of sprayed material. The rate for Ti particles reaches 75, NiCr particles — 70, W particles — 45 m/s.

The investigation of figure of metallization for MPS using NiCr wire was carried out. It was established that profile of figure of metallization is described by Gauss distribution. The diameter of spraying spot is 5–10 mm, the angle of jet opening is in the limits of $4.6\text{--}9.4^\circ$, which is comparable with the data for laminar plasma jets and, probably, connected with the presence of reduction jet of shielding gas. It was shown that in connection with decrease of distance of spraying during wire MPS down to 40–60 mm the decreased content of oxide and nitride phases in the coatings is achieved. Thus, for Ti coating the minimal values were O₂ — 0.88, N₂ — 0.57 %.

As a result of establishment of possibility to control macroporosity of Ti coatings during wire MPS, the compliance of value of their engagement with the base of Ti alloy for detachment ($25.6 \pm 4.6 \text{ MPa}$) and for shear ($24.2 \pm 3.5 \text{ MPa}$), with ASTM C633 requirements, and also with data of tests of these coatings in-vivo the efficiency of their application is shown during manufacture of endoprostheses of different purpose (hip, dental and other).



E.O. Paton Electric Welding Institute of the NAS of Ukraine

I.A. Ryabtsev (E.O. Paton Electric Welding Institute) defended thesis for a Doctor's degree on February 2, 2011 on the subject «Restoration and strengthening of parts operating under the conditions of wear and different kinds of cyclic loads using surfacing methods».

The thesis is devoted to the development of theoretical assumptions about a part to be surfaced as a multilayer structure, where each its layer has its functional purpose and contributes to stress-strain state of the part on the whole and influences its operational properties, service life and feasibility of multiple restoration surfacing.

Based on the modern models of tough-plastic non-isothermal flow, thermokinetic diagrams of decay of overcooled austenite of deposited and base metal using numerical finite element method, the methods of calculation of residual stress-strain and structural state of cylindrical and plane parts during single and multilayer deposition and their influence on fatigue strength at cyclic mechanical or thermomechanical loads were developed. The calculations were confirmed by the tests of thermal and mechanical fatigue strength of deposited specimens and parts.

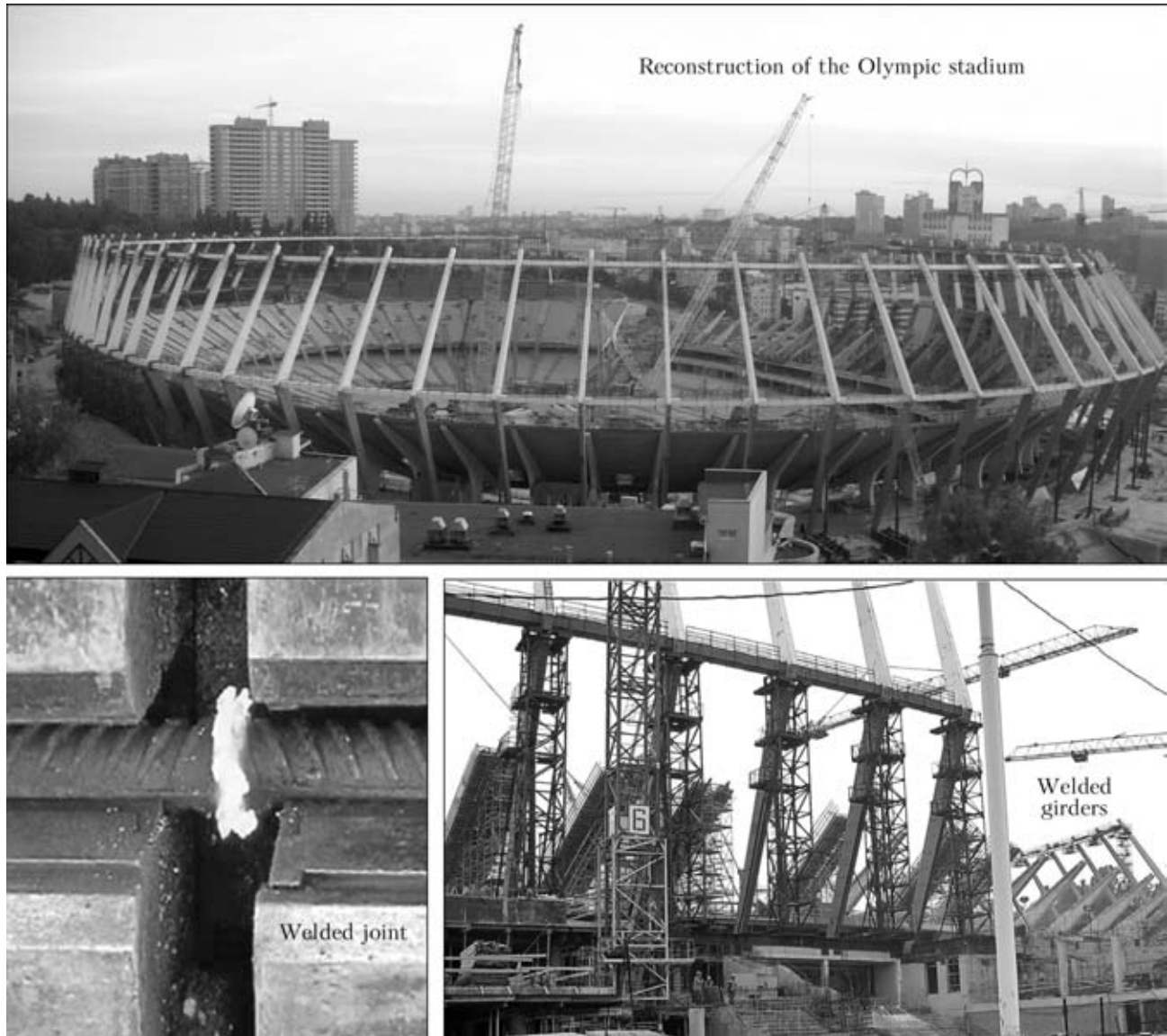
The methods were developed and calculation of stress-strain and structural state in the process of deposition and service cyclic thermal loads of parts of the type of mill rolls deposited by tool steel with and without plastic underlayer was carried out. Using calculations it was established that deposition with a plastic underlayer provides decrease of stresses by 25–30 % in the most loaded external working layer, which results in increase of thermal resistance of deposited part approximately by 35 %. The experimental investigations of thermal resistance of deposited specimens confirmed the results of calculations. To control the structure and properties of deposited metal it was offered to use effect of structure heredity in the electrode (filler) material–weld pool–deposited metal system. It was established that in arc surfacing the method of preparation of charge materials and their structure influence the structure and wear resistance of deposited metal. At similar chemical composition in the structure of metal deposited using wire with charge of powders of ferroalloys including high-carbon ferrochrome, the content of carbides is approximately 1.2–1.3 times higher than in the structure of metal deposited using wire with charge of preliminary melted and sprayed highly-alloyed powder. The effect of structural heritage is offered to be used for refining structure and increase of thermal resistance of wear-resistant deposited metal of the type of tool steels by adding of surfacing flux-cored wires of ultradispersed eutectic carbide compositions of main alloying elements of chromium, tungsten, vanadium and other into the charge.

The carried out investigations allowed developing the new high-efficient surfacing materials and technologies of surfacing the parts, operating under the conditions of wear and cyclic mechanical or thermomechanical loads. The developed materials and technologies of surfacing have passed pilot-industrial tests and used in mining and metallurgical enterprises of Ukraine.



FLASH-BUTT WELDING OF ROD REINFORCEMENT IN RECONSTRUCTION OF OLYMPIC NSC (Kiev)

In Kiev during preparation to the Football European Championship EURO 2012 a large complex of works is performed for the reconstruction of available and construction of new objects of Olympic NSC.



The E.O. Paton Electric Welding Institute of the NAS of Ukraine has contributed to realize large-scale projects in the planned terms. In particular, the Department of Pressure Welding of the Institute has developed technologies of flash-butt welding of rod reinforcement of ferroconcrete and model of mobile complex for realization of these technologies directly at the construction site. The complex includes flash-butt welding machines, earlier designed at the E.O. Paton Electric Welding Institute. In the period of June–October 2010 a large volume of works on flash-butt welding of ferroconcrete rod reinforcement of 20, 25, 28, 32 and 36 mm diameter for manufacture of twenty girders of upper tier of spectators stand of the VIP-zone and monolithic plates of the zone for arriving team buses was performed.

The carried out metallographic investigations and mechanical tests showed that quality of welded joints completely meets the requirements of acting standard documents.

This development can be widely used in construction of industrial and residential structures, bridges, viaducts and other objects.